UNCLASSIFIED
SECURITY CLASSIFICATION OF THIS PAGE

(2)

AD-A240 642

DTIC ELECTE SEP 23 1991 S D

Form Approved
OMB No. 0704-0188

REPORT DOCUMENTATIC

1a. REPORT SECURITY CLASSIFICATION
UNCLASSIFIED

2a. SECURITY CLASSIFICATION AUTHORITY

2b. DECLASSIFICATION / DOWNGRADING SCHEDULE

3. DISTRIBUTION / AVAILABILITY OF REPORT
Approved for public release; distributic unlimited.

4. PERFORMING ORGANIZATION REPORT NUMBER(S)
N00014-89-J-3088-TR1

5. MONITORING ORGANIZATION REPORT NUMBER(S)

6a. NAME OF PERFORMING ORGANIZATION
Washington State University

6b. OFFICE SYMBOL (If applicable)

7a. NAME OF MONITORING ORGANIZATION
Office of Naval Research

6c. ADDRESS (City, State, and ZIP Code)
Department of Physics
Washington State University
Pullman, WA 99164-2814

7b. ADDRESS (City, State, and ZIP Code)
Physics Division Code 1112
Arlington, VA 22217-5000

8a. NAME OF FUNDING / SPONSORING ORGANIZATION

8b. OFFICE SYMBOL (If applicable)

9. PROCUREMENT INSTRUMENT IDENTIFICATION NUMBER
N00014-89-J-3088

8c. ADDRESS (City, State, and ZIP Code)

10. SOURCE OF FUNDING NUMBERS

PROGRAM ELEMENT NO.	PROJECT NO.	TASK NO.	WORK UNIT ACCESSION NO
	uri 5004		

11. TITLE (Include Security Classification) Scattering of Tone Bursts from Spherical Shells: Computations Based on Fourier Transform Method

12. PERSONAL AUTHOR(S)
Zhang, L. G.

13a. TYPE OF REPORT	13b. TIME COVERED	14. DATE OF REPORT (Year, Month, Day)	15. PAGE COUNT
Technical	FROM 900816 TO 910731	910830	xii + 142 = 154

16 SUPPLEMENTARY NOTATION This is the M.S. dissertation of Ligang Zhang. The grant P. I. was P. L. Marston, Telephone (509) 335-5343 or 335-9531.

17 COSATI CODES		
FIELD	GROUP	SUB-GROUP
20	01	

18. SUBJECT TERMS (Continue on reverse if necessary and identify by block number)
Acoustical Scattering, Lamb Waves

19. ABSTRACT (Continue on reverse if necessary and identify by block number)

An algorithm to compute the transient scattering of sound by elastic spheres and shells has been developed and tested. Short tone bursts incident on elastic spherical shells under various conditions have been investigated. Previous experiment results for elastic spheres and shells have been confirmed. Some interesting physical aspects concerning the basics of the scattering mechanism have been detected. A mid-frequency enhancement has been examined for thin shells and compared with the ray model results. The ray model is found to closely approximate the enhanced backscattering for tone burst associated with a subsonic wave on thin shells. A related filter-like effect of thin

20. DISTRIBUTION / AVAILABILITY OF ABSTRACT	21. ABSTRACT SECURITY CLASSIFICATION
☒ UNCLASSIFIED/UNLIMITED ☐ SAME AS RPT ☐ DTIC USERS	UNCLASSIFIED

22a. NAME OF RESPONSIBLE INDIVIDUAL	22b. TELEPHONE (Include Area Code)	22c. OFFICE SYMBOL
L. E. Hargrove	(703) 696-4221	ONR Code 1112

DD Form 1473, JUN 86 Previous editions are obsolete.

SECURITY CLASSIFICATION OF THIS PAGE
UNCLASSIFIED

19. ABSTRACT (continued)

shells for the selected frequencies of the enhancement has been detected and quantitatively described and the impulse response has been computed. The subsonic wave associated with the mid-frequency enhancement is referred to as the Scholte-Stoneley wave by some authors. The present computations can be of practical use and can be compared with observations or ray models of the scattering from shells under the same conditions if such observations or models become available later on. The scattering of tome bursts from shells was calculated when the carrier frequency is at or close to the frequency of resonance associated with a reverberation of longitudinal waves across the thickness of the shell. When the shell is a fluid, the results are easily interpreted in terms of an existing ray model. When the shell is elastic, they suggest the presence of a mechanism for prompt radiation noninvolving complete circumnavigation of the sphere by guided elastic waves.

SCATTERING OF TONE BURSTS FROM SPHERICAL SHELLS: COMPUTATIONS BASED ON FOURIER TRANSFORM METHOD

By

LIGANG ZHANG

A thesis submitted in partial fulfillment of the requirements

for the degree

Master of Science in Physics

Washington State University

Department of Physics

August 1991

Technical Report, Grant N00014-89-J-3088

To the Faculty of Washington State University:

The members of the committee appointed to examine the thesis of Ligang Zhang find it satisfactory and recommend that it be accepted.

Philip L. Marston

Chair

Robert J. Cole

Michael Muller

Naihua Sun

Acknowledgements

This work was done under the supervision of Dr. Philip L Marston. I would like to thank him for his wonderful directions during the whole process of the work. He has always lead me out of problems and made the job go smoothly. Without his guidance, I would have spent much longer time to make progress, let alone obtain any meaningful results. His instructions have been the key to the accomplishment of the job.

I would also like to take the opportunity to give my sincere thanks to Dr. Naihua Sun whom I never hesitated to turn to whenever a problem came up and from whom I have obtained many useful suggestions. I am also grateful to her for allowing me to use the plots from her research (Fig. 8, 9, 10). I would also like to express my gratitude to Mr. Greg Kaduchak for plot in Fig.D1.

Also my thanks go to Dr. Michael Miller and the members of the Marston research group for their support concerning the computing questions.

The work is partly sponsored by the Office of Naval Research. Without their funding, the writing of the report would not have been possible.

My stay here was financially supported by the Department of Physics at WSU. Without the support, It would not have been possible for me to just stay in Pullman, not to mention to study for the degree. I am very grateful for it.

SCATTERING OF TONE BURSTS FROM SPHERICAL SHELLS: COMPUTATIONS BASED ON FOURIER TRANSFORM METHOD

Abstract

by Ligang Zhang, M.S.

Washington State University

August 1991

Chair: Philip L. Marston

An algorithm to compute the transient scattering of sound by elastic spheres and shells has been developed and tested. Short tone bursts incident on elastic spherical shells under various conditions have been investigated. Previous experiment results for elastic spheres and shells have been confirmed. Some interesting physical aspects concerning the basics of the scattering mechanism have been detected. A mid-frequency enhancement has been examined for thin shells and compared with the ray model results. The ray model is found to closely approximate the enhanced backscattering for tone bursts associated with a subsonic wave on thin shells. A related filter-like effect of thin shells for the selected frequencies has been detected and quantitatively described and the impulse response has been computed. The present computations can be of practical use and can be compared with observations or ray models of the scattering from shells under the same conditions if such observations or models become available later on. The scattering of tone bursts from shells was calculated when the carrier frequency is at or close to the frequency of resonance associated with a reverberation of longitudinal waves across the thickness of the shell.

When the shell is a fluid, the results are easily interpreted in terms of an existing ray model. When the shell is elastic, they suggest the presence of a mechanism for prompt radiation noninvolving complete circumnavigation of the sphere by guided elastic waves.

Table of Contents

List of Illustrations

Figures

List of Tables

Table

To Wei Luo

CHAPTER 1

Introduction

Scattering from well-shaped smooth objects such as solid spheres and spherical shells has been of interest and investigated for a long time, yet some basic physical aspects still remain not well understood or even unknown. Recent attention has been focused on the geometrical representation of scattering and its extension to arbitrary objects. For the last a couple of years, Dr. Marston and his research group have done marvelous jobs on the modeling of the scattering problem by ray synthesis method which has turned out to work excitingly well. The modeling is, however, not perfect. There are still some unclear physics which presumably can be seen by investigating scattering of various transient waves.

There have been numerous papers and researches on the scattering from solid spheres and hollow spheres, nevertheless, relatively few transient experiments or calculations can be found[1-6]. One of the difficulties in applying the geometrical theory of diffraction (GTD) to elastic objects is that the contributions due to surface guided elastic waves (SEW), such as Rayleigh and Lamb waves[7,8], can be important. Present work is to compute the transient backscattering from elastic spheres and spherical shells by using the Fourier Transform Method. This report is written in a consistent $e^{-i\omega t}$ time convention where $i = \sqrt{-1}$. Results verified the previous experiments, and most importantly, have revealed some exciting physics concerning the backscattering mechanism, hence helped better understand the scattering process and can be helpful in further modeling of ray method.

The arrangement of the report is as follows. First, the steady state scattering will be briefly discussed in Chapter 2 following the introduction. Chapter 3 presents the transient scattering formulation and the method used in the calculations. In Chapter 4, some more detailed computational considerations can be found and tests against previous experimental work for elastic sphere will be conducted . Chapter 5 deals with the main part of the report --- backscattering from elastic shells. Quite a few interesting results are presented in this chapter. A short conclusion and discussion can be found in Chapter 6. Appendices will present the programs used to finish the job and some illustrations about the writing of the programs which can be regarded as a "user's guide". Also presented in the appendices are some additional data and graphs for reference purpose.

CHAPTER 2

Steady-State Scattering

2.1 Far field scattering

Figure 1 illustrates a generic problem of interest. The center of an elastic sphere or a smooth empty shell having a circular profile is fixed at the origin of a spherical coordinate system.

Considering an infinitely extended incident plane pressure wave of a single frequency travelling in the +z direction

$$P_i(t) = P_o e^{ikz-i\omega t} = P_o e^{ik(z-ct)}, \qquad (2.1)$$

where Po is the pressure amplitude , $k=2\pi/\lambda$ is the wavenumber, λ is the wavelength and c is the sound speed in the fluid. The exact PWS (Partial Wave Series) solution can be obtained by solving the differential equations subject to proper boundary conditions. The solution is based on the summation of infinite terms of spherical Bessel and Hankel functions of the first kind. This response to a single frequency incident wave has been given a widely accepted name as the reflection form function denoted here by F(ka), where ka is the dimensionless wavenumber. Let $F(ka)e^{-i\omega t}$ be the solution for constant frequency, then at point P, which is at a distance $r>>ka^2$ from the center, harmonic scattered wave is produced[3]

$$P_r(t) = \left(\frac{a}{2r}\right) P_o e^{ik(r-ct)} F(ka) \qquad (2.2)$$

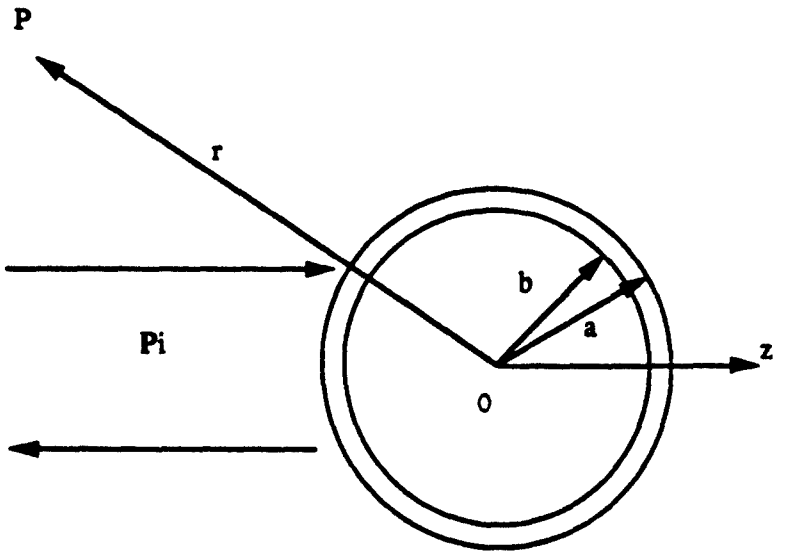

Fig.1 Geometrical illustration of problem . The incident pressure wave is an infinitely extended plane wave for the steady state scattering and a few cycles sine burst for the transient scattering. The scatterer can be an elastic sphere or a spherical shell. The thickness of shell is h = a - b.

Eq.(2.2) has the form of an outgoing spherical wave modified by the form function. For convenience, we define two dimensionless variables as following:

$$x = ka = (\omega/c)\, a$$

$$\tau = (ct - r)/a \ , \text{or} \quad x\tau = k(ct - r). \tag{2.3}$$

For the incident wave, r in above expression should be replaced by z. Obviously, τ is a dimensionless time interval, which is analogous to retarded time, with a unit corresponding to the time period necessary for the wave to travel a distance equal to the radius of the sphere or the out radius of the shell in the speed of sound in water. Equation(2.2) can then be rewritten as

$$P_r(\tau) = \left(\frac{a}{2r}\right) P_o\, e^{-ix\tau}\, F(x). \tag{2.4}$$

2.2 Form Function

The complex scattering amplitude or form function in the backscattering direction has the exact partial wave series representation

$$F(x) = \frac{2}{ix} \sum_{n=0}^{\infty} (-1)^n (2n+1) \frac{B_n(x)}{D_n(x)}, \tag{2.5}$$

where the functions Bn(x) and Dn(x) are 3×3 or 5×5 determinants obtained by satisfying the appropriate boundary conditions for elastic sphere[9,10],fluid shell[11] or elastic shell[12].

The computation of the form function requires the truncation of the infinite summation in Eq. (2.4). The minimum number of terms (or the maximum number of terms used in the calculation) n_{max} retained for sufficient convergence of F(x) exceeds x. The

following criterion discussed by S. Kargl and P.L.Marston will be used throughout this work[13].

$$n_{max} = 2 + [\, x + 4.0x^{1/3}] \,, \qquad x < 8$$

$$n_{max} = 3 + [x + 4.05x^{1/3}] \,, \qquad x \geq 8 \tag{2.6}$$

where the square brackets imply truncation to the nearest integer.

Chapter 3

Transient Analysis

3.1 Signal in Time and Frequency domain

For any incident time signal g(t), we can write down its frequency spectrum as Fourier integral

$$G(\omega) = \int_{-\infty}^{\infty} g(t)\, e^{+i\omega t}\, dt \tag{3.1}$$

and

$$g(t) = \frac{1}{2\pi}\int_{-\infty}^{\infty} G(\omega)\, e^{-i\omega t}\, d\omega \tag{3.2}$$

We can also rewrite these expressions in terms of our dimensionless variables x and τ as

$$G(x) = \int_{-\infty}^{\infty} g(\tau)\, e^{ix\tau}\, d\tau \tag{3.3}$$

and

$$g(\tau) = \frac{1}{2\pi}\int_{-\infty}^{\infty} G(x)\, e^{-ix\tau}\, dx \tag{3.4}$$

For each single frequency component G(x), we have for its scattering response in frequency domain

$$P(x) = G(x)\, F(x)\,. \tag{3.5}$$

The total far-field scattering wave in the time domain is hence given by

$$p(\tau) = \frac{P_0 a}{2r}\frac{1}{2\pi}\int_{-\infty}^{\infty} G(x)\, F(x) e^{-ix\tau}\, dx \tag{3.6}$$

Since only the backscattering is of interest in this report, F(x) in above equation is the form function at specific angle $\theta = \pi$.

3.2 Transient Formulation

If, in Eq. (3.6), one writes

$$p'(\tau) = \frac{1}{2\pi}\int_{-\infty}^{\infty} G(x)\, F(x) e^{-ix\tau}\, dx \tag{3.7}$$

then by computing $p'(\tau)$ as a function of τ, the scattered wave as a function of time observed at point P will be obtained. In other word, a pulseform will be seen at the point P developing like that computed according to Eq. 3.7 as value of τ increases.

For a real incident wave we have $g^*(\tau) = g(\tau)$, therefore

$$G(-x) = \int_{-\infty}^{\infty} g(\tau)\, e^{-ix\tau}\, d\tau$$

$$= \int_{-\infty}^{\infty} \left(g(\tau)\, e^{ix\tau}\right)^* d\tau$$

$$= \left(\int_{-\infty}^{\infty} g(\tau)\, e^{ix\tau}\, d\tau\right)^*$$

$$= G^*(x) .$$

So we obtain

$$G(-x) = G^*(x) \tag{3.8}$$

Let the incident wave be a Dirac delta function $\delta(\tau)$, then $G(x) \equiv 1$ and

$$p'(\tau) = \frac{1}{2\pi} \int_{-\infty}^{\infty} F(x) e^{-ix\tau}\, dx$$

We see that $p'(\tau)$ and $F(x)$ are the impulse response and the transfer function of the system (scatterer) respectively. They are a Fourier Transform pair. Since $p'(\tau)$ is a real function, following the above derivation, we immediately write down

$$F(-x) = F^*(x) \tag{3.9}$$

Now, we are ready to simplify our Eq.(3.7) as

$$p'(\tau) = \frac{1}{2\pi} \int_{-\infty}^{\infty} G(x)\, F(x) e^{-ix\tau}\, dx$$

$$= \frac{1}{2\pi} \int_{-\infty}^{0} G(x)\, F(x) e^{-ix\tau}\, dx + \frac{1}{2\pi} \int_{0}^{\infty} G(x)\, F(x) e^{-ix\tau}\, dx$$

$$= \frac{1}{2\pi}\int_0^{\infty} G(-x)\,F(-x)e^{ix\tau}\,dx + \frac{1}{2\pi}\int_0^{\infty} G(x)\,F(x)e^{-ix\tau}\,dx$$

$$= \left(\frac{1}{2\pi}\int_0^{\infty} G(x)\,F(x)e^{-ix\tau}\,dx\right)^{*} + \frac{1}{2\pi}\int_0^{\infty} G(x)\,F(x)e^{-ix\tau}\,dx$$

$$= \frac{2}{2\pi}\mathrm{Re}\int_0^{\infty} G(x)\,F(x)e^{-ix\tau}\,dx \qquad (3.10)$$

Eq. (3.10) is the basic formula we will use throughout the work. By using Eq.(3.10), we don't need to worry about the physical meaning of negative frequency. This equation has turned out to be important in understanding the algorithm developed later by using Digital Fourier Transform method.

Chapter 4

Computational Consideration and tests

4.1 Upper limit of the integration

First, a Fortran program computing the frequency spectrum of an incident several cycles sine burst was developed. It was checked by determining the backscattering from a hypothetical body for which the form function $F(x) \equiv 1$. Eq.(3.7) immediately leads that $p'(\tau)$ is the inverse transform of the incident wave, therefore an exactly the same signal is expected. However, since it is impractical to do the integration in Eq.(3.10) over the x range of $(0, +\infty)$, we truncated the upper limit of the integration at xmax. For a b-cycle sine tone burst

$$g(t) = \begin{cases} \sin \omega_o t & 0 \le t \le \dfrac{2\pi b}{\omega_o} \\ 0 & \text{otherwise} \end{cases}, \tag{4.1}$$

or, in terms of x and τ

$$g(\tau) = \begin{cases} \sin x_o \tau & 0 \le \tau \le \dfrac{2\pi b}{x_o} = B \\ 0 & \text{otherwise} \end{cases}, \tag{4.2}$$

where ω_o is the carrying frequency of the burst and $x_o = k_o a = \omega_o a/c$ is its dimensionless counterpart. Its spectrum can be calculated as follows,

$$G(x) = \int_{-\infty}^{\infty} g(\tau)\, e^{ix\tau}\, d\tau$$

$$= \int_{0}^{B} \sin\, x_o\tau\, e^{ix\tau}\, d\tau$$

$$= \frac{1}{2}\left[\frac{1}{\alpha}\left(1-e^{iB\alpha}\right) - \frac{1}{\beta}\left(1 - e^{iB\beta}\right)\right] \qquad (4.3)$$

where $\alpha = x+x_o$, $\beta = x-x_o$. The integration in Eq.(3.10) was accomplished by utilizing the simple trapezoidal method. To assure the detail of the scattered wave be properly displayed, the interval between successive τ values has to be chosen small enough. This value has been set to $\Delta\tau = \frac{B}{25\,b}$ so that there are 25 points over one cycle of sine burst (see more detail in Appendix A6). For the case of a 4-cycle burst with $x_o = 49.1$, $\Delta\tau = 0.02$ and xmax was chosen to be 400. This value of xmax is determined by the fact that the inverse transformed version has been good enough for a cut-off frequency of 400 and the convergence beyond 400 is so slow that in order to get significant improvement over the case of xmax = 400, xmax has to be greater than 1000, which implies whole lot a more computational work. The ideal incident tone burst and computed backscattering from an object with $F(x) \equiv 1$, or the real incident burst are both shown in Fig. 2.

Replacing the integral's upper limit with a finite value is the same as letting the signal pass through an ideal low-pass filter. Therefore a filtered replica of the ideal incident burst is expected. This effect is clearly shown by the actual incident burst depicted in Fig. 2 where the sharp part of the ideal burst has been rounded off since the high frequency information above the xmax have been lost. But the amplitude of those high frequency components are small enough that the difference is not significant as far as the transient scattering is concerned. Physical aspects are still there and almost unaffected.

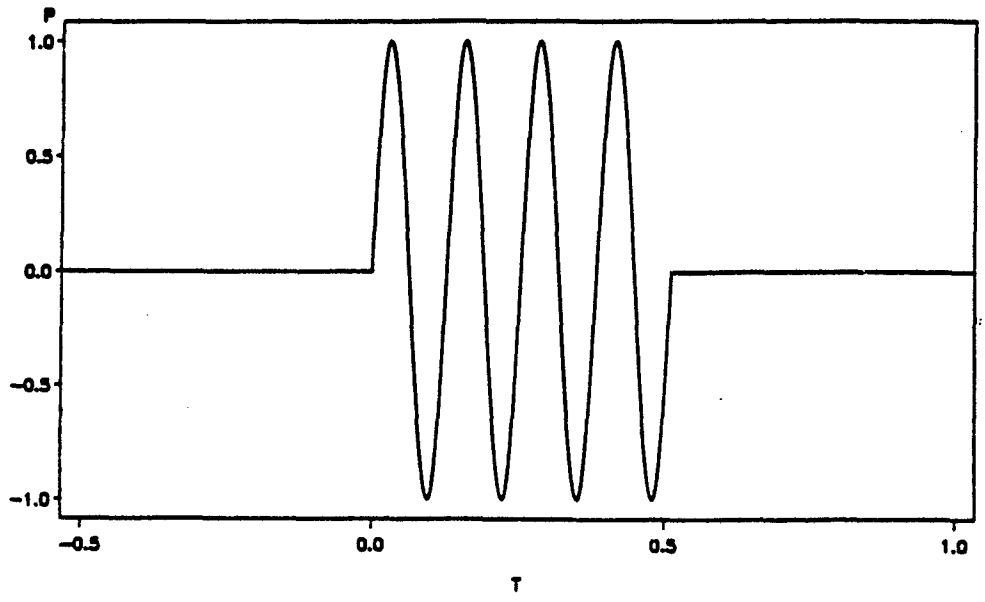

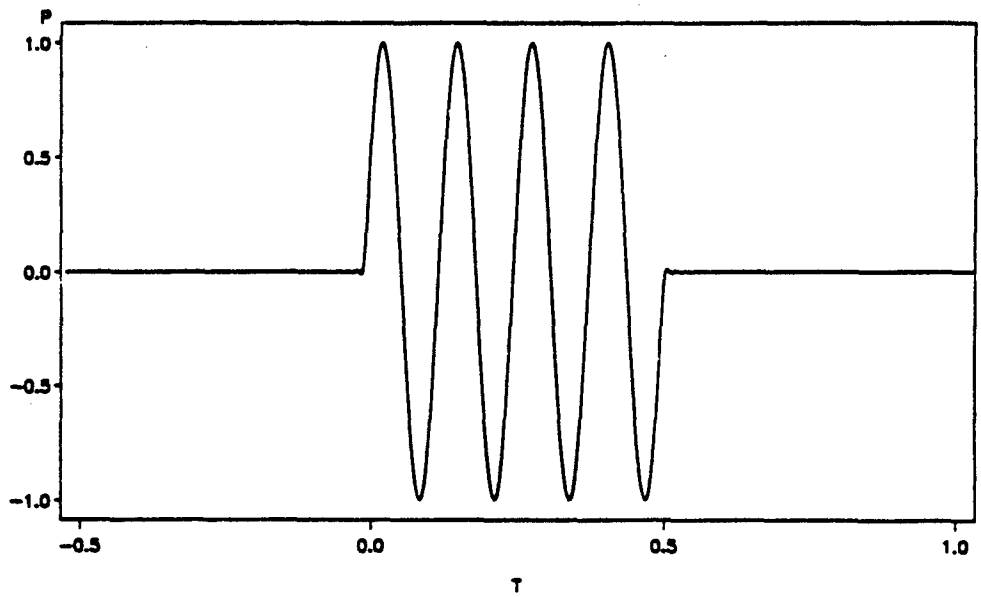

Fig2a. Ideal incident burst and its practical version. The 4-cycle sine burst has a carrier frequency $x_0 = 49.1$. The cut-off frequency is xmax = 400. The real burst is good enough, which shows that the xmax = 400 is sufficient.

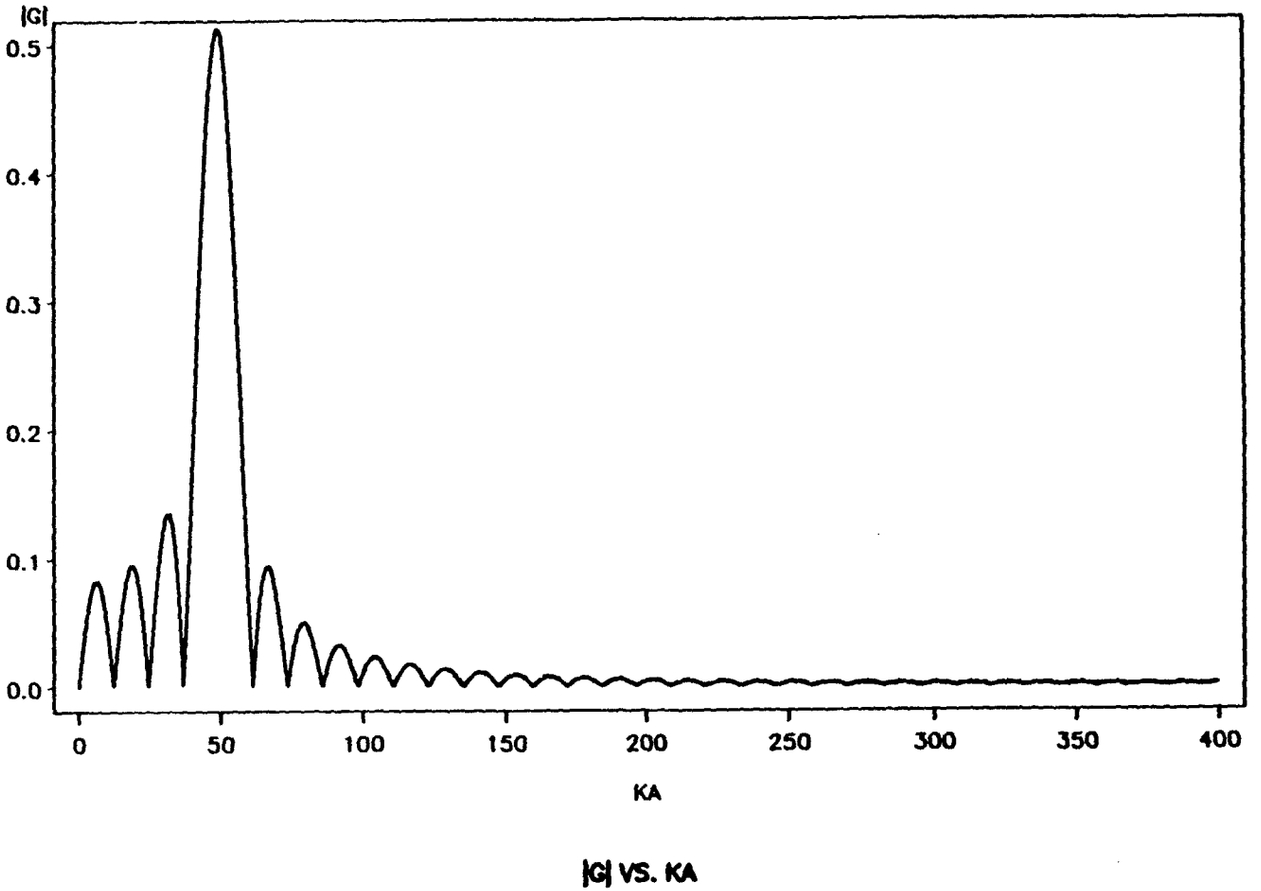

Fig.2b. Frequency spectrum of a 4-cycle sine burst with $x_0 = 49.1$.

4.2 Test against experiment

The test against the experiment result obtained by William and Marston[9] for a tungsten carbide sphere in water was then carried out. The material parameters used for tungsten carbide were: density ρ= 13.80 g/cm^3, longitudinal wave speed c_l= 6.860 $\times 10^5$ cm/s, shear wave speed = 4.185 $\times$ 10^5 cm/s. Those for water were: density ρ_w= 1g/cm^3, longitudinal wave speed = 1.4760 $\times$ 10^5 cm/s. The incident burst is again chosen as stated in Eq. 4.2 with b=4. The form function F(x), calculated on the Dec station in the range of $0<x<400$ with an interval $\Delta x = 0.05$ and plotted on HP-7475A plotter, is shown as Fig.3b for completeness. Both the experiment and calculated results are also shown in Fig. 3 where we have seen that they match each other reasonably well. The form function is referenced at the center of the sphere so that scattered wave leads the incident wave by $\tau = 2$. This test simply verified that the approach to the transient problem is successful.

4.3 DFT Approach

To do the computation more effectively we utilize the FFT programs provided by the CMS main frame. To better understand the algorithm we are using we have to talk about the DFT (abbreviation for Digital Fourier Transform) first.

DFT [14] of a sequence of N samples, f(nT), $0<n<N-1$, is defined as another sequence

$$F(j\Omega) = \sum_{n=0}^{\infty} f(nT)e^{i\Omega Tnj} \qquad (4.4)$$

Material	ρ (g/cm^3)	c_l (km/s)	c_s (km/s)
Tungsten carbide	13.80	6.860	4.185
Water	1.00	1.476	

Table 1. Material parameters for tungsten carbide sphere and water.

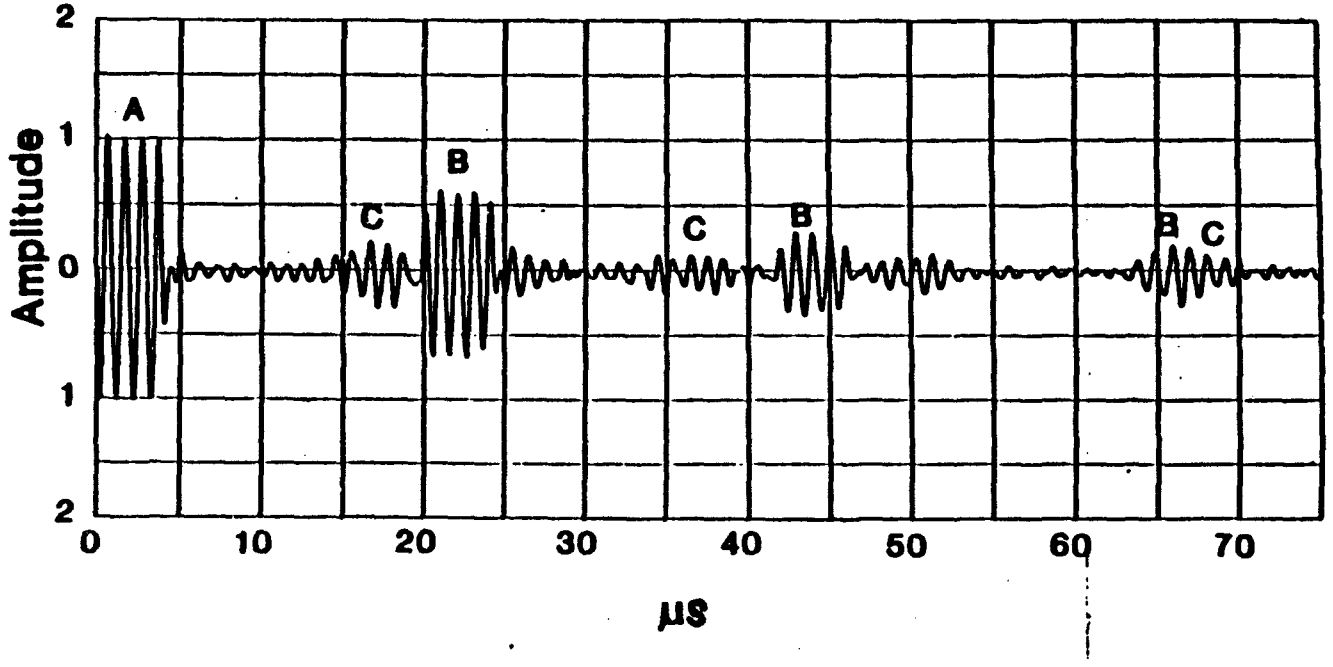

Fig.3a. Experiment result of the backscattering from a tungsten carbide sphere in water. The incident 4-cycle sine burst has a carrier frequency $x_0 = 49.1$. The individual echoes are labeled as follows: A-- specular reflection, B--Rayleigh surface wave echoes, C--other surface waves and transmitted bulk waves.

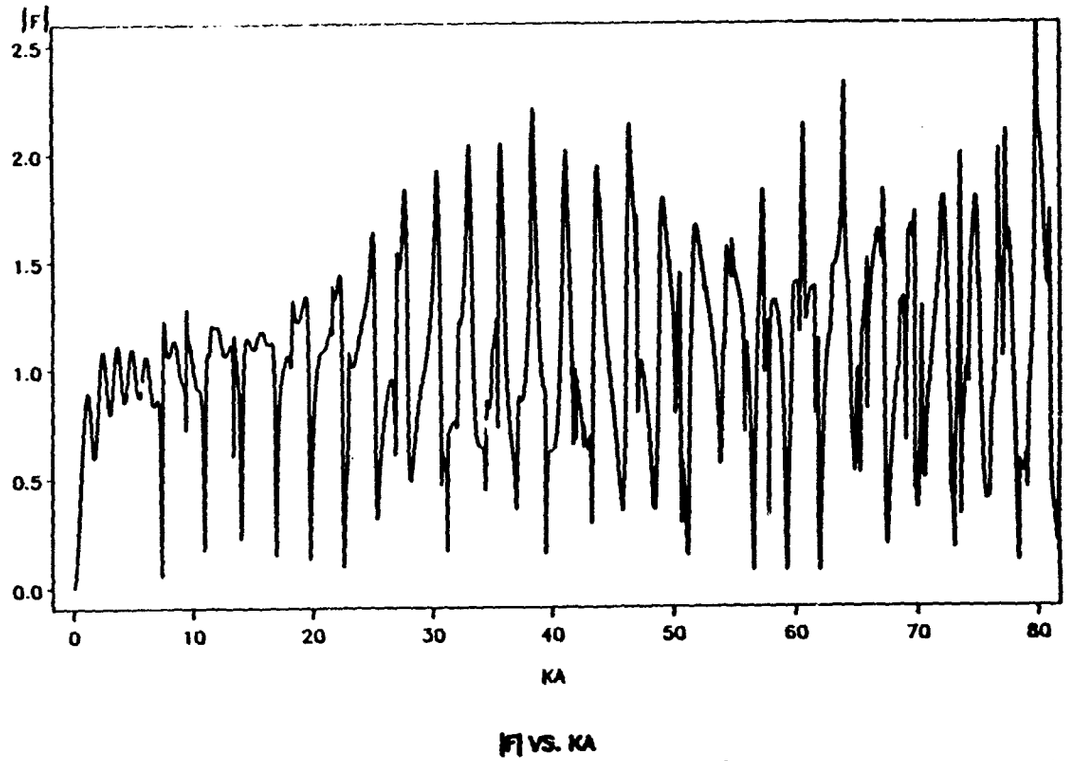

Fig.3b. Form function of a tungsten carbide sphere in water.

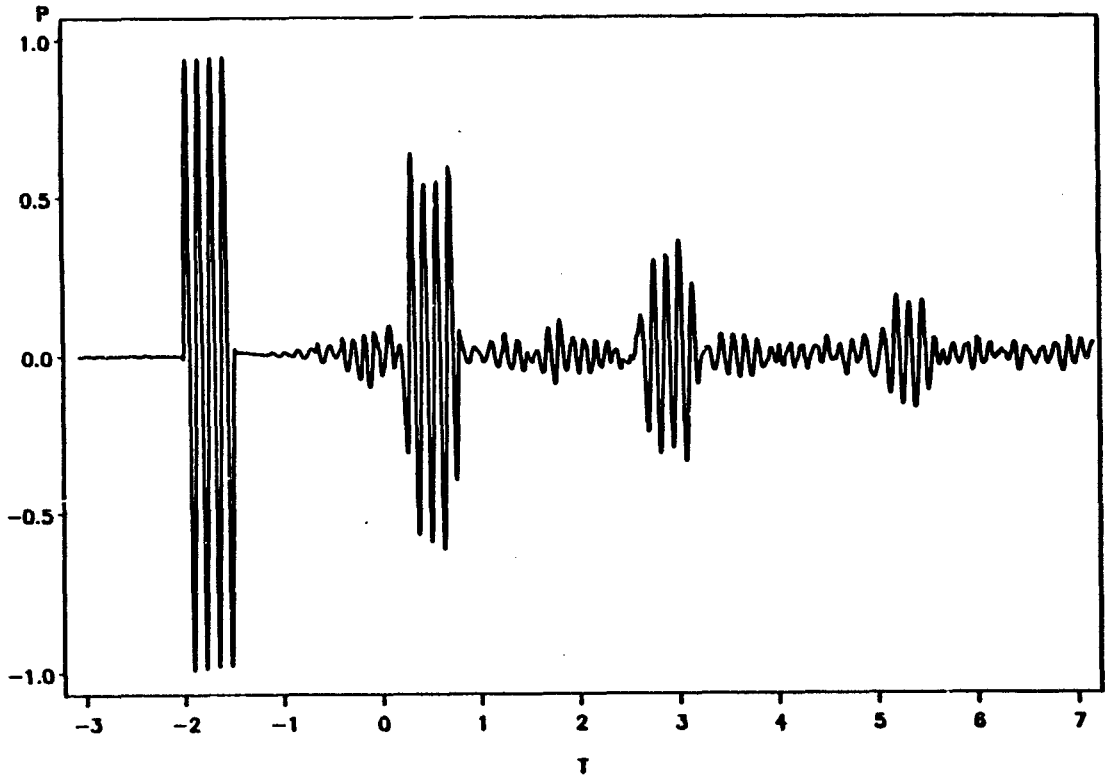

Fig.3c. Computational backscattering from a tungsten carbide sphere in water. The incident wave is a 4-cycle sine burst with xo = 49.1. The form function is referenced at the center of the sphere, so the backscattering starts at $\tau = -2$.

The inverse DFT is given by

$$f(nT) = \frac{1}{N} \sum_{j=0}^{\infty} F(j\Omega)\, e^{-i\Omega Tnj} \quad , \tag{4.5}$$

where $0 \le n \le N-1$, $0 \le j \le N-1$ and

$$\Omega = \frac{2\pi}{NT} \quad . \tag{4.6}$$

Clear enough, N has to be very large if we intent to have both frequency and time intervals to be sufficiently small so that we don't lost any detailed information during the computations.

4.4 Sampling

Now we consider an input sequence Y_j obtained by sampling the incident sine burst at an equal interval $\Delta\tau$. Since DFT regards the input sequence as one period of a periodic signal, we let Y_j be described as

$$Y_j = \begin{cases} \sin(x_0 Bm/M) & m=0,1,.....M-1 \\ 0 & m= M, M+1,....N \end{cases} \quad , \tag{4.7}$$

where M is the number of points over the duration of the burst while N is the length of the input sequence. A look at the measurements of backscattering by elastic sphere and shells tells us that the ratio of N/M must be greater than 16 if we want to distinguish at least the first few scattered surface waves. By letting the ratio big enough, we can assure the period of the input sequence to be long enough to cover the transient time interval we are interested in. Otherwise, the second period of the specular reflection would get back to our

measurement point P before the SEW due to the first burst. This is the intrinsic disadvantage of the method over the previous one where we only have one period of burst. This turns out not to be a problem because in order to satisfy other conditions to be discussed below, N has to be very large compared with M, which ensures the above condition in any case.

Sampling period $\Delta\tau$ has to be chosen so that there are sufficient sampling points over one cycle of the burst. And at the same time we need to be sure that the frequency interval Δx is small enough. But calculating of the form function involves a lot of computing time, Δx is therefore set to be 0.05 which has been proven sufficient by the later computational results. Actually one can not ordinarily discern the results of $\Delta x = 0.05$ and $\Delta x = 0.01$. Suppose we want L points per cycle, then,

$$M = L \times b \tag{4.8}$$

$$\Delta\tau = \frac{2\pi}{L\, x_o} \tag{4.9}$$

and

$$N = \frac{2\pi}{\Delta\tau\, \Delta x} = \frac{L\, x_O}{\Delta x} \tag{4.10}$$

for L = 20 and x_O=49.1, N=19,640. The maximum x_O value involved in this work is about 340 and resulting huge number of N can be a computing problem. To avoid this we will have to decrease the value of L and increase the value of Δx sometimes (see more detail in the Appendix A6).

4.5 FFT Algorithm

FFT programs we used are FFTCF and FFTCB routines in the IMSL bank[15]. FFTCF routine computes the discrete complex Fourier Transform of a complex vector of size N while FFTCB computes the inverse discrete transform of a complex vector of size N. The method used is a variant of the Cooley- Tukey algorithm which is most effective when N is a product of small prime factors. Specifically, given an N-vector Y, FFTCF returns another N-vector Z

$$Z_j = \sum_{n=0}^{N-1} Y_n e^{2\pi inj/N}, \qquad j = 0,1,\ldots N-1 \tag{4.11}$$

and given an N-vector Z, FFTCB returns another N-vector Y

$$Y_n = \frac{1}{N}\sum_{j=0}^{N-1} Z_j e^{-2\pi inj/N}. \qquad n = 0,1,\ldots N-1 \tag{4.12}$$

For a real sequence $Y_n^* = Y_n$, we have

$$\begin{aligned} Z_{N-j} &= \sum_{n=0}^{N-1} Y_n e^{2\pi in(N-j)/N} \\ &= \sum_{n=0}^{N-1} Y_n e^{2\pi in} e^{-2\pi inj/N} \\ &= \sum_{n=0}^{N-1} \left(Y_n e^{2\pi inj/N}\right)^* \\ &= Z_j^* \end{aligned}$$

or,

$$Z_{N-j} = Z_j^* \tag{4.13}$$

Above equation is analogous to Eq.(3.8). Clearly, Z_j (j>[N/2]) corresponds to the negative frequency components and $Z_{N/2}$ is the highest frequency component calculated by the FFT. Therefore we can also write

$$Y_n = 2\,\mathrm{Re}\left(\frac{1}{N}\sum_{j=0}^{[N/2]} Z_j\, e^{-2\pi inj/N}\right) \qquad n = 0,1,...,N-1 \tag{4.14}$$

Eq.(3.10) becomes

$$p'_n = 2\,\mathrm{Re}\left(\frac{1}{N}\sum_{j=0}^{[N/2]} Z_j F_j\, e^{-2\pi inj/N}\right) \qquad n = 0,1,...,N-1 \tag{4.15}$$

The problem of reference point can be serious for the FFT calculation. If we still let the incident burst be described by Eq.(4.7), we would expect the backscattering echoes leading the incident burst by $\tau = 2$. In other word, backscattering would start at $\tau = -2$. But FFT routines do not provide any data in the negative time scale. In fact, since the incident burst is regarded as one period of a periodic input sequence, the echo starting at $\tau = -2$ would appear at the end of the first period of computed backscattering. Basically, there are two ways to solve the problem. One way is to multiply each frequency component of incident burst by a phase shift factor exp(i2ka) before doing the integration or summation. This is equivalent to taking the convolution of the incident burst with $\delta(\tau-2)$. But this δ function could not be perfect due to the upper limit of integration or summation. This will cause some distortion on the real incident burst. The other way is to directly shift the incident burst over the time scale so that is starts at $\tau = 2$ instead of $\tau = 0$. This is in

principle the same as the first method but avoids the other unwanted effect. In order to see the early stage of the backscattering clearly, we have actually shifted the incident burst so that it starts at $\tau = 3$. The backscattering echoes therefore starts at $\tau = 1$ in any case. The ideal and real (inverse transformed assuming a hypothetical body with $F(x) \equiv 1$) incident bursts for FFT routines are shown in Fig.4a. The spectrum of the burst was computed by FFTCF routine and the backscattered wave was computed by FFTCB routine according to Eq.(4.15) where we have let $Z_j = 0$ for $j = [n/2]+1, \ldots N-1$. As we see from Fig.4b, The backscattered wave calculated by using the DFT is exactly the same as our previous computed result by doing the integration directly (Fig.3).

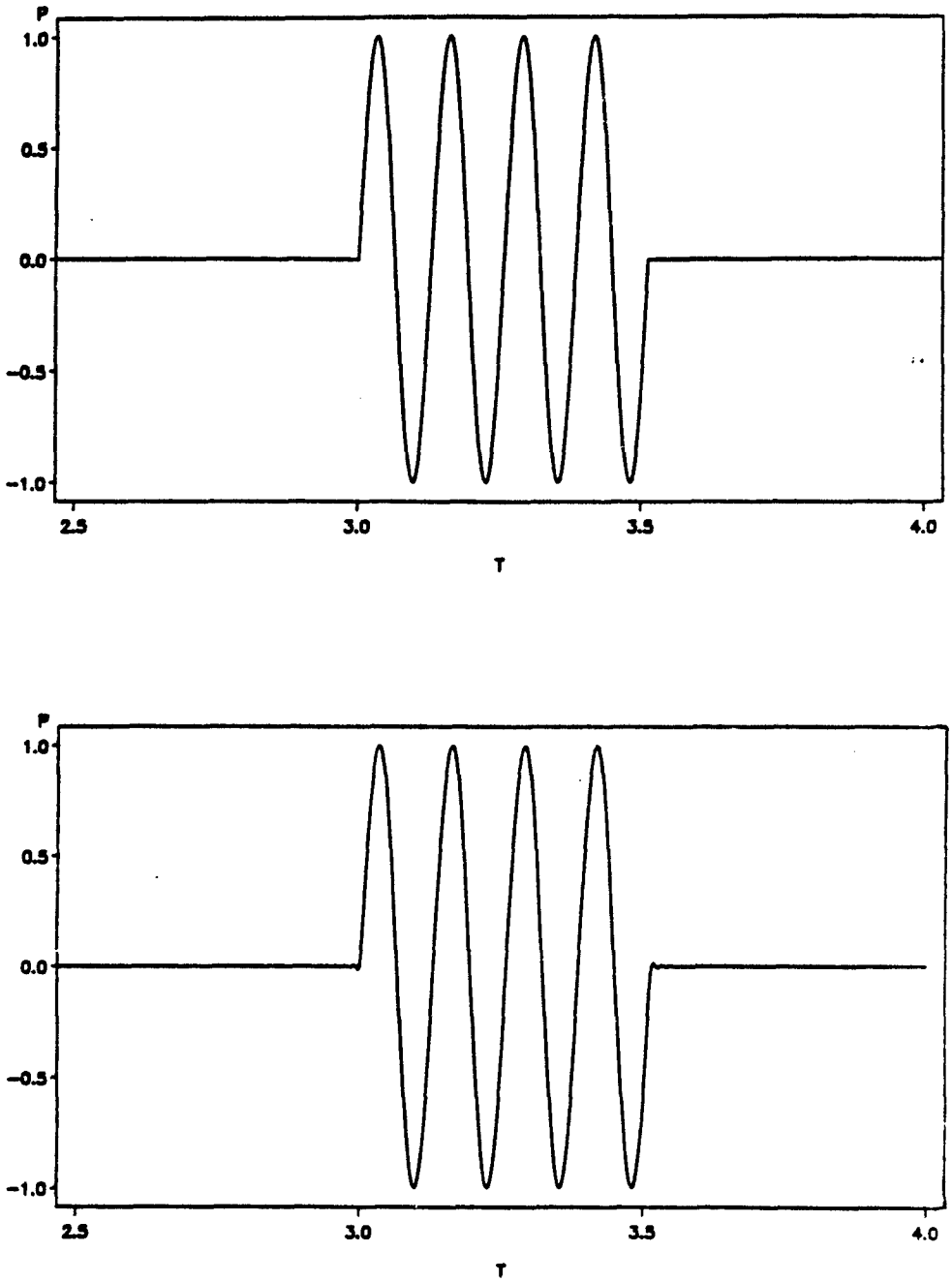

Fig.4a. Ideal incident burst and its practical version for FFT algorithm. They start at $\tau = 3$ instead of 0. The xmax is again chosen to be 400.

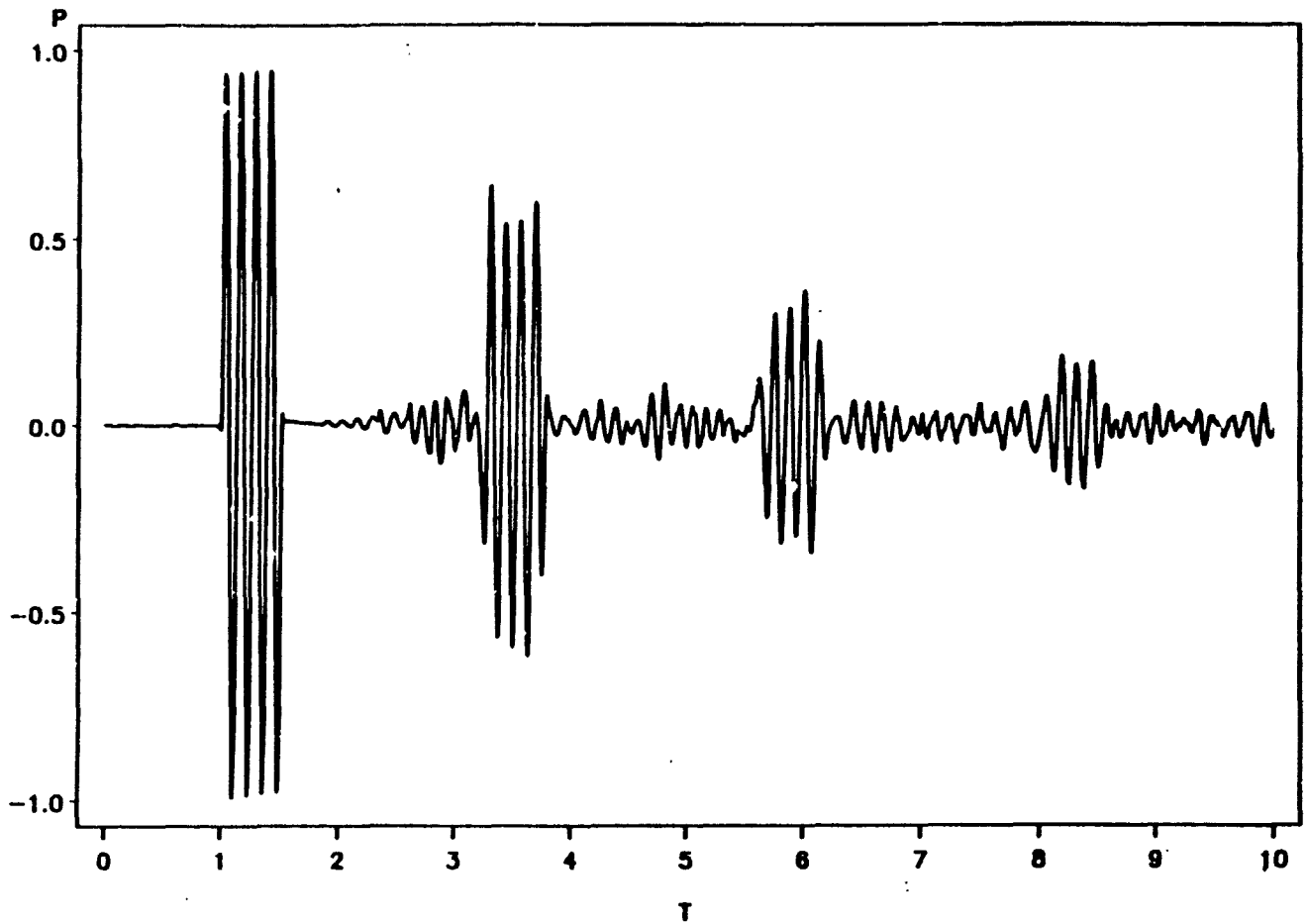

Fig.4b.Backscattering from a tungsten carbide sphere computed by using FFT algorithm. Compare with Fig. 3c.

Chapter 5

Backscattering From Elastic Shells

5.1 Verification with Experiments

The same FFT algorithm was applied to the case of a 16.2% - thick spherical shell. The material constants are listed in Table 2. The results for ka = 68.8, 64.7, 36.4 are presented in Fig. 5. Incident burst was again chosen to be four-cycle sine wave. These results reasonably match the previous experiment result obtained by S. Kargl and P.L. Marston[12] which is also shown in Fig.5 for comparison. Evidently, there are some significant difference. In the computation case a slow varying wave packet shows up, which was not expected and understood at the very beginning of the report at all. But we can get some clue by looking at the form function of such a shell which is also given in Fig.5. Clearly there is a big hump at the very low frequency. This phenomenon explains, at least tentatively, why the low frequency components of the incident wave were sort of amplified and the effect was so evident. The central dimensionless wavenumber of the hump is around x = 5. For the a = 1.905cm shell, it corresponds a low frequency of f_h = 62kHz which is much lower than the actual carrier frequency of the incident burst. This enhancement of the low frequency response may have been suppressed during the experiments since the combined transmitting and receiving apparatus would not have had the broad bandwidth assumed in the calculation. It is especially plausible that the four-cycle source burst used in the experiments did not have the low frequency spectral components implicit in Eq.(4.3). For thinner shells, the enhancement is shifted to a higher frequency and becomes what is known as the mid-frequency enhancement of the backscattering.

Material	ρ (g/cm^3)	c_l (km/s)	c_s (km/s)
440 C stainless stell	7.84	5.854	3.150
Water	1.00	1.479	

Table 2. Material parameters for SS440C shell and water.

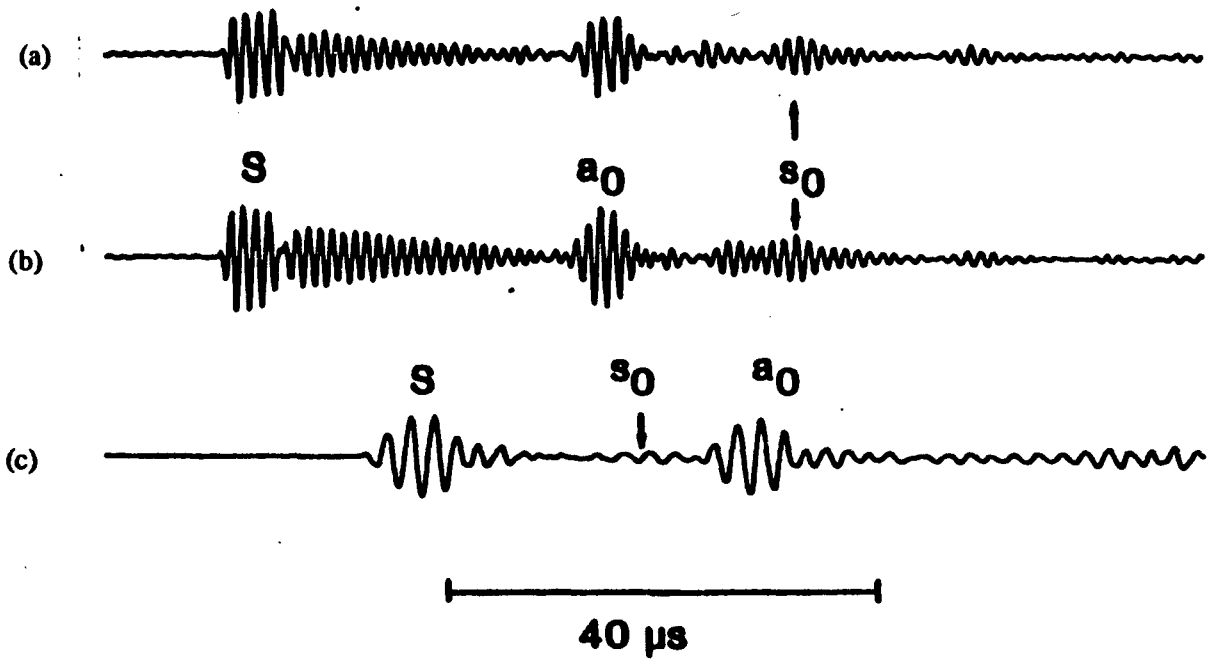

Fig.5a. Experiment results of backscattering from a 16.2%-thick stainless steel 440C shell. In each case, the specular echo is denoted by S. In (a) - (c), x_0 is, respectively, 64.7, 68.8, and 36.4.

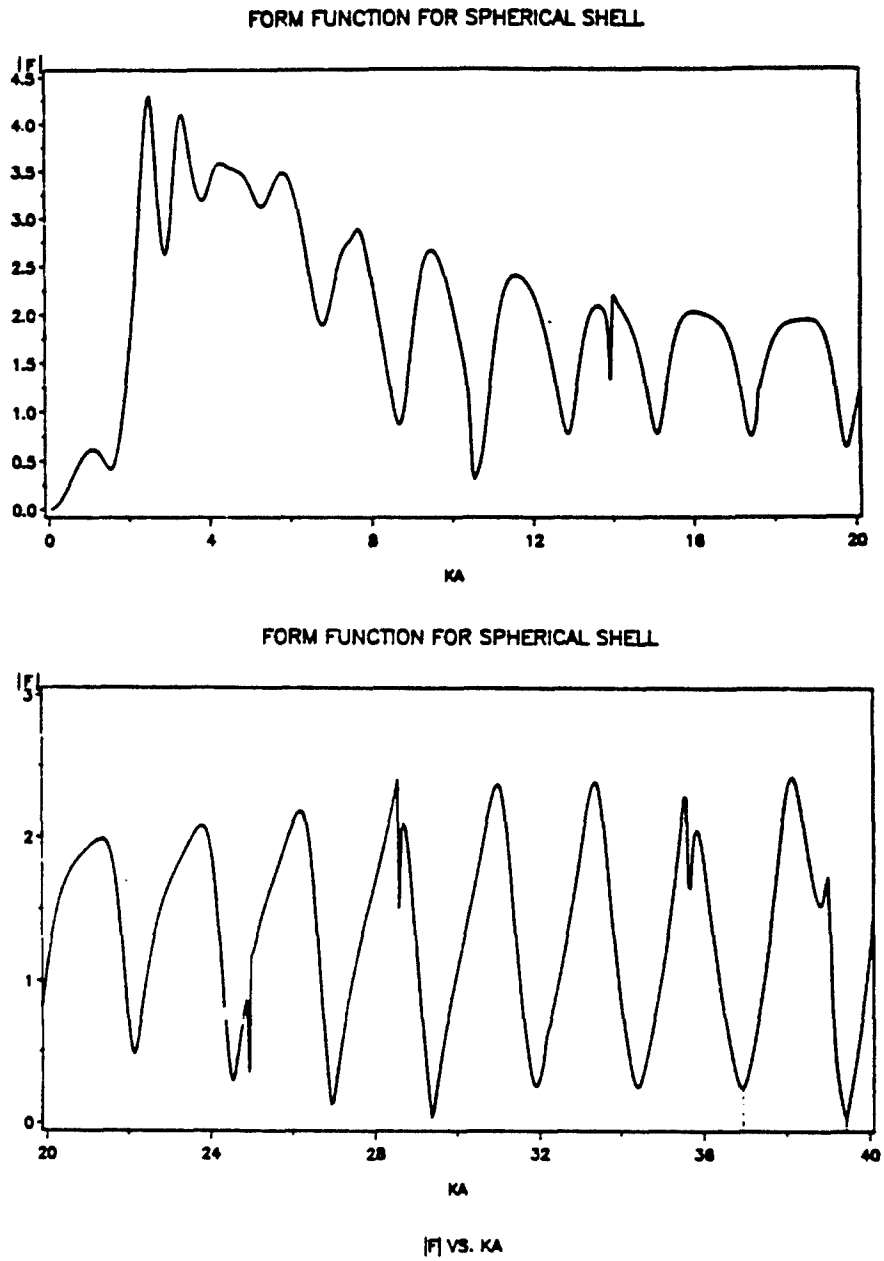

Fig.5b. The form function of a 16.2%-thick SS440C shell.

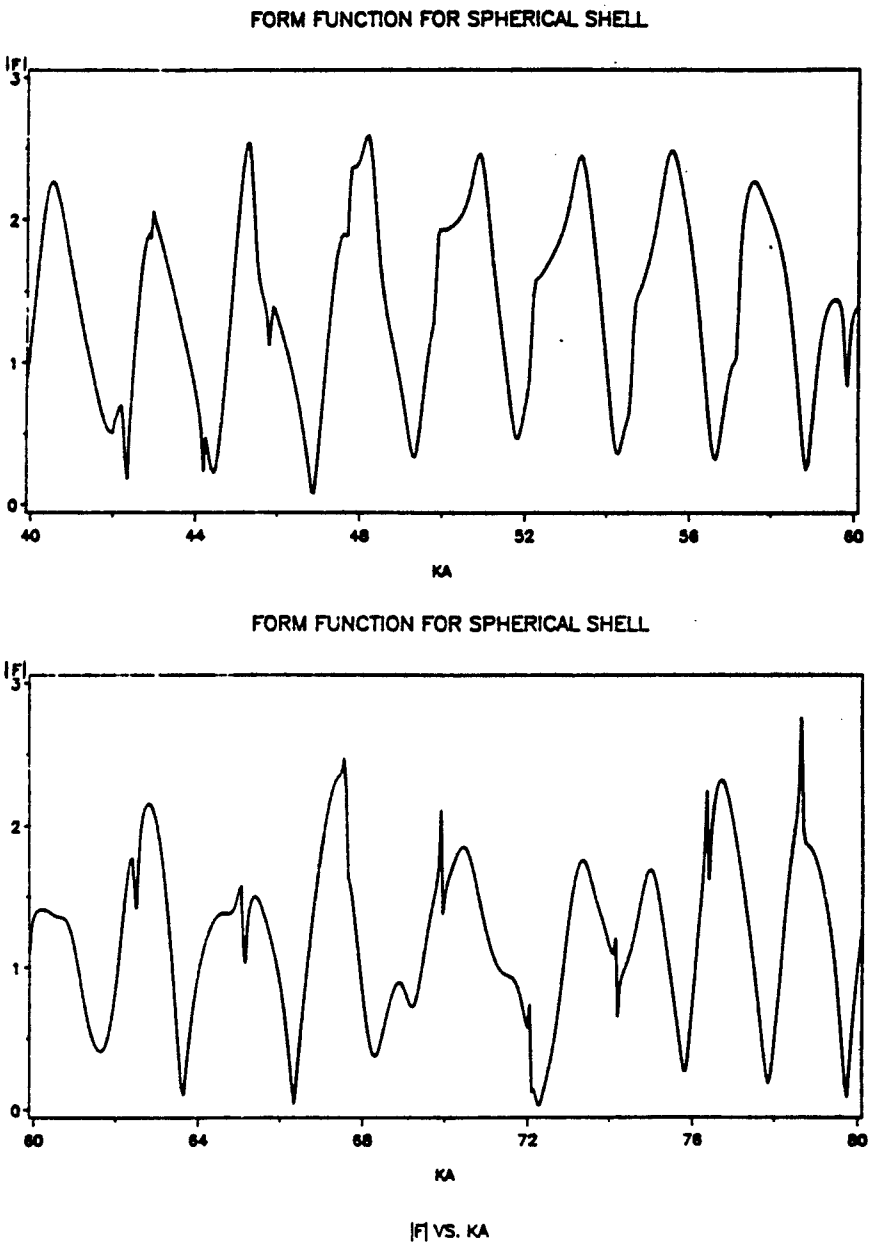

Fig.5b. The form function of a 16.2%-thick SS440C shell (continued).

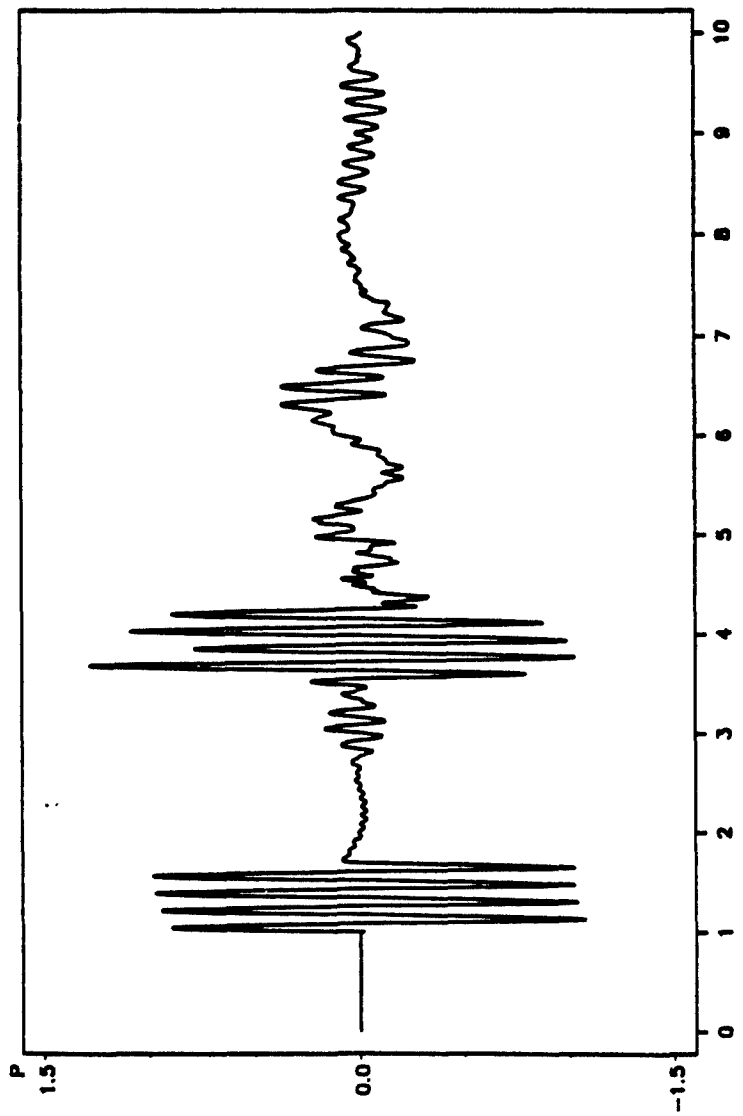

Fig.5c(a). Computational backscattering from a 16.2%-thick SS440C shell for a 4-cycle sine burst with $x_0 = 36.4$.

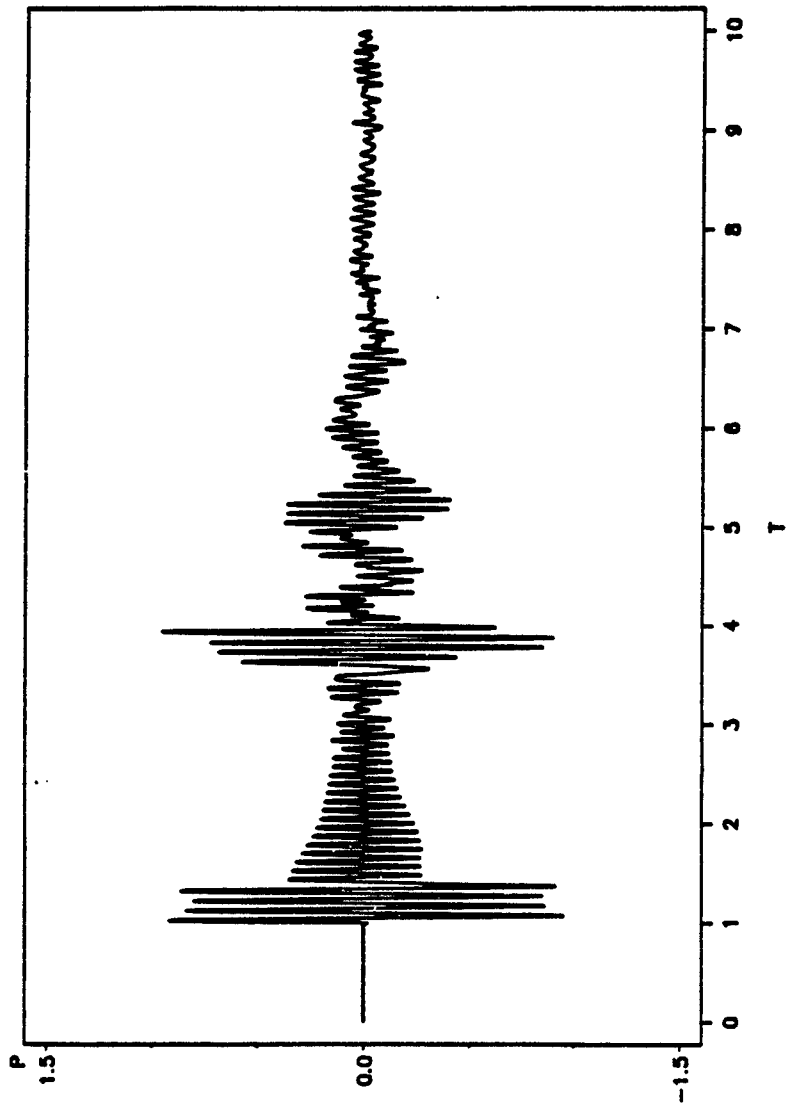

Fig.5c(b). Computational backscattering from a 16.2%-thick SS440C shell for a 4-cycle sine burst with $x_0 = 64.7$.

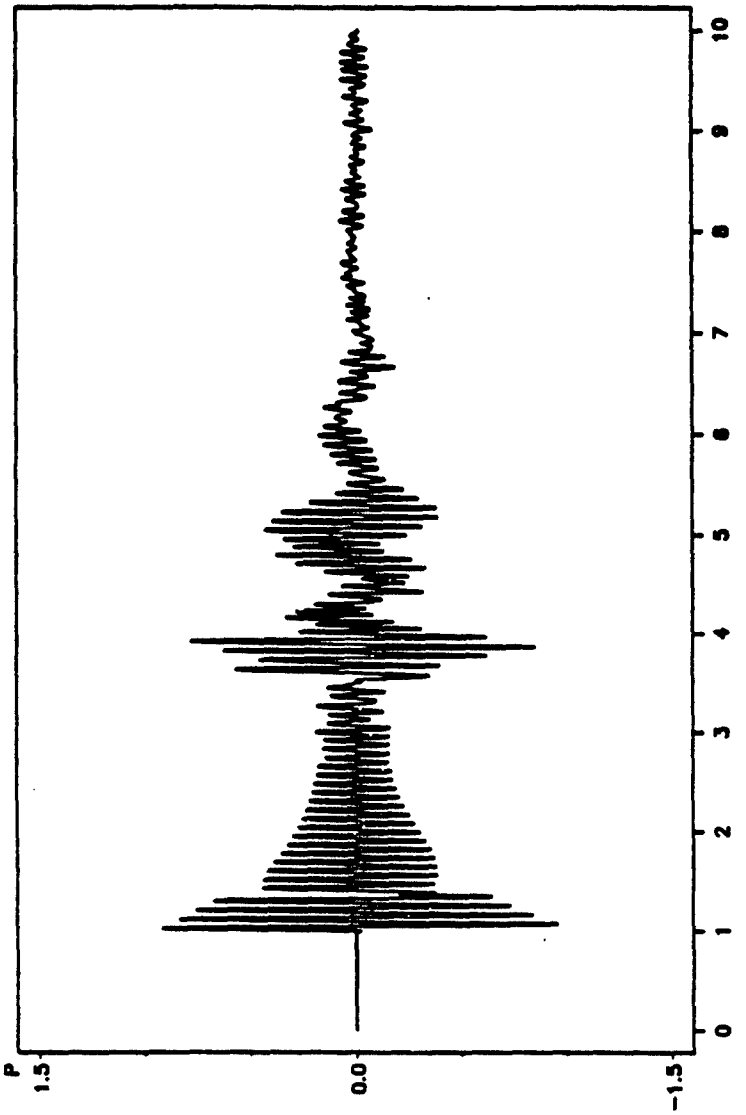

Fig.5c(c). Computational backscattering from a 16.2%-thick SS440C shell for a 4-cycle sine burst with $x_0 = 68.8$.

5.2 More on Mid-frequency Enhancement

The unexpected phenomenon and the tentative yet reasonable explanation lead us to the further examination of some other shell cases. Because the hump effect will most likely happen for thin shells, the backscattering of a 4-cycle sine burst incident on a 5% - thick spherical shell was computed. The carrier frequency $x_0 = 66.3$ was chosen, which happens to be a form function minimum. Shown in Fig.6 are the form function, spectrum of the incident burst and the transient backscattering. This time we see a huge hump or "hill" in the range of ka values 18-24 in Fig.6a and a relatively large amplitude of components in this range for the incident burst in Fig.6b. These combined factors clearly explain the low frequency signal detected in Fig.6c. There is a relatively large response to the initial weak low frequency component of the incident burst.

In the system point of view, the shell is acting like a filter with a big response for ka = 18-24. Any significant frequency component in this range for any input signal will be singled out. Then what about a burst with a carrier frequency in that range? The question is well answered by the huge echo following the specular reflection as shown in Fig.6d for a 4-cycle sine burst with $x_0 = 22.1$. This particular value of x_0 was picked up because in Fig.6c we see the low frequency response looks like a sine wave of 1/3 of original sine signal carrier frequency. The existence of a mid-frequency enhancement or "hill" in the form function for the steady state backscattering of elastic shells has been noted by various authors including Talmant, Uberall, Miller, and Dickey[8] and Sammelmann, Trivett, and Hackman[16,17]. The effect is interesting enough that it deserves further investigation.

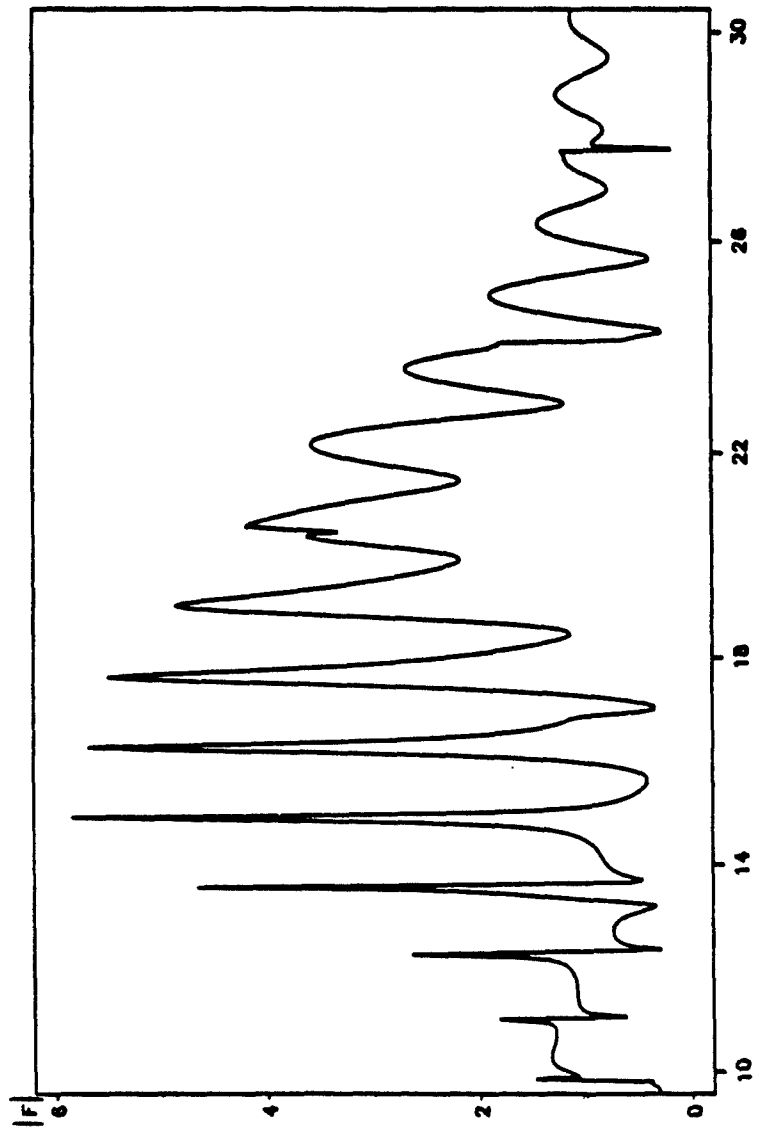

Fig.6a. Form function of a 5%-thick SS440C shell.

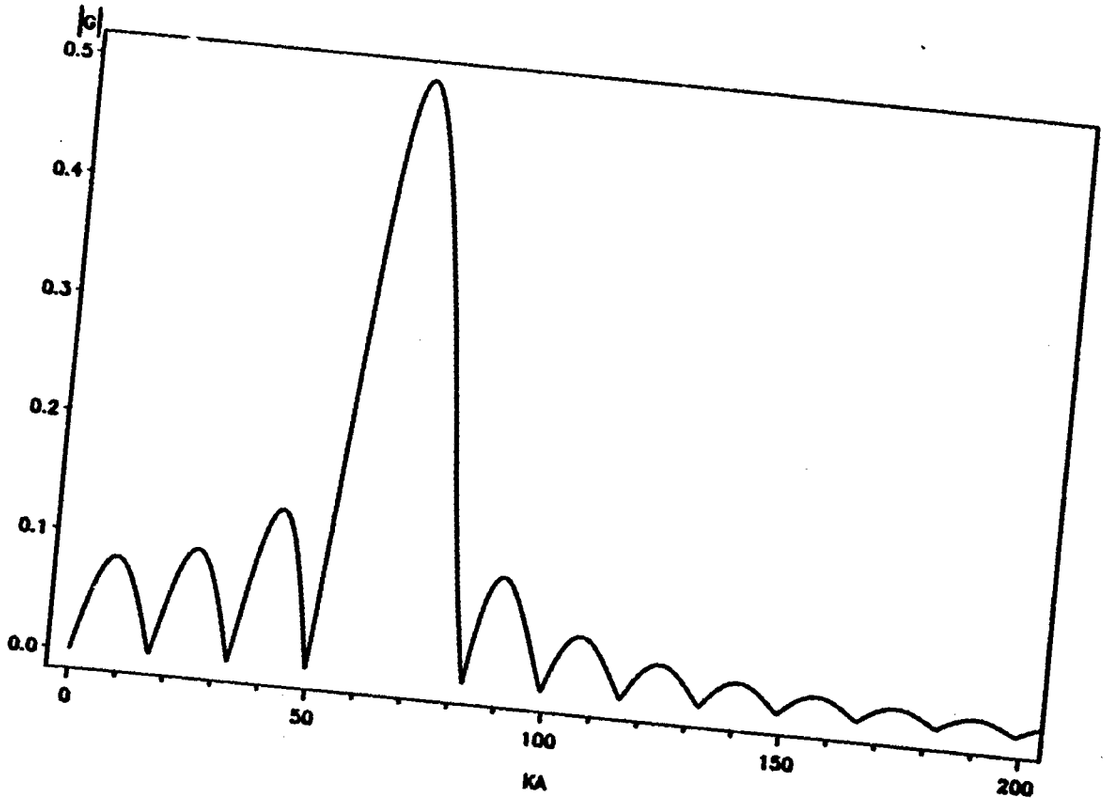

Fig.6b. Spectrum of a 4-cycle sine burst with $x_o = 66.3$.

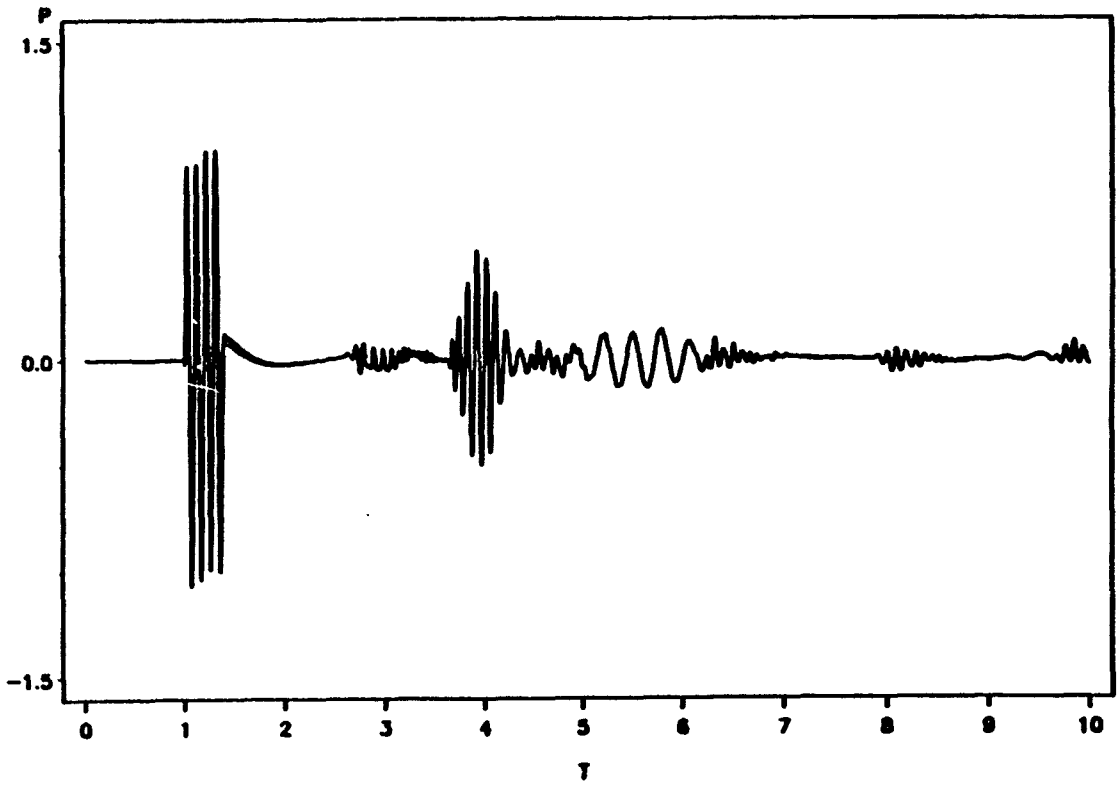

Fig.6c. Computational backscattering from a 5%-thick SS440C shell for a 4-cycle sine burst with $x_0 = 66.3$. The low frequency response is a manifestation of the mid-frequency enhancement.

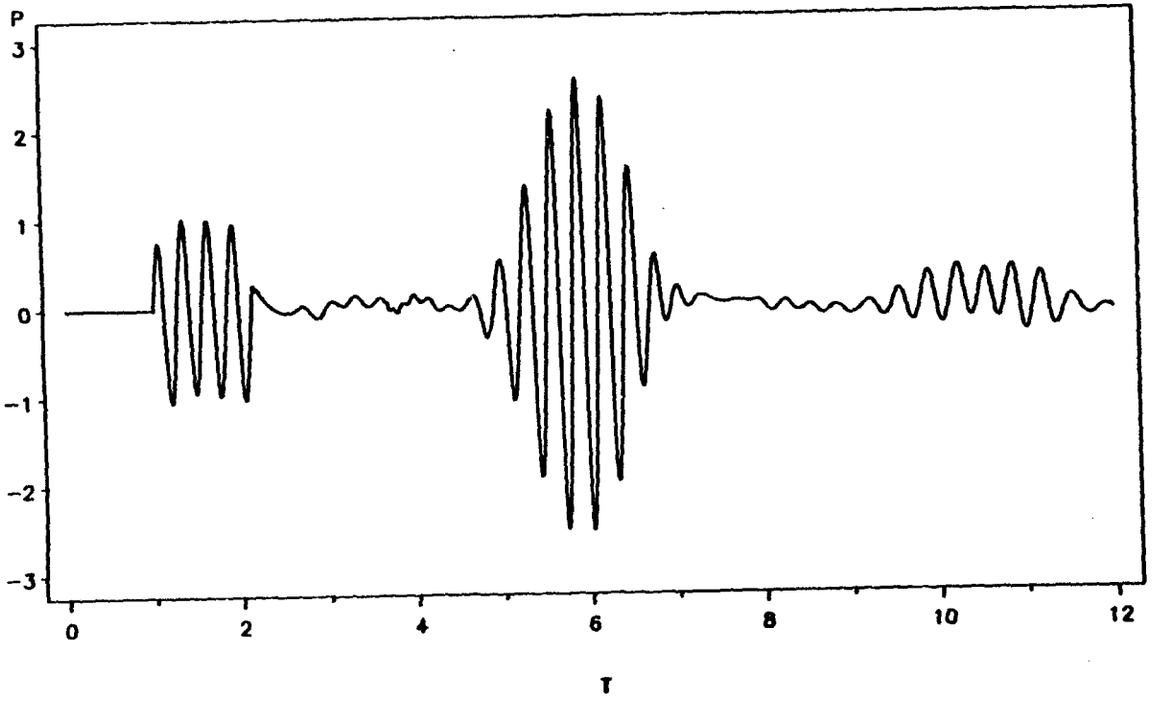

Fig.6d. Computational backscattering from a 5%-thick SS440C shell for a 4-cycle sine burst with $x_0 = 22.1$. The huge echo following the specular reflection is a manifestation of mid-frequency enhancement.

5.3 Mid-frequency Enhancement: Ray model and Verification

First of all, we notice the arrival time of the echo. Relative to the specular response, this particular echo always has a time delay of $\tau_d \approx 4$-5, that is the time period necessary for the signal to travel a distant equal to the 4 or 5 times of out radius of the shell in terms of the speed of sound in water. To facilitate the understanding of the major scattering mechanisms, the ray model analysis borrowed from Marston ,Kargl and Williams[11,18,20] is simply restated here. Fig.7a shows the ray diagram for leaky Lamb waves where a trace-velocity matching condition gives for $c_l > c$

$$\theta_l = \arcsin (c/c_l) . \tag{5.1a}$$

Ray synthesis of form function has basically two parts, one is due to the specular reflection and the other is the contribution of the variety of SEW. It can be written in the following form where *l* denoted the class of SEW:

$$f = f_{sp} + f_{l=s_0} + f_{l=a_0} + f_{l=a_0'} + \ldots , \tag{5.1b}$$

where $f_{l=a_0'}$ term is thought to be especially important for thin shells. Some authors[16,17] use A_0' to denote the wave a_0'. The geometric series for repeated leaky wave contributions gives for the steady state scattering from a spherical shell[18,19]

$$f_l = \frac{-G_l \exp[-2(\pi - \theta_l)\beta_l] \exp(i\eta_l)}{1 + \exp(-2\pi\beta_l)\exp(i2\pi kac/c_l)} , \tag{5.2}$$

where

$$\eta_l = 2ka[(c/c_l)(\pi - \theta_l) - \cos\theta_l] - \pi/2$$

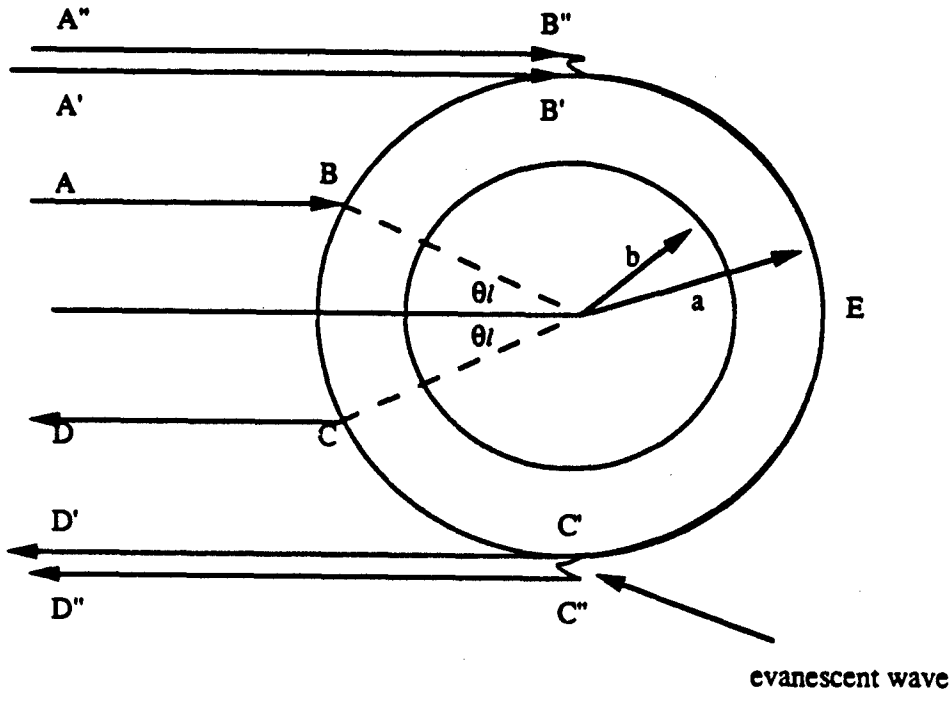

Fig.7a. Ray diagram for contributions to backscattering due to various kinds of surface wave (of type *l*) excited on an elastic spherical shell. Ray path ABECD is the usual case where $c_l > c$. Ray path A'B'E C'D' and AA"B"E C"D" correspond to $c_l = c$ (known as "creeping wave") and $c_l < c$ (known as "trapped wave"). In the case of $c_{gl} < 0$, The energy follows the short path of ABCD without circumnavigating the shell.

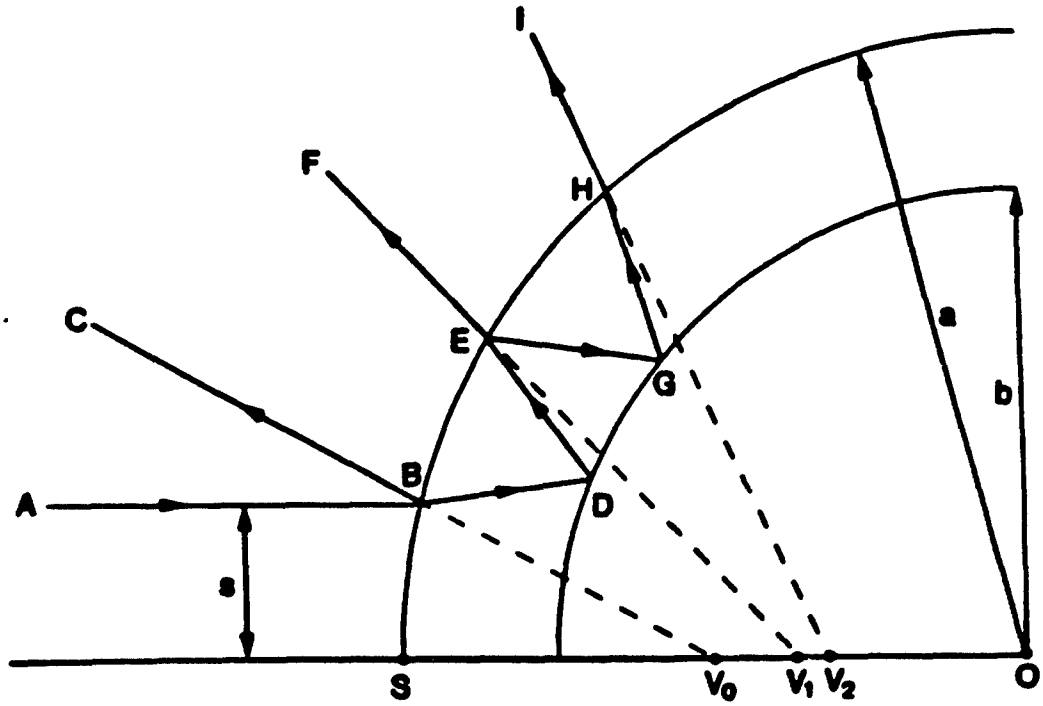

Fig.7b. The ray diagram for the specular reflection from an elastic spherical shell. The point S is the vertex of the refracting surface. The ray AB infinitesimally close to the z-axis is incident on the shell with impact parameter s. The ray ABC is the ordinary specular ray: while ABDEF and ABDEGHI are the first two internal specular reflection contributions. Intersection of the projection (dashed lines) of the outgoing rays and the z-axis define locations of virtual point sources, V_n, which describe local curvature of the wavefront associated with each ray. The specular reflection contribution to the form function for backscattering is determined from a superposition of the wavefields from the virtual sources.

and[18-20]

$$|G_l| \approx 8\pi\beta_l c/c_l \ . \qquad (5.3)$$

Some comments on the nature of the specular reflection are appropriate. Fig.7b shows the ray diagram for the external specular reflection and the other specular contributions associated with the reverberation of longitudinal waves within the shell. The point S is the vertex of the refracting surface. The ray AB is infinitesimally close to the z-axis. The ray ABC is the external specular ray; while ABDEF and ABDEGHI are the first two internal specular reflection contributions. At the internal surface, the rays are totally reflected and the rays are partially reflected and/or transmitted at the water-shell interface. Intersection of the projection (dashed lines) of the outgoing rays and the z-axis define locations of virtual point sources, V_n, which describe local curvature of the wavefront associated with each ray. For thin shells numerical computations of steady-state scattering[19] suggest that it is satisfactory to neglect the multiple reverberations in the region of the mid-frequency enhancement and to approximate the specular contribution is that due to ray ABC.

Fig.8,9,10 calculated by Dr. Sun for a 2.5%-thick SS304 shell show how the radiation damping parameter β_l (in np/radian), the phase velocity c_l and the group velocity c_{gl} of a_o,s_o and a_o' waves vary with ka. For the thickness of the shell we are considering here these are the only relevant surface guided waves. The method of computing these surface wave properties is based on applying the Watson transform methodology to the exact elastic equations for shells as discussed in Refs. 12,13,and 20. In Fig.8, we see that in the region of $34<x<62$, β_l is near zero for a_o and is large for s_o wave. Eq.(5.2) and (5.3) tell us that the contribution to the form function due to a surface wave will be small if

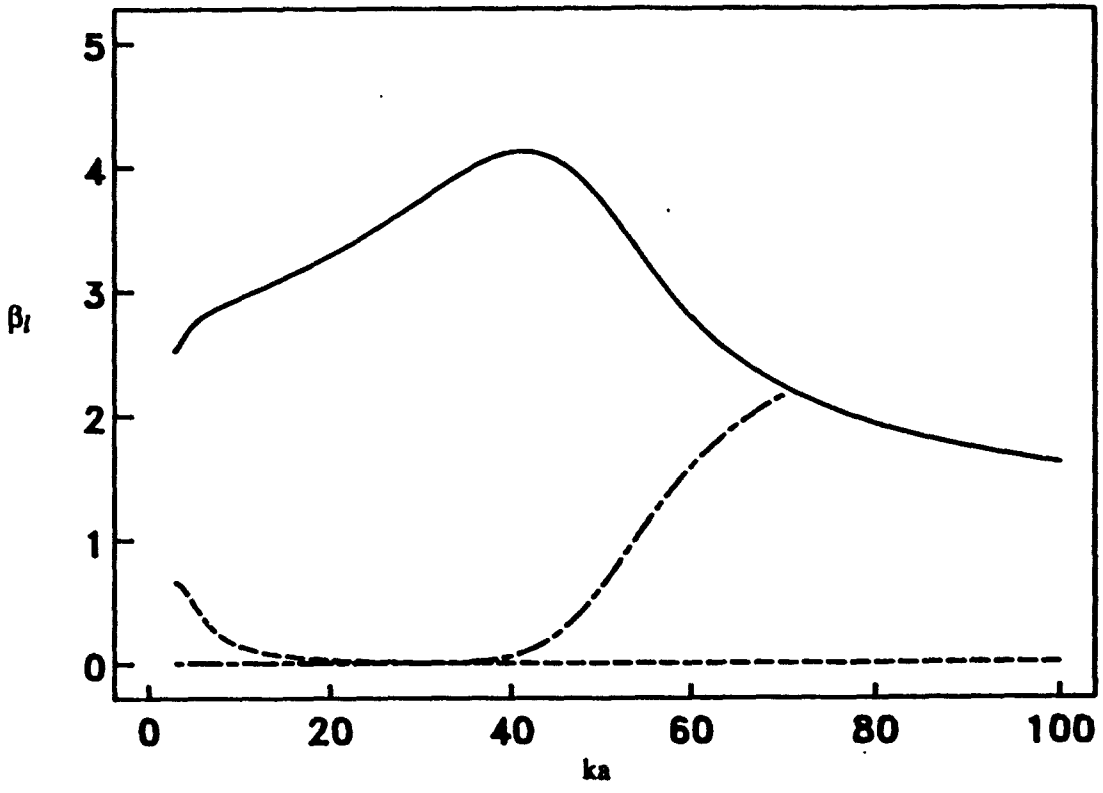

Fig.8. Radiation damping parameter β_l varies with ka for a 2.5%-thick SS304 shell. The solid curve is for $l = a_0$, the short-dashed curve is for $l = s_0$, and the short-long-dashed curve is for $l = a_0'$.

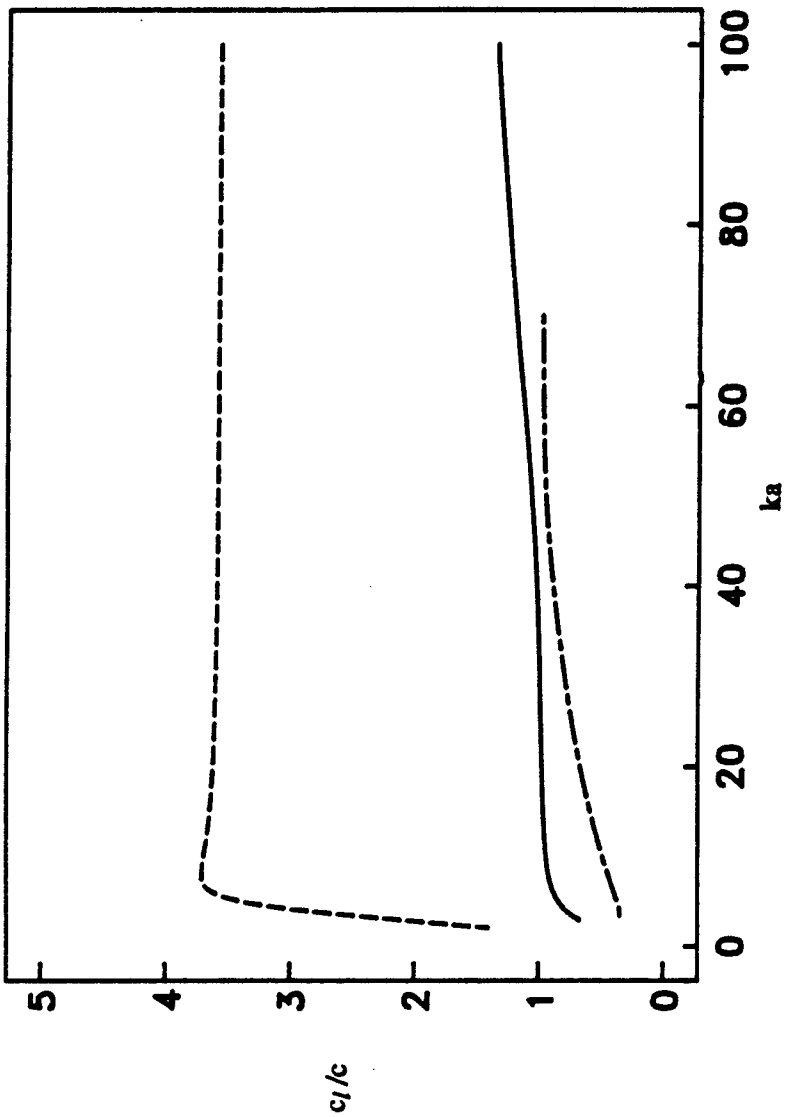

Fig.9. Phase velocity c_l varies with ka for a 2.5%-thick SS304 shell. The solid curve is for $l = a_0$, the short-dashed curve is for $l = s_0$, and the short-long-dashed curve is for $l = a_0'$.

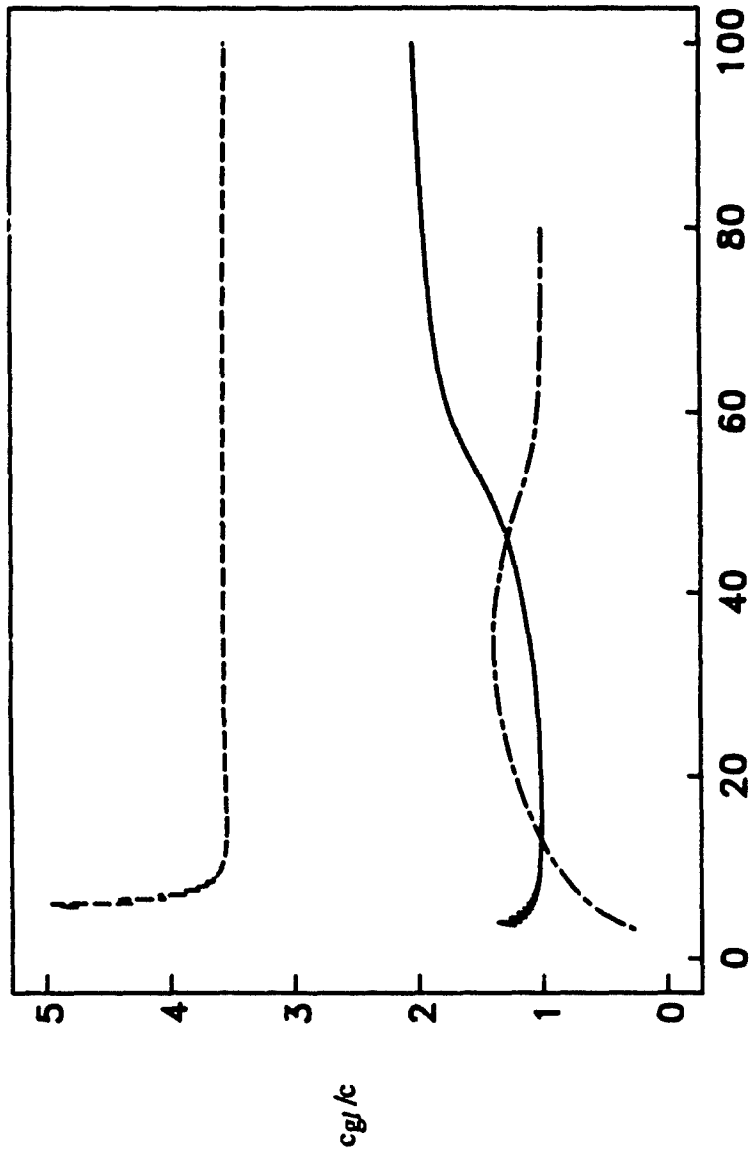

Fig.10. Group velocity c_{gl} varies with ka for a 2.5%-thick SS304 shell. The solid curve is for $l = a_0$, the short-dashed curve is for $l = s_0$, and the short-long-dashed curve is for $l = a_0'$.

β_l value of the surface wave is either small (coupling coefficient G_l will be small) or large (big damping will kill it), hence only the a_o' wave is important in this analysis. Fig.9 tells us that the phase velocity for a_o' in the ka range we are dealing with is very close to the sound speed in water c, which means that we are near the coincident condition. Eq.(5.1b) immediately gives $\theta_l = \pi/2$ for $c_l = c$. In Fig.7a, a traveling path of the wave is drawn as A'B'E C'D'. The wave first travels with speed of c straight along the ray A'B' and couples with the surface of the shell in the vicinity of point B', then goes with speed of c_{gl} along a ray path B'E C' that lies along the periphery of the shell. Finally travels to D' with speed c straight along the path C'D'. This is the case of "creeping wave". For $c_l < c$, a "trapped wave" exist where the wave is tunnelling into the shell in the form of an evanescent wave as indicated by the rays A"B"E C"D" in Fig.7a. The terminology is that of Ho and Felsen[21]. For both cases, the incident angle is taken to be $\pi/2$. The applicability of Eq.(5.1b) to steady state scattering from thin shells was recently demonstrated by Sun and Marston[19]. Inspection of Fig.9 shows that $c_l < c$ for the a_o' wave which exhibits "trapped" wave behavior at low frequencies becoming "creeping wave" like as ka is increased above ≈ 40.

Consider now the implication of Fig.7a to the scattering of tone bursts. The arrival time of the burst follows from the inspection of Fig.7a. Since $\theta_l = \pi/2$ for creeping and trapped waves the time delay of a_o' wave τ_d relative to the specular reflection in terms of the dimensionless time interval can be approximated as

$$\tau_d = (1 + \pi c / c_{gl} + 1), \tag{5.4}$$

where the actual time delay is $t_d = \tau_d a/c$. Fig.10 states that the group velocity for a_o' is close to and a little bit bigger than c. In the region of $34<x<62$, $c_{gl}/c \approx 1.38$-1.03, which corresponds to a τ_d value of 4.28 - 5.05. The property of c_l and c_{gl} for a_o' wave was

found to be common to other thin shells and hence the above analysis should also apply to the general arrival time of the a_0' wave burst for the 5%-thick SS440c shell. We see that this simple approximation agrees with our previous observation in Fig.6.

To further test the validity of this ray model and investigate the backscattering under the mid-frequency enhancement condition, we have made the computations for the backscattering of bursts with various carrier frequencies. Since the available ray method calculation by Sun is for the case of a 2.5% - thick SS304 shell, the same parameters were chosen and listed in table 3. The carrier frequencies picked up were ka =34, 38, 42, 46, 50, 54, 58, 62. In order to measure the correct amplitude for the transient waves the incident burst has to be long enough so that the near steady state response can be achieved before the signal turns off. On the other hand, it could not be too long, otherwise additional echoes would come in and make the measurement impossible. The establishment of the steady state response has turned out to be slow; as a compromise, a 20-cycle burst was finally chosen. The calculated transient backscattering are depicted in Fig.11. For each case, the amplitude of this particular type of wave relative to the specular echo were measured by looking at the data presented in Table 4 and averaging the closest four maximum values highlighted by the rectangular boxes. Table 5 provides the predicted amplitude value by the ray model and that of present calculation for each ka value we picked up. The amplitude measured from the transient backscattering is depicted by the stars in Fig.12 where the ray model calculation has been drawn as a solid line in the same figure for comparison. The ray model calculation was based on the following equation

$$|f_{l=a_0,m=0}| = 8\pi\beta_l\frac{c}{c_l}\exp(-\beta_l\pi), \tag{5.5}$$

where m = 0 indicates that the contribution is only due to the first radiation after circumnavigating half the circle which is suitable to compare with the transient

Material	ρ (g/cm^3)	c_l (km/s)	c_s (km/s)
SS304	7.570	5.675	3.141
Water	1.00	1.479	

Table 3. Material parameters for stainless steel 304 shell and water.

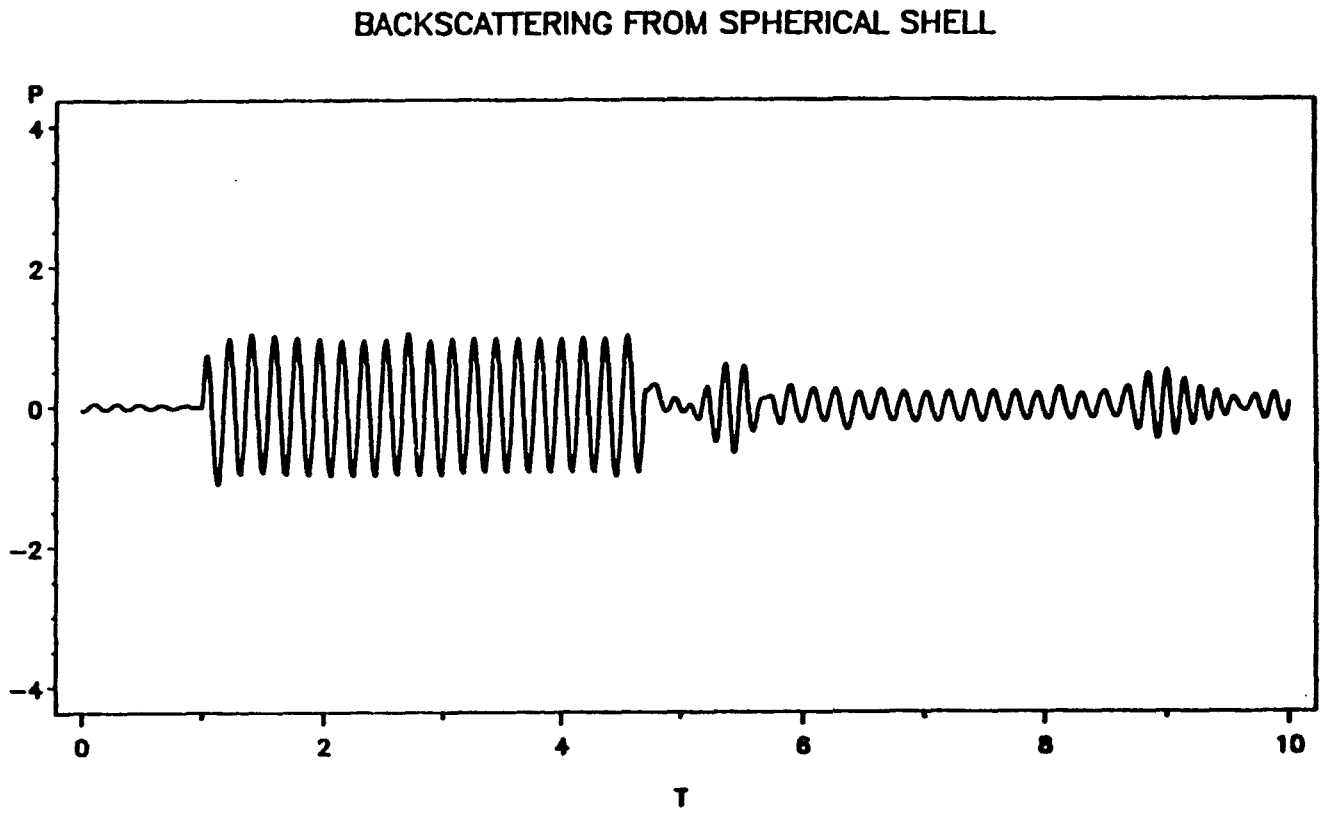

Fig.11a. Computational backscattering from a 2.5%-thick SS304 shell for a 20-cycle sine burst with $x_0 = 34.0$.

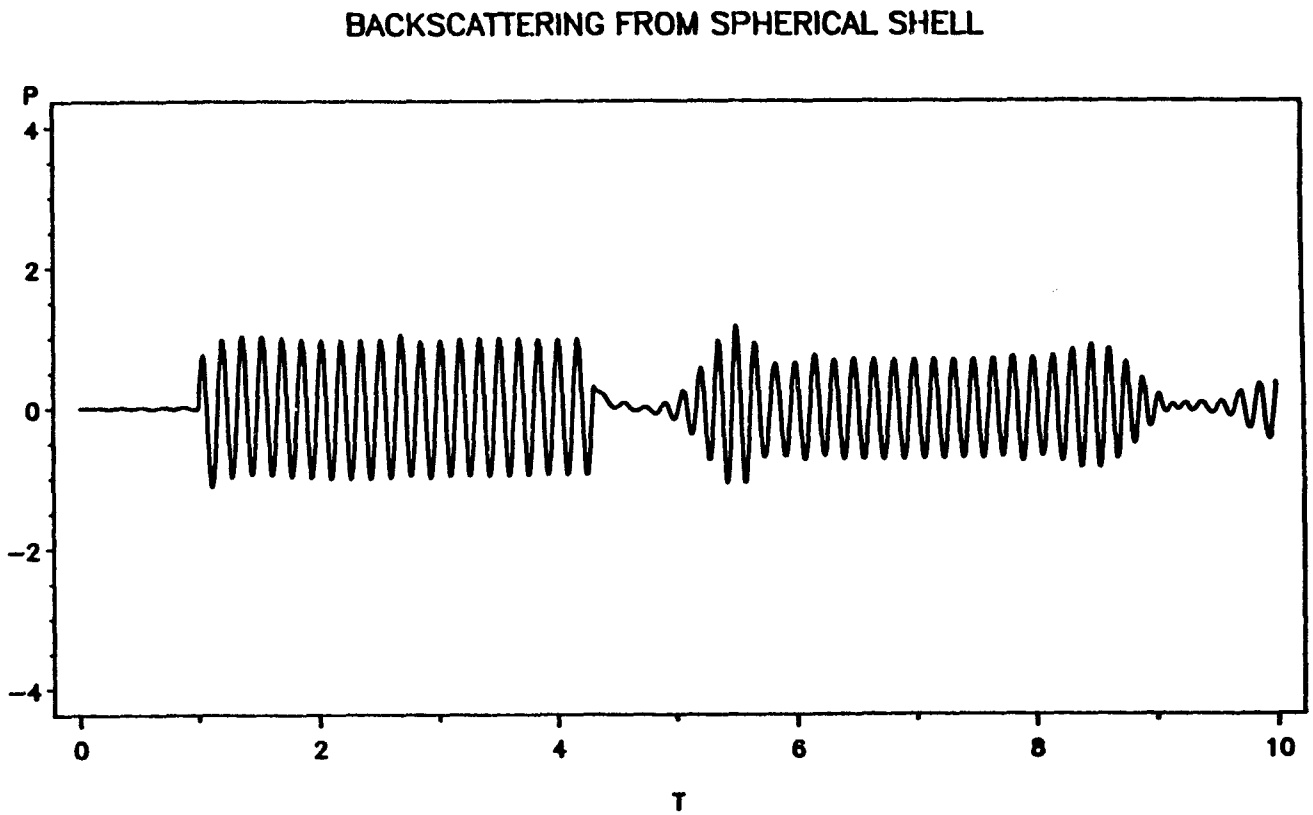

Fig.11b. Computational backscattering from a 2.5%-thick SS304 shell for a 20-cycle sine burst with $x_0 = 38.0$.

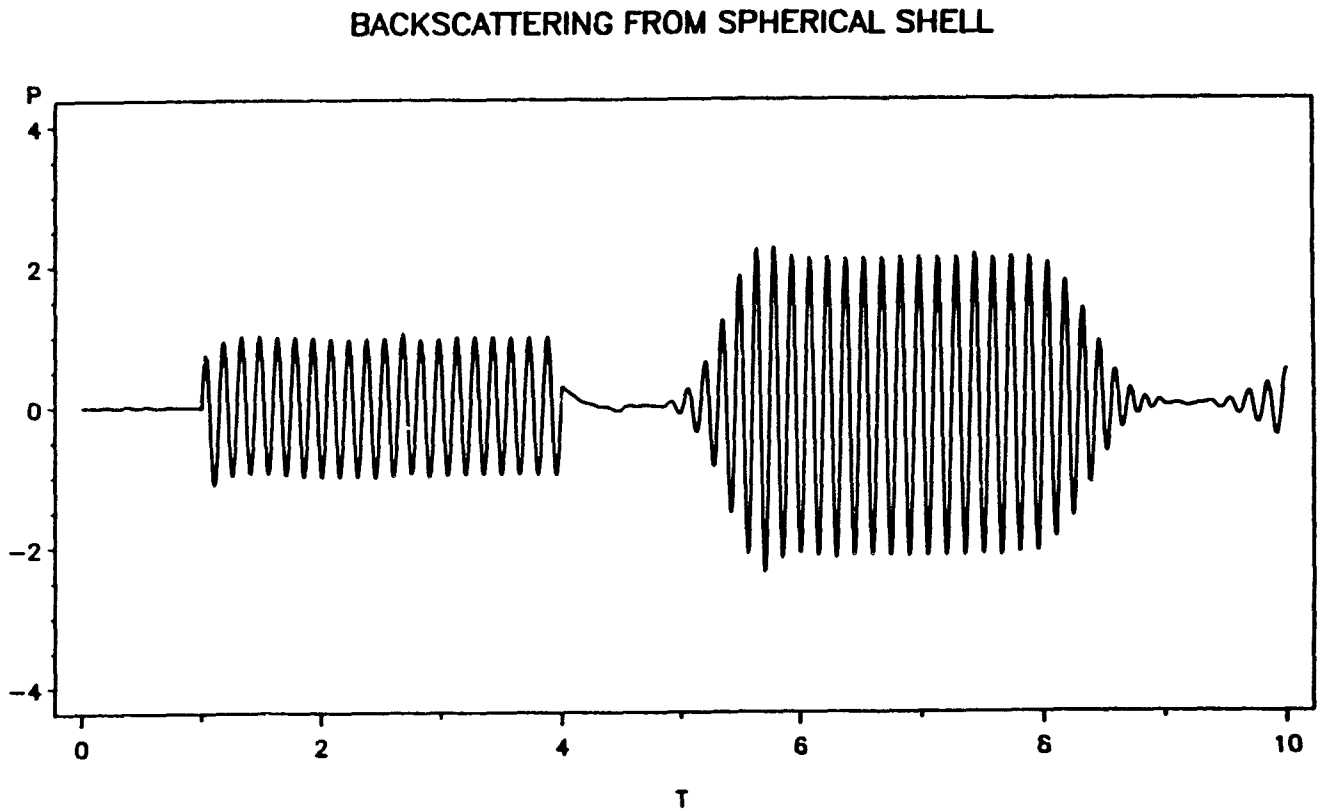

Fig.11c. Computational backscattering from a 2.5%-thick SS304 shell for a 20-cycle sine burst with $x_0 = 42.0$.

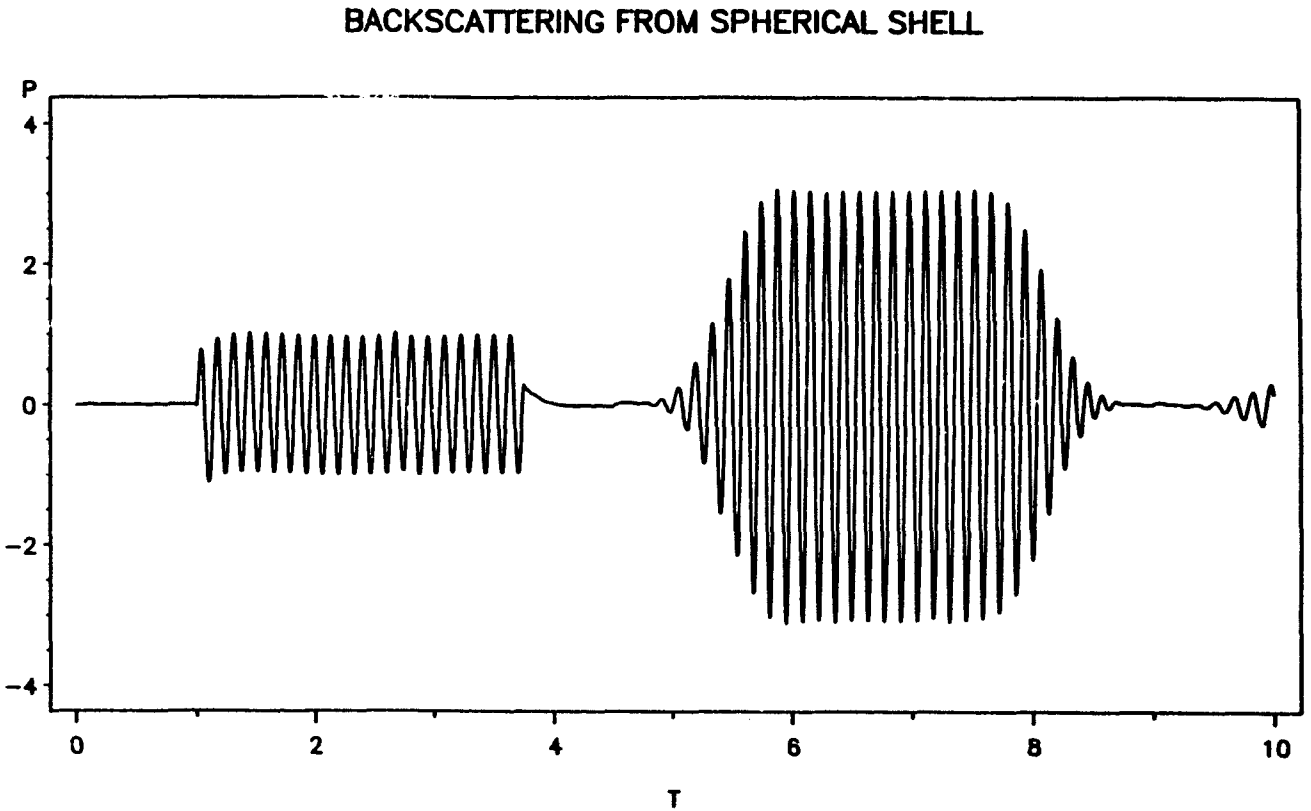

Fig.11d. Computational backscattering from a 2.5%-thick SS304 shell for a 20-cycle sine burst with $x_O = 46.0$.

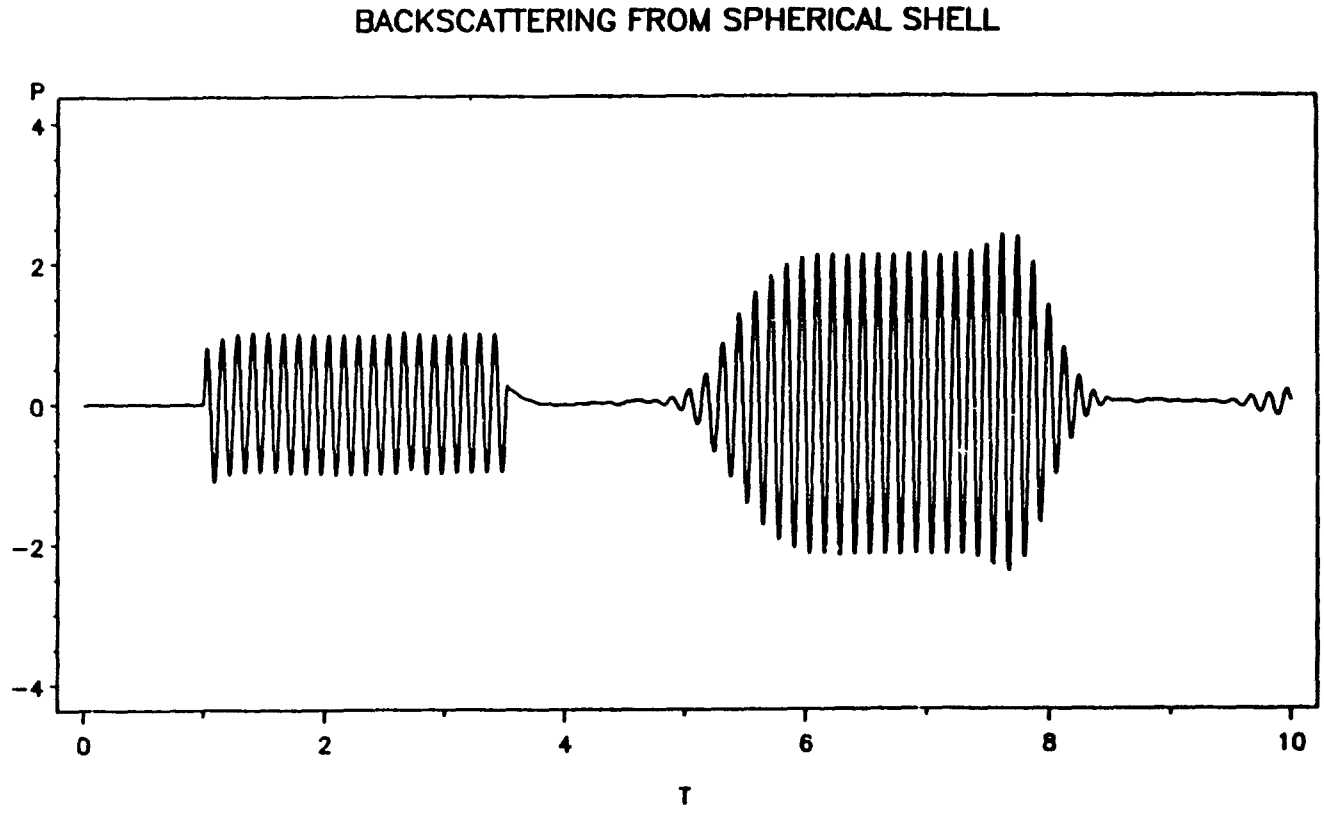

Fig. 11e. Computational backscattering from a 2.5%-thick SS304 shell for a 20-cycle sine burst with $x_0 = 50.0$.

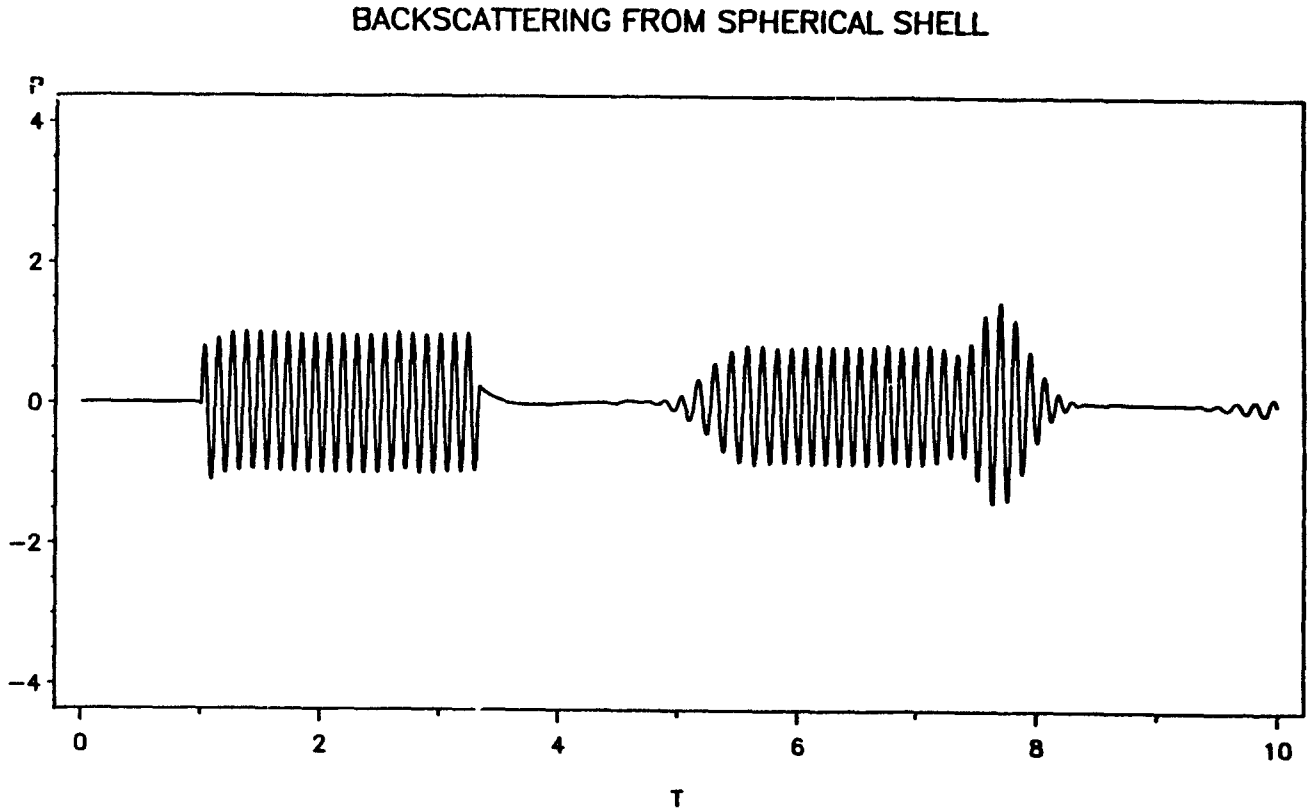

Fig.11f. Computational backscattering from a 2.5%-thick SS304 shell for a 20-cycle sine burst with $x_O = 54.0$.

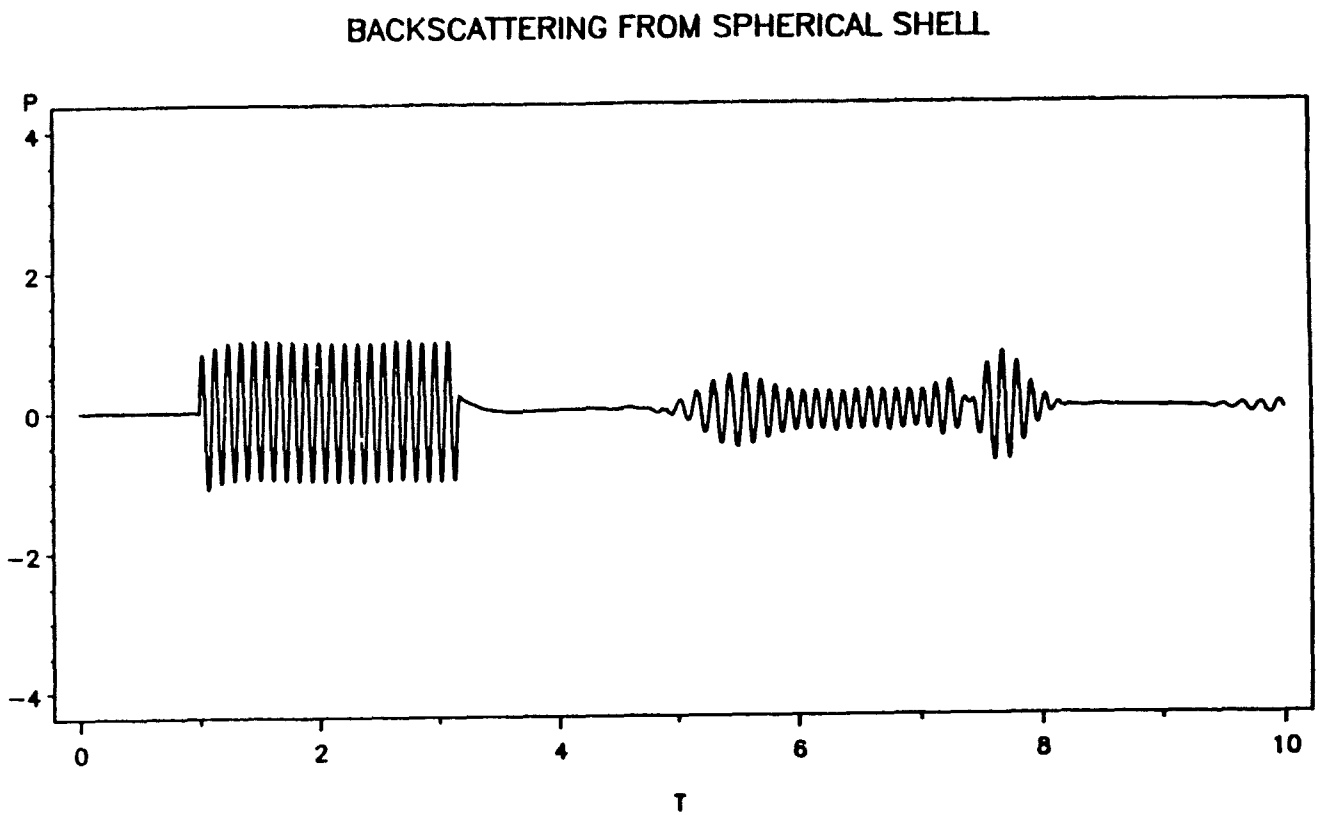

Fig.11g. Computational backscattering from a 2.5%-thick SS304 shell for a 20-cycle sine burst with $x_o = 58.0$.

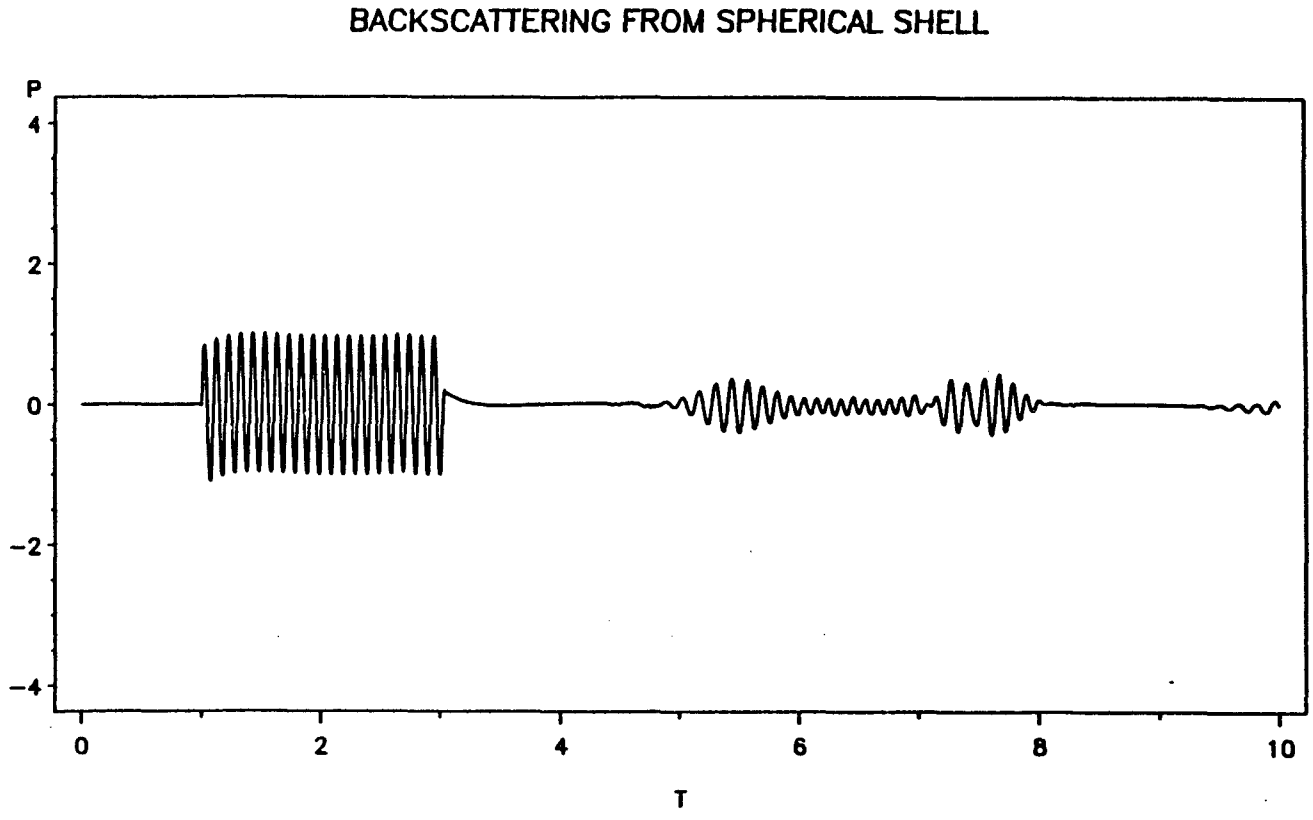

Fig.11h. Computational backscattering from a 2.5%-thick SS304 shell for a 20-cycle sine burst with $x_O = 62.0$.

T	P	T	P
6.596870	0.036035	6.606110	0.111537
6.615349	0.159312	6.624588	0.209079
6.633827	0.235192	6.643066	0.232162
6.652306	0.223170	6.661545	0.178535
6.670784	0.126900	6.680023	0.062583
6.689262	-0.012010	6.698502	-0.075965
6.707741	-0.142101	6.716980	-0.184319
6.726219	-0.216449	6.735458	-0.222948
6.744698	-0.208140	6.753937	-0.178558
6.763176	-0.123631	6.772415	-0.068047
6.781654	0.002376	6.790894	0.064782
6.800133	0.122427	6.809372	0.166800
6.818611	0.191209	6.827850	0.198699
6.837090	0.181139	6.846329	0.148974
6.855568	0.095020	6.864807	0.036073
6.874046	-0.034133	6.883286	-0.098084
6.892525	-0.157116	6.901764	-0.202599
6.911003	-0.227852	6.920242	-0.237273
6.929482	-0.219966	6.938721	-0.188992
6.947960	-0.136223	6.957199	-0.076677
6.966438	-0.007875	6.975677	0.056634
6.984917	0.116522	6.994156	0.160240
7.003395	0.189328	7.012634	0.194753
7.021873	0.182232	7.031113	0.147074
7.040352	0.097537	7.049591	0.035587
7.058830	-0.032350	7.068069	-0.096843
7.077309	-0.157209	7.086548	-0.199349
7.095787	-0.228534	7.105026	-0.232535
7.114265	-0.218630	7.123505	-0.183318
7.132744	-0.131329	7.141983	-0.069772
7.151222	-0.000209	7.160461	0.065476
7.169701	0.124636	7.178940	0.171080
7.188179	0.195974	7.197418	0.206602
7.206657	0.187360	7.215897	0.158368
7.225136	0.102800	7.234375	0.044973
7.243614	-0.025200	7.252853	-0.089960
7.262093	-0.148125	7.271332	-0.194823
7.280571	-0.219536	7.289810	-0.229761
7.299049	-0.212095	7.308289	-0.181532
7.317528	-0.127805	7.326767	-0.068328

Table 4.1 Data for backscattered wave under coincident condition with $x_o = 34.0$.

T	P	T	P
6.365273	-0.023188	6.373540	-0.238160
6.381806	-0.439772	6.390073	-0.597940
6.398339	-0.706256	6.406606	-0.741619
6.414872	-0.700890	6.423139	-0.604760
6.431405	-0.446606	6.439672	-0.246643
6.447938	-0.021616	6.456204	0.203273
6.464471	0.399340	6.472737	0.564193
6.481004	0.670664	6.489270	0.705618
6.497537	0.672829	6.505803	0.571213
6.514070	0.416703	6.522336	0.212836
6.530602	-0.011839	6.538869	-0.232127
6.547135	-0.438064	6.555402	-0.600266
6.563668	-0.707348	6.571935	-0.743429
6.580201	-0.713637	6.588468	-0.615201
6.596734	-0.455063	6.605000	-0.257137
6.613267	-0.034457	6.621533	0.188746
6.629800	0.393084	6.638066	0.553324
6.646333	0.658783	6.654599	0.699054
6.662866	0.665960	6.671132	0.565667
6.679399	0.410796	6.687665	0.209122
6.695931	-0.012120	6.704198	-0.236750
6.712464	-0.437461	6.720731	-0.602479
6.728997	-0.705638	6.737264	-0.745843
6.745530	-0.713730	6.753797	-0.614909
6.762063	-0.457097	6.770329	-0.258647
6.778596	-0.036101	6.786862	0.187598
6.795129	0.390068	6.803395	0.551739
6.811662	0.659242	6.819928	0.697035
6.828195	0.667313	6.836461	0.568729
6.844728	0.413183	6.852994	0.214244
6.861260	-0.005725	6.869527	-0.229921
6.877793	-0.431122	6.886060	-0.593886
6.894326	-0.699590	6.902593	-0.740077
6.910859	-0.707751	6.919126	-0.611882
6.927392	-0.453401	6.935658	-0.257104
6.943925	-0.033302	6.952191	0.188291
6.960458	0.393116	6.968724	0.554449
6.976991	0.662974	6.985257	0.702523
6.993524	0.672867	7.001790	0.577343
7.010056	0.419696	7.018323	0.222881
7.026589	0.002894	7.034856	-0.220533
7.043122	-0.426468	7.051389	-0.587425
7.059655	-0.694408	7.067922	-0.734579

Table 4.2 Data for backscattered wave under coincident condition with $x_0 = 38.0$.

T	P	T	P
6.350278	0.559239	6.357758	1.161832
6.365237	1.646473	6.372717	1.967741
6.380197	2.097844	6.387676	2.019434
6.395156	1.732595	6.402636	1.275286
6.410115	0.689955	6.417595	0.042314
6.425075	-0.617974	6.432554	-1.220983
6.440034	-1.708334	6.447514	-2.024584
6.454993	-2.145013	6.462473	-2.060061
6.469953	-1.777786	6.477432	-1.320424
6.484912	-0.730696	6.492392	-0.079298
6.499871	0.582484	6.507351	1.179777
6.514831	1.670031	6.522310	1.985994
6.529790	2.108430	6.537270	2.020617
6.544749	1.737244	6.552229	1.280616
6.559709	0.691401	6.567188	0.039001
6.574668	-0.622499	6.582148	-1.221521
6.589627	-1.709781	6.597107	-2.025415
6.604587	-2.147242	6.612066	-2.060807
6.619546	-1.774627	6.627026	-1.316886
6.634505	-0.727802	6.641985	-0.075336
6.649465	0.585943	6.656944	1.189285
6.664424	1.671964	6.671904	1.991014
6.679383	2.109529	6.686863	2.026320
6.694343	1.737120	6.701822	1.275133
6.709302	0.690124	6.716782	0.034059
6.724261	-0.627559	6.731741	-1.234824
6.739221	-1.717731	6.746700	-2.035459
6.754180	-2.158458	6.761660	-2.069981
6.769139	-1.785295	6.776619	-1.325667
6.784099	-0.735967	6.791578	-0.078363
6.799058	0.587846	6.806538	1.188315
6.814017	1.675397	6.821497	1.995219
6.828977	2.116850	6.836456	2.034254
6.843936	1.746574	6.851416	1.286531
6.858895	0.699010	6.866375	0.039062
6.873855	-0.623633	6.881334	-1.229516
6.888814	-1.714690	6.896294	-2.033982
6.903773	-2.160228	6.911253	-2.072351
6.918733	-1.788444	6.926212	-1.330139
6.933692	-0.741370	6.941172	-0.084951
6.948651	0.580860	6.956131	1.187328
6.963611	1.674013	6.971090	1.997989
6.978570	2.120455	6.986050	2.036927
6.993529	1.750979	7.001009	1.290996

Table 4.3 Data for backscattered wave under coincident condition with $x_0 = 42.0$.

T	P	T	P
6.597102	-0.025907	6.603931	-0.973626
6.610761	-1.825780	6.617590	-2.503560
6.624419	-2.936231	6.631248	-3.079511
6.638078	-2.929365	6.644907	-2.493511
6.651736	-1.812736	6.658566	-0.959201
6.665395	-0.012516	6.672224	0.933062
6.679053	1.785619	6.685883	2.464755
6.692712	2.897599	6.699541	3.043399
6.706370	2.893751	6.713200	2.455397
6.720029	1.773091	6.726858	0.918041
6.733687	-0.031260	6.740517	-0.978651
6.747346	-1.832103	6.754175	-2.510407
6.761004	-2.942909	6.767834	-3.089663
6.774663	-2.939170	6.781492	-2.501066
6.788321	-1.819549	6.795151	-0.964964
6.801980	-0.016426	6.808809	0.932137
6.815639	1.786369	6.822468	2.464557
6.829297	2.899034	6.836126	3.047814
6.842956	2.897290	6.849785	2.459860
6.856614	1.779217	6.863443	0.924893
6.870273	-0.024116	6.877102	-0.973685
6.883931	-1.826900	6.890760	-2.505418
6.897590	-2.941862	6.904419	-3.089979
6.911248	-2.938947	6.918077	-2.503733
6.924907	-1.823455	6.931736	-0.967920
6.938565	-0.020529	6.945395	0.928623
6.952224	1.783107	6.959053	2.461402
6.965882	2.898016	6.972712	3.047017
6.979541	2.896656	6.986370	2.462214
6.993199	1.782508	7.000029	0.927581
7.006858	-0.018170	7.013687	-0.966861
7.020516	-1.820955	7.027346	-2.497132
7.034175	-2.933331	7.041004	-3.032415
7.047833	-2.930409	7.054663	-2.495530
7.061492	-1.816685	7.068321	-0.960380
7.075150	-0.013899	7.081980	0.934126
7.088809	1.790331	7.095638	2.468091
7.102468	2.904951	7.109297	3.057021
7.116126	2.907706	7.122955	2.474592
7.129785	1.799615	7.136614	0.947236

Table 4.4 Data for backscattered wave under coincident condition with $x_O = 46.0$.

T	P	T	P
6.504855	0.011539	6.509044	-0.436678
6.513232	-0.867708	6.517421	-1.262138
6.521609	-1.602292	6.525798	-1.873637
6.529986	-2.064192	6.534175	-2.164548
6.538363	-2.169625	6.542552	-2.080113
6.546741	-1.901734	6.550929	-1.643118
6.555118	-1.314392	6.559306	-0.927864
6.563495	-0.499779	6.567683	-0.050313
6.571872	0.399248	6.576060	0.829382
6.580249	1.222500	6.584437	1.561802
6.588626	1.831941	6.592814	2.021164
6.597003	2.121951	6.601192	2.129898
6.605380	2.043390	6.609569	1.865207
6.613757	1.603903	6.617946	1.272740
6.622134	0.886852	6.626323	0.461651
6.630511	0.013940	6.634700	-0.436558
6.638888	-0.868439	6.643077	-1.262070
6.647265	-1.601197	6.651454	-1.871750
6.655643	-2.061283	6.659831	-2.161029
6.664020	-2.167546	6.668208	-2.081394
6.672397	-1.905348	6.676585	-1.645490
6.680774	-1.313410	6.684962	-0.925579
6.689151	-0.500037	6.693339	-0.054200
6.697528	0.394307	6.701716	0.826047
6.705905	1.220548	6.710093	1.559359
6.714282	1.828331	6.718471	2.017086
6.722659	2.117488	6.726848	2.124104
6.731036	2.036243	6.735225	1.858479
6.739413	1.598993	6.743602	1.268452
6.747790	0.880678	6.751979	0.453133
6.756167	0.005424	6.760356	-0.442877
6.764544	-0.873113	6.768733	-1.267176
6.772922	-1.607440	6.777110	-1.877936
6.781299	-2.066348	6.785487	-2.165199
6.789676	-2.171248	6.793864	-2.084203
6.798053	-1.906754	6.802241	-1.645953
6.806430	-1.313712	6.810618	-0.925399
6.814807	-0.498067	6.818995	-0.049818
6.823184	0.400200	6.827373	0.832200

Table 4.5 Data for backscattered wave under coincident condition with $x_0 = 50.0$.

T	P	T	P
6.382811	0.035442	6.386688	0.209292
6.390566	0.372359	6.394444	0.518352
6.398321	0.641011	6.402199	0.735356
6.406076	0.798002	6.409954	0.826164
6.413832	0.817231	6.417709	0.769973
6.421587	0.686021	6.425465	0.569997
6.429342	0.428413	6.433220	0.268459
6.437098	0.097275	6.440975	-0.078245
6.444853	-0.251158	6.448730	-0.414271
6.452608	-0.560668	6.456486	-0.684435
6.460363	-0.780417	6.464241	-0.843409
6.468119	-0.868711	6.471996	-0.854340
6.475874	-0.802352	6.479752	-0.717329
6.483629	-0.603766	6.487507	-0.465459
6.491385	-0.307072	6.495262	-0.135321
6.499140	0.041802	6.503017	0.216520
6.506895	0.381673	6.510773	0.530038
6.514650	0.654073	6.518528	0.747090
6.522406	0.805060	6.526283	0.827153
6.530161	0.814186	6.534039	0.766641
6.537916	0.684721	6.541794	0.570449
6.545671	0.429062	6.549549	0.267968
6.553427	0.094795	6.557304	-0.083125
6.561182	-0.258108	6.565060	-0.422186
6.568937	-0.568257	6.572815	-0.690728
6.576693	-0.784984	6.580570	-0.846725
6.584448	-0.872268	6.588326	-0.859543
6.592203	-0.808948	6.596081	-0.723501
6.599958	-0.608078	6.603836	-0.468155
6.607714	-0.309112	6.611591	-0.136769
6.615469	0.041721	6.619347	0.218022
6.623224	0.383811	6.627102	0.531717
6.630980	0.655401	6.634857	0.749476
6.638735	0.809840	6.642612	0.834087
6.646490	0.821553	6.650368	0.773008
6.654245	0.690296	6.658123	0.576243
6.662001	0.435166	6.665878	0.273601
6.669756	0.100009	6.673634	-0.077046
6.677511	-0.250588	6.681389	-0.414793
6.685266	-0.563140	6.689144	-0.687918
6.693022	-0.782125	6.696899	-0.841541
6.700777	-0.864707	6.704655	-0.851418
6.708532	-0.801931	6.712410	-0.717605
6.716288	-0.601830	6.720165	-0.460004
6.724043	-0.298634	6.727921	-0.124493

Table 4.6 Data for backscattered wave under coincident condition with $x_o = 54.0$.

T	P	T	P
6.074376	-0.004603	6.078709	-0.073365
6.083041	-0.138927	6.087374	-0.198649
6.091706	-0.247784	6.096039	-0.281372
6.100371	-0.297811	6.104704	-0.298039
6.109036	-0.281832	6.113369	-0.247893
6.117702	-0.197849	6.122034	-0.137058
6.126367	-0.070412	6.130699	-0.000069
6.135032	0.071267	6.139364	0.137669
6.143697	0.192945	6.148029	0.234435
6.152362	0.261705	6.156694	0.273110
6.161027	0.266137	6.165359	0.240549
6.169692	0.199254	6.174025	0.146085
6.178357	0.083878	6.182690	0.015065
6.187022	-0.056422	6.191355	-0.124831
6.195687	-0.184968	6.200020	-0.234247
6.204352	-0.271104	6.208685	-0.292394
6.213017	-0.294801	6.217350	-0.278369
6.221683	-0.245890	6.226015	-0.199158
6.230348	-0.138985	6.234680	-0.068894
6.239013	0.004546	6.243345	0.075609
6.247678	0.140881	6.252010	0.196614
6.256343	0.237589	6.260675	0.259815
6.265008	0.262724	6.269341	0.247984
6.273673	0.217343	6.278006	0.172367
6.282338	0.115705	6.286671	0.051692

Table 4.7 Data for backscattered wave under coincident condition with $x_0 = 58.0$.

T	P	T	P
5.962266	-0.015721	5.966319	-0.047572
5.970372	-0.077883	5.974425	-0.103375
5.978478	-0.122413	5.982532	-0.135460
5.986585	-0.143257	5.990638	-0.145075
5.994691	-0.139266	5.998744	-0.125686
6.002797	-0.106693	6.006850	-0.084866
6.010903	-0.060525	6.014956	-0.033032
6.019010	-0.003971	6.023063	0.023066
6.027116	0.045946	6.031169	0.065132
6.035222	0.080809	6.039275	0.090985
6.043328	0.093645	6.047381	0.089184
6.051435	0.079337	6.055488	0.064762
6.059541	0.045096	6.063594	0.020878
6.067647	-0.005789	6.071700	-0.032454
6.075753	-0.057588	6.079806	-0.080598
6.083859	-0.100811	6.087913	-0.116554
6.091966	-0.125670	6.096019	-0.127319
6.100072	-0.122697	6.104125	-0.113186
6.108178	-0.098435	6.112231	-0.077523
6.116284	-0.051724	6.120337	-0.024494
6.124391	0.001606	6.128444	0.026482
6.132497	0.050305	6.136550	0.071073
6.140603	0.085678	6.144656	0.092797
6.148709	0.093451	6.152762	0.088778
6.156816	0.078462	6.160869	0.061804
6.164922	0.039610	6.168975	0.014311

Table 4.8 Data for backscattered wave under coincident condition with $x_0 = 62.0$.

x	Amplitude by ray model	Amplitude by modified ray model	Amplitude by PWS
34.0	0.169133	0.140835	0.2158
38.0	0.768413	0.667904	0.7213
42.0	2.132889	1.919801	2.1363
46.0	3.167944	2.930751	3.0686
50.0	2.394250	2.260151	2.1482
54.0	1.088952	1.041594	0.8506
58.0	0.433748	0.418051	0.2822
62.0	0.195738	0.189482	0.1149

Table 5. The amplitudes of a_0' wave for SS304 shell by ray methods and PWS calculation.

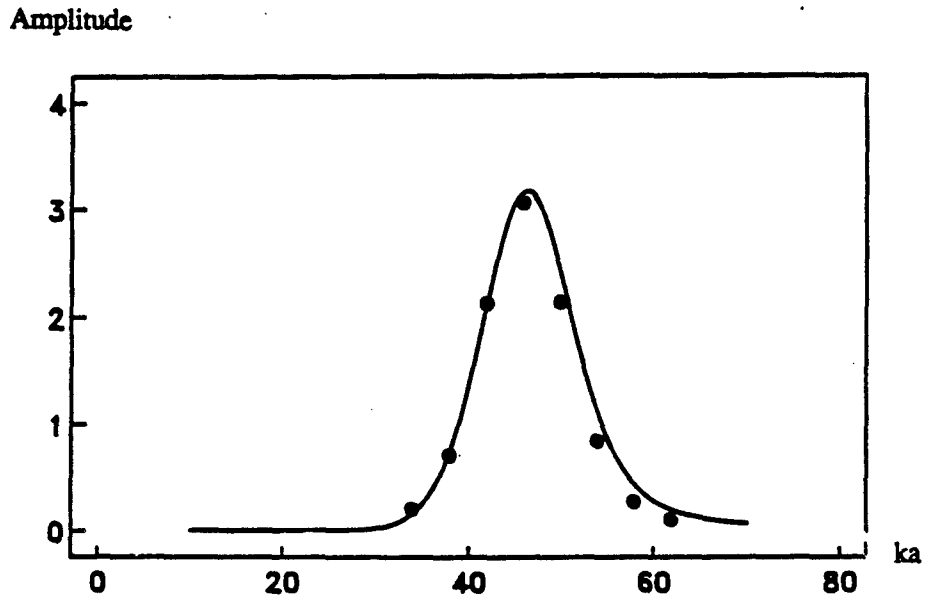

Fig.12a. Comparison of the amplitude for the ray model and PWS calculation. The solid curve is for the ray model calculation which is based on the Eq.(5.5); while the dots are for the PWS computation.

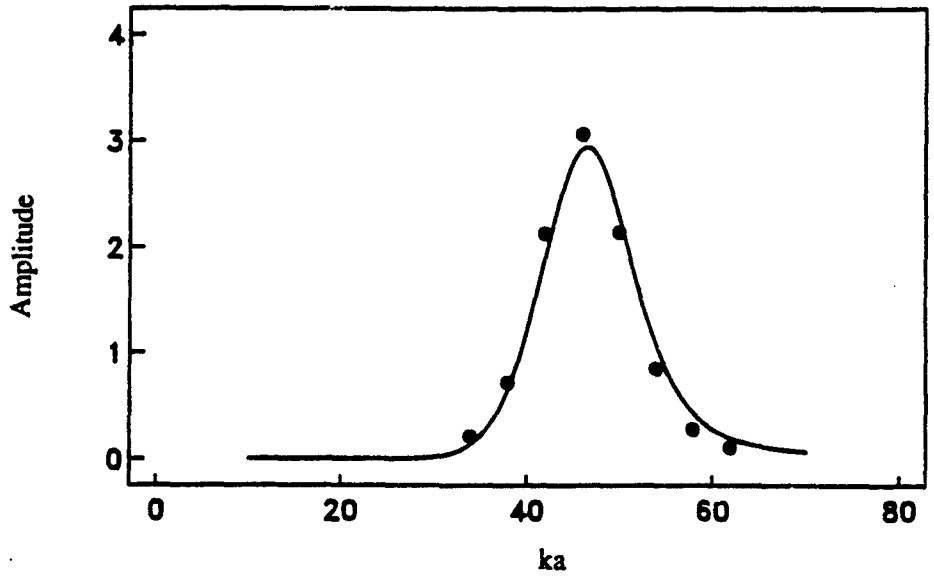

Fig.12b. Comparison of the amplitude for the ray model and PWS calculation. The solid curve is for the ray model calculation which is based on a modification to Eq.(5.5) in which c/c_l is omitted; while the dots are for the PWS computation. Comparison of Fig.12a and 12b shows that the exact ray model is somewhere between these two.

computations. The large second echo visible in Fig.11d is seen to be the contribution from the a_0' ray which has circumnavigated only the backside of the shell. Excellent agreement of the results in terms of this simple calculation is a manifestation of the validity of the ray model. Of course, s_0 can still be seen especially in the case of short bursts where we have more low frequency components as presented in the appendix A. In addition, the overlap of weak a_0 wave on a_0' can also be seen at high frequencies.

5.4 Reverberations of longitudinal waves and resonance scattering--fluid shells

Next, we turn our attention to the resonance backscattering of shells. Consider the longitudinal resonance conditions[11,20]

$$k_L h = n\pi \qquad (n = 1,2,...) \tag{5.6}$$

$$k_L h = (n+1/2)\pi \qquad (n = 0,1,...) \ , \tag{5.7}$$

where h is the thickness of the shell. These conditions are obtained from the requirement of constructive interference of consecutive internally reflected waves upon transmission back into the water. These reflections are shown in Fig.7b. Eq.(5.6) corresponds to the usual case considered here where the acoustic impedance of the elastic material $\rho_e c_l$ is greater than the impedance of the water ρc while Eq.(5.7) is valid for the case where $\rho_e c_l$ is less than ρc. First assume an ideal fluid shell whose physical constants are the same as the real aluminum shell (to be called aluminum/fluid shell) and are listed in Table 6b. By investigating such an ideal object, we are able to get rid of the effects due to elastic surface waves and transverse waves and concentrate on the longitudinal resonance echoes. The

Material	ρ (g/cm^3)	c_l (km/s)	c_s (km/s)
Aluminum	2.70	6.42	3.04
Water	1.00	1.4825	

Table 6a. Material parameters for Aluminum shell and water.

Fluid/water	ρ_e (g/cm^3)	c_l (km/s)	c (km/s)	ρ (g/cm^3)
Aluminum/water	2.70	6.42	1.4825	1.00
SS440C/water	7.84	5.854	1.479	1.00

Table 6b. Material parameters for fluid shells.

form functions of a 4%-thick aluminum/fluid shell is shown in Fig.13 for c_l = 6.42 km/s where the form function for a real aluminum shell is also plotted for comparison. Eq.(5.6) predicts a longitudinal resonance at $x_{Lr} \approx$ 340. The minimum in both cases is a manifestation of this longitudinal resonance. This dip has been modeled in detail by a ray method[11]. The cause of the large peak near x = 302 for the real aluminum shell has not been well understood yet. It has been explained as the prompt radiation in Ref.20 and described as a "thickness quasiresonance" in Ref.17. The form function for a 16.2%-thick SS440c/fluid shell is shown in Fig.14. This time Eq.(5.6) predicts a longitudinal resonance at $x_{Lr} \approx$ 76.8. Again a dip near x = 76.8 in Fig.14 corresponds to the presence of the longitudinal resonance. The computed backscattered waves for the aluminum/fluid shell at x_0 = 302 and 340 are both shown in Fig.15. Various burst lengths have been tested. Presented in Fig.15a and 15b are the case of 20-cycle burst. For reference, some additional figures are presented in the Appendix B. The results are just expected. For x_0 = 340, the decay of the echoes immediately following the specular reflection is the manifestation of a longitudinal resonance. The form function predicts a minimum amplitude of 0.17, as incident burst gets longer, the backscattered echo does reach the limit as shown in Fig.15c where a 40-cycle burst has been used. The measured amplitude is 0.17 which agree with the form function prediction and the region of measurement has been marked. We don't see anything anomalous from the x_0 = 302 plot, which demonstrates that the anomaly around x = 302 in the elastic form function is not the direct effect of the longitudinal resonance. We then computed the backscattering for the SS440c/fluid shell for x_0 = 71 and 76.8. The reason we are interested in the case of x_0 = 71 will become clear later in Section 5.5. The results are Fig.16 and again are fully expected. The decay of the echoes corresponds to the longitudinal resonance which is not responsible for any possible anomalous behavior around x = 71. As in the case of Aluminum/fluid shell, we checked the

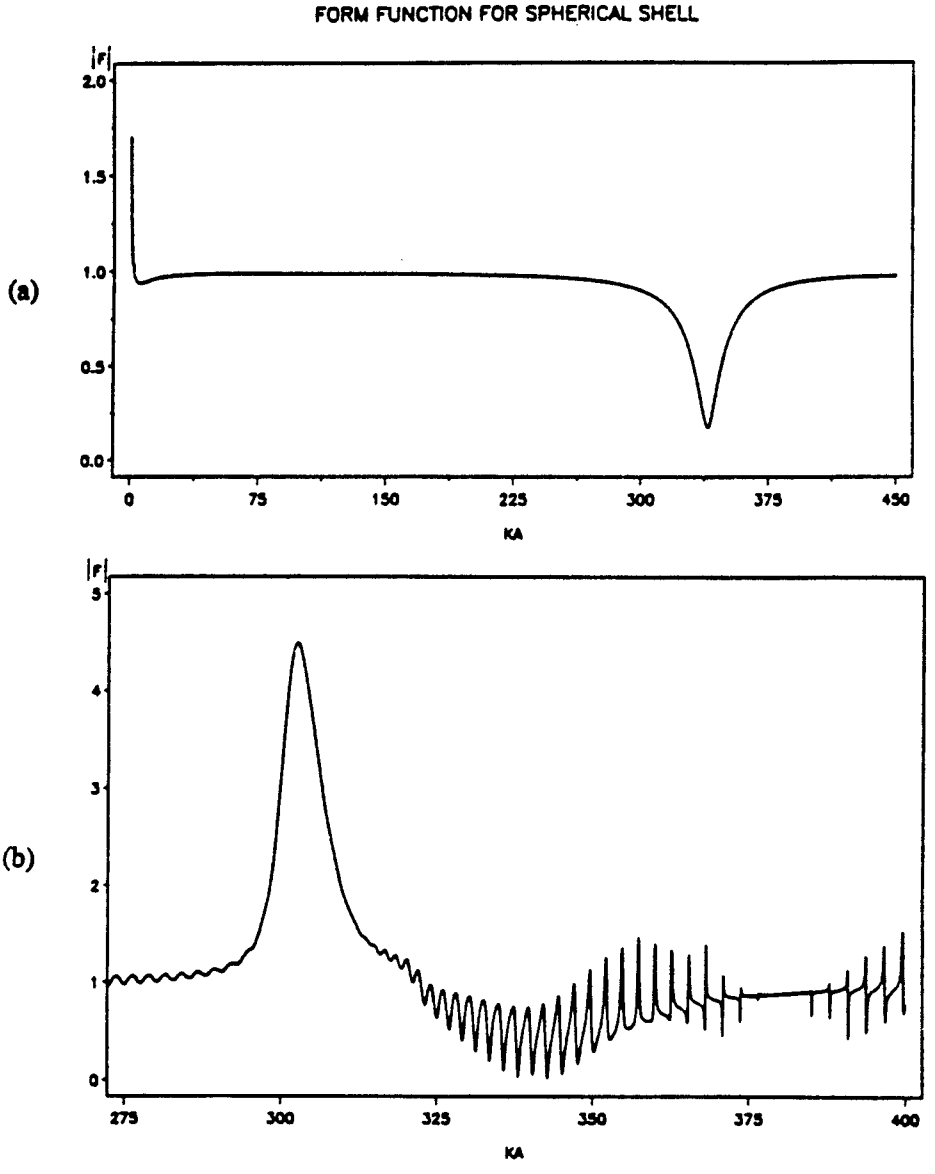

Fig.13. Form functions of 4%-thick aluminum/fluid(a) and aluminum(b) shells.

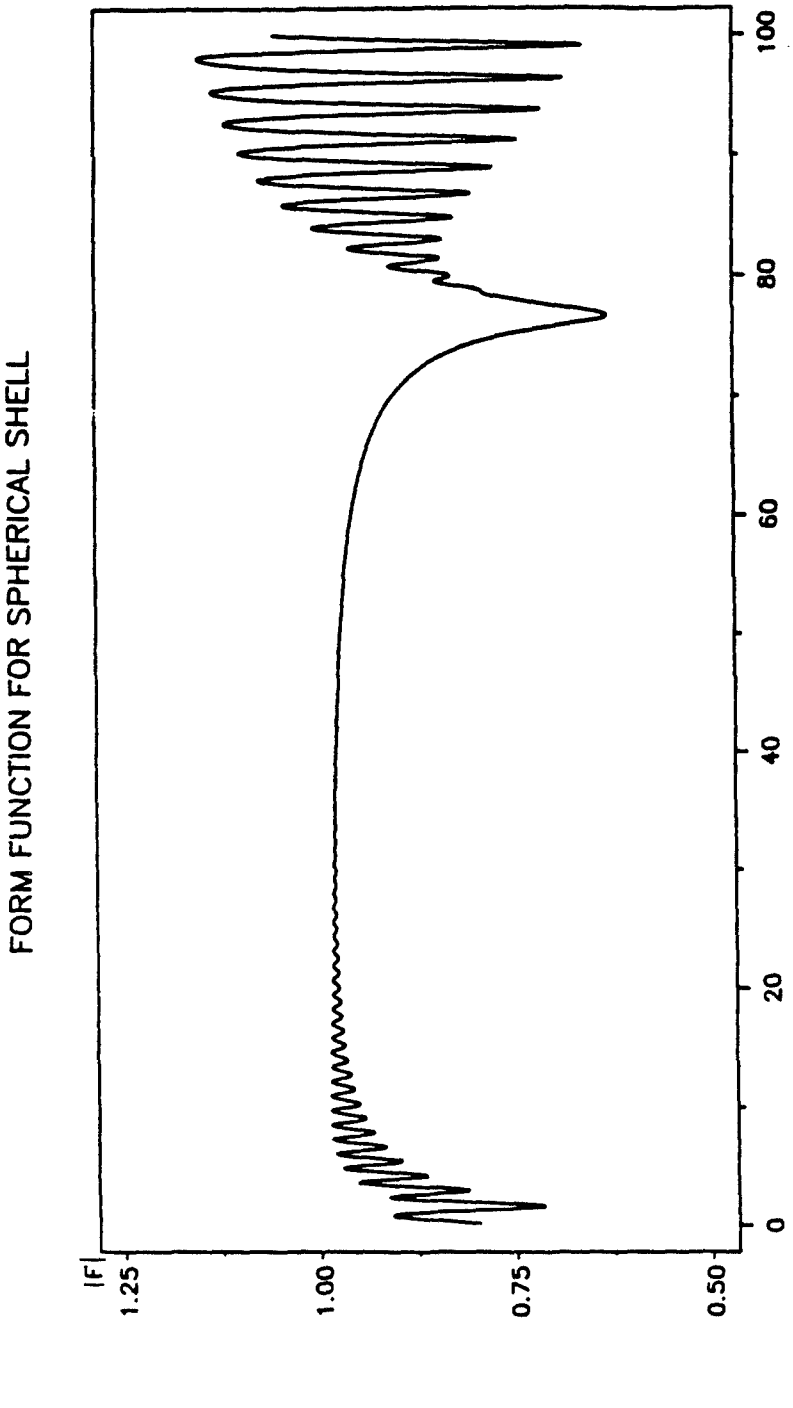

Fig.14. Form function of a 16.2%-thick SS440C/fluid shell.

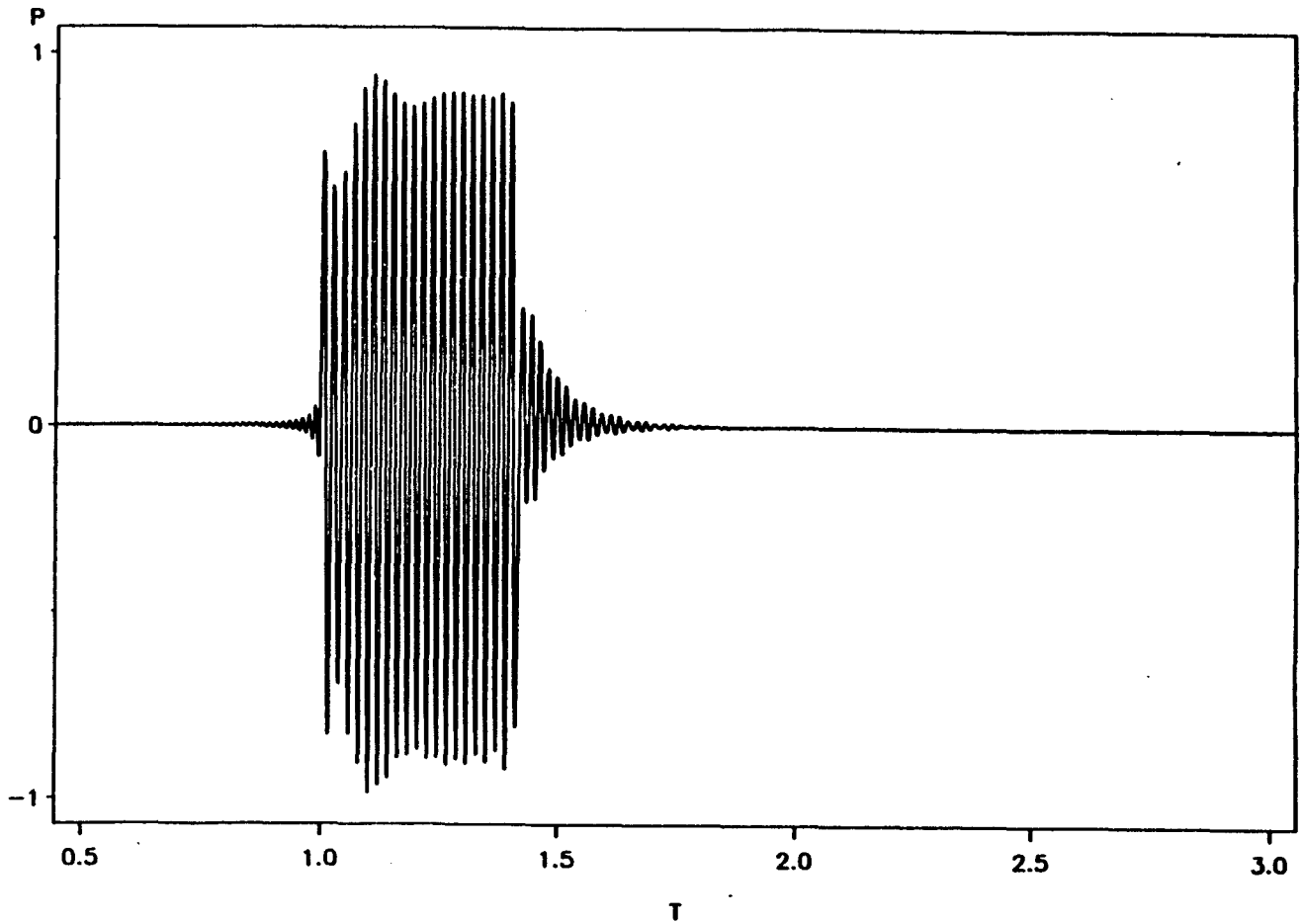

Fig.15a. Computational backscattering from a 4%-thick aluminum/fluid shell for a 20-cycle sine burst with $x_0 = 302$.

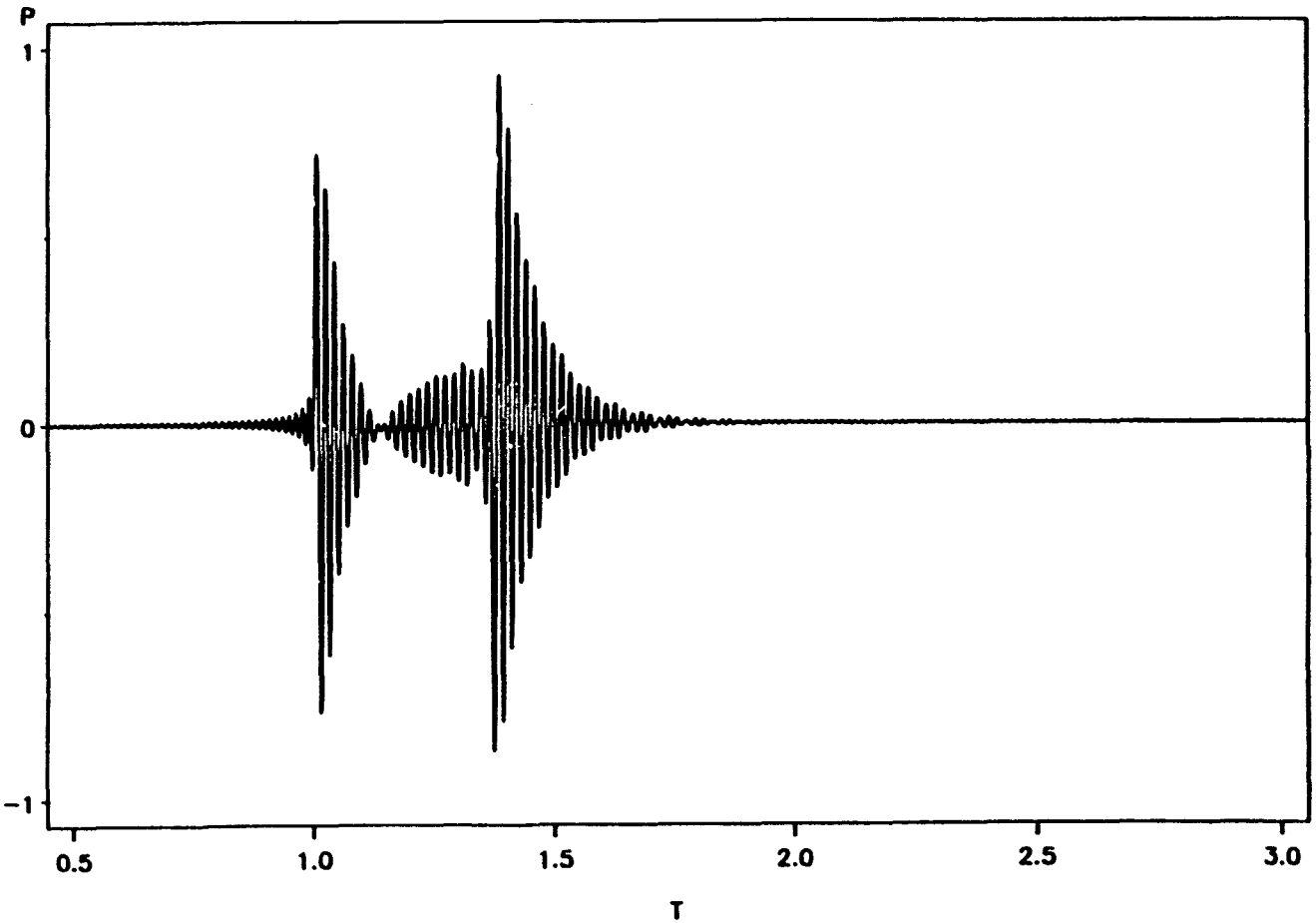

Fig.15b. Computational backscattering from a 4%-thick aluminum/fluid shell for a 20-cycle sine burst with $x_0 = 340$.

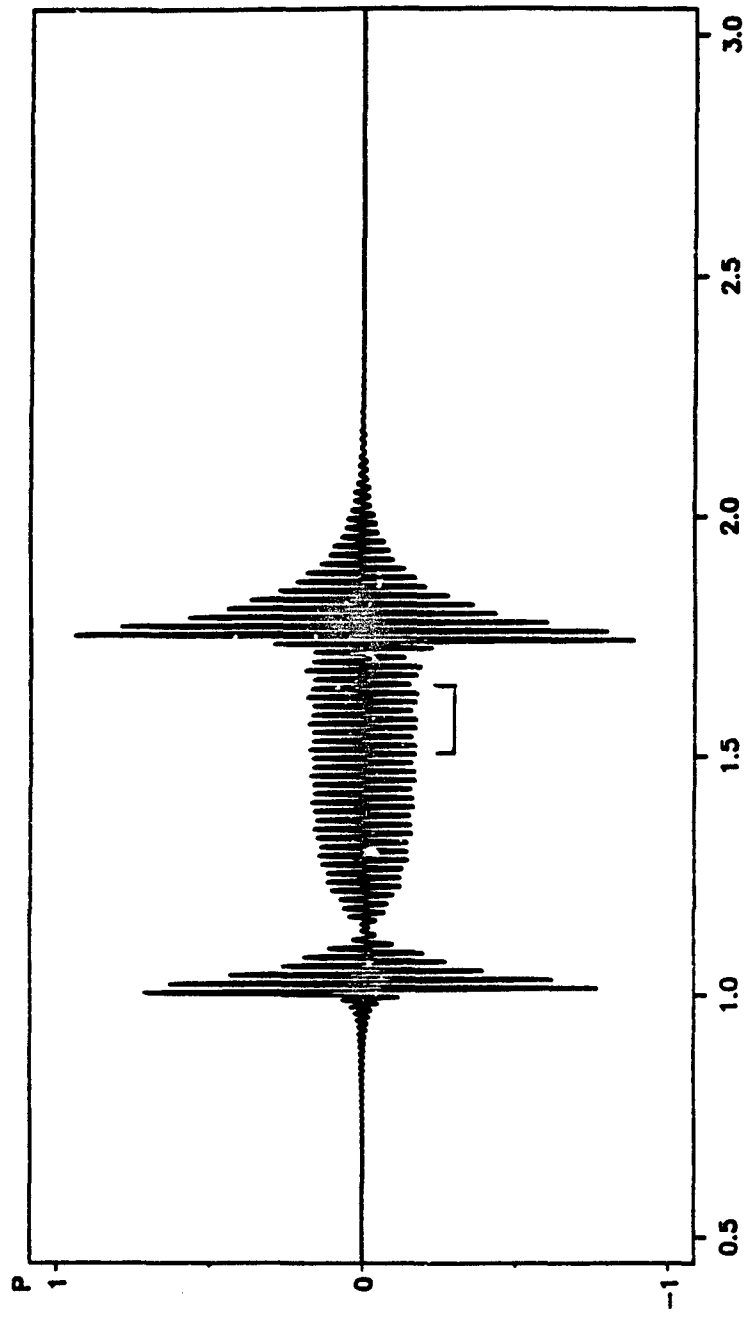

Fig.15c. Computational backscattering from a 4%-thick aluminum/fluid shell for a 40-cycle sine burst with $x_0 = 340$ The measured amplitude as marked agrees with the form function prediction.

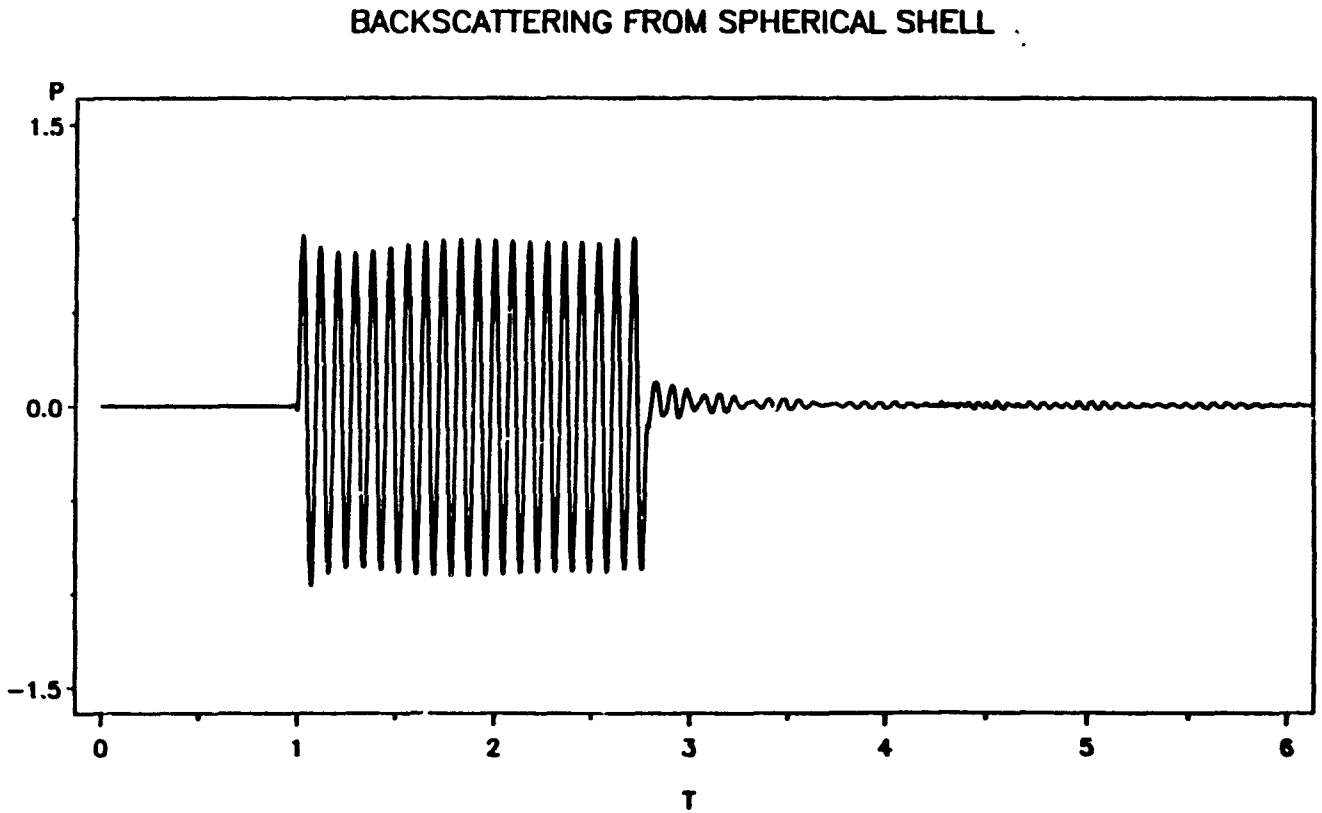

Fig.16a. Computational backscattering from a 16.2%-thick SS440C/fluid shell for a 20-cycle sine burst with $x_0 = 71.0$.

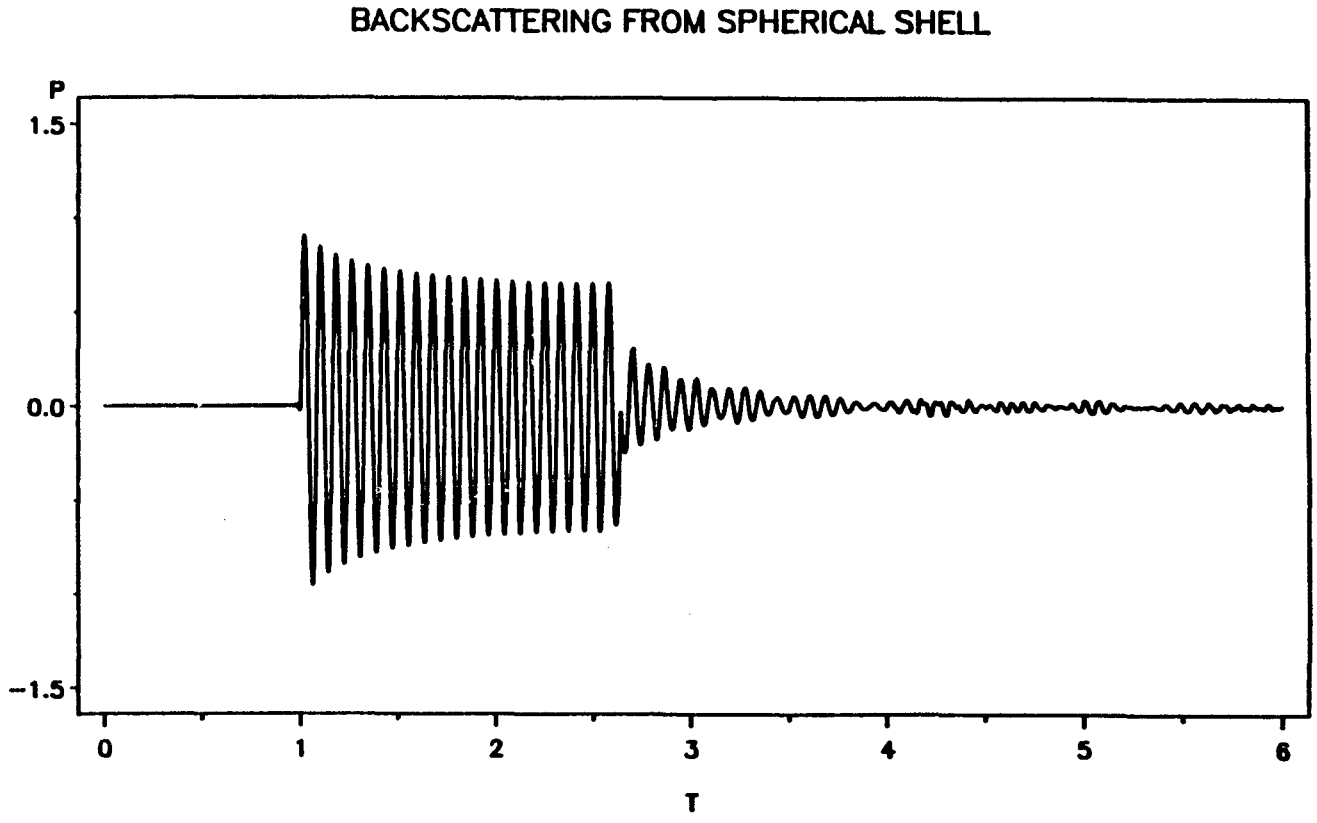

Fig.16b. Computational backscattering from a 16.2%-thick SS440C/fluid shell for a 20-cycle sine burst with $x_0 = 76.8$.

minimum amplitude which is predicted by the form function to be 0.63. The near steady state amplitude measured from Fig.16b is 0.64 which is very close to the form function prediction.

5.5 Reverberations of longitudinal waves and resonance scattering--elastic shells

Next we investigate the on resonance and below resonance backscattering for a real aluminum shell. Results for a 20-cycle incident burst for x_0 = 302 and 340 are depicted in Fig.17. The buildup and decay at the very early stage of the backscattered wave under the constructive and destructive resonance conditions are both evident. The form function predicts a maximum amplitude of 4.26 times that of the incident bursts. We do see that as input burst gets longer, the amplitude of the backscattering reaches the limit as shown in Fig.17c.

The form function calculated for the SS440c shell using the current ray model fails to recover the form function from the exact PWS calculation in the x range of 70--74 [20]. One possible cause of the anomalous behavior near x = 71 is due to the fact that the phase velocity becomes large for the s_1 Lamb wave, hence the trace-velocity matching angle θ_l defined in Eq.(5.1) becomes small and the group velocity for the s_1 Lamb wave becomes negative around x = 71. It has been suggested (P.L.Marston, private communication) that the energy of the burst is taking a short path and travelling along the path of BC in Fig.7a directly without circumnavigating the shell at all. This is one ray mechanism for producing prompt radiation, which was not included in the analysis in Ref.20. The computed backscattered waves from a real SS440C shell for x_0 = 71.0 and 76.8 are shown in Fig.18

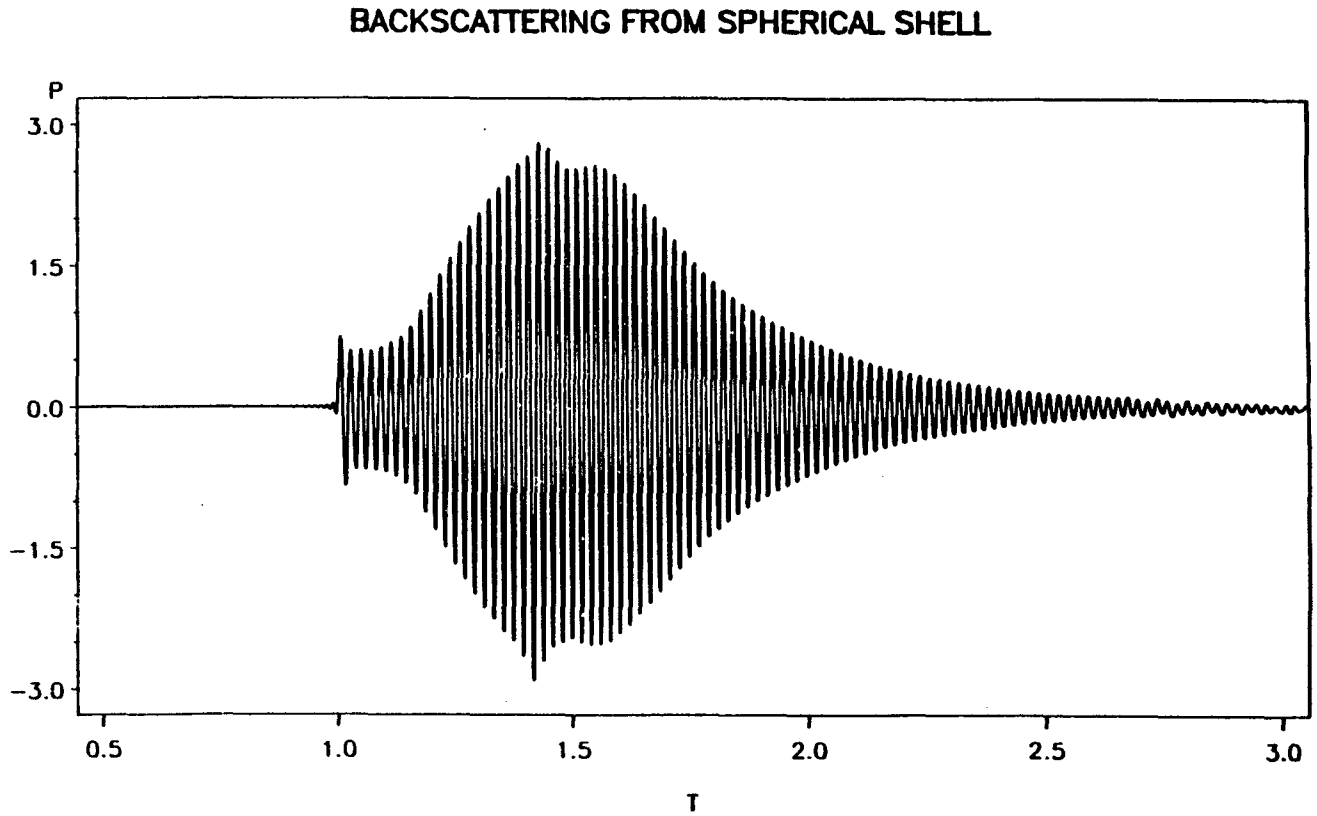

Fig.17a. Computational backscattering from a 4%-thick aluminum shell for a 20-cycle sine burst with $x_O = 302$.

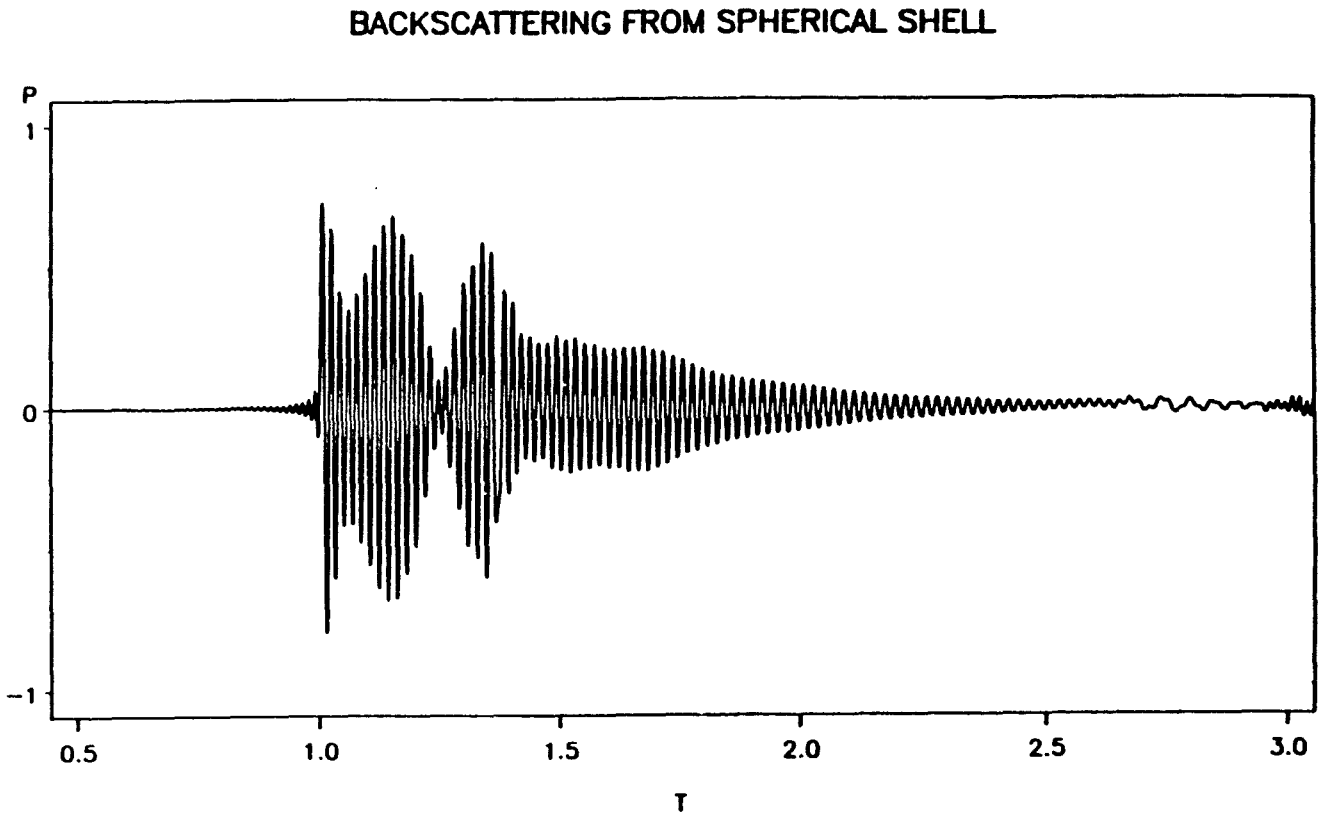

Fig. 17b. Computational backscattering from a 4%-thick aluminum shell for a 20-cycle sine burst with $x_0 = 340$.

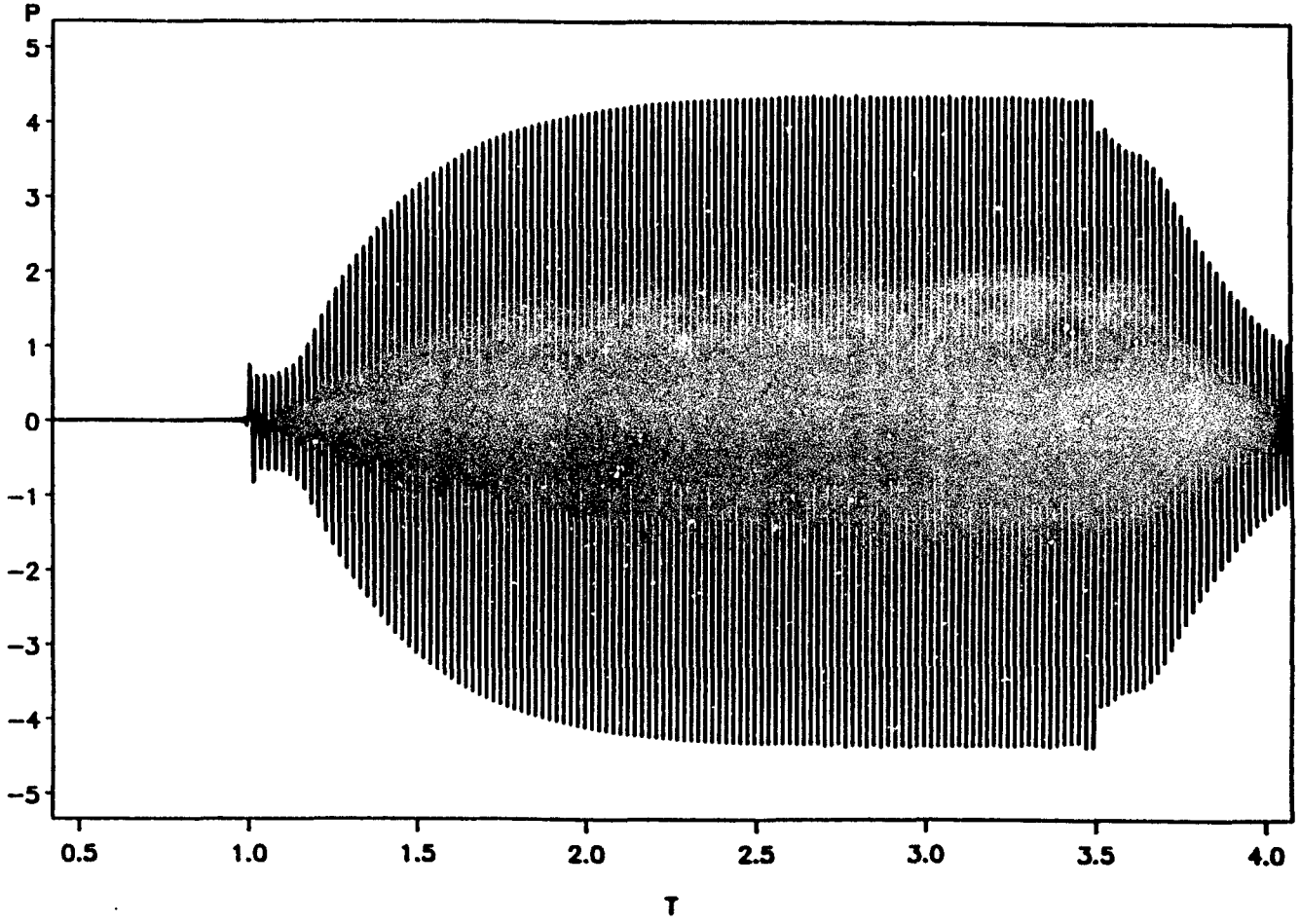

Fig.17c. Computational backscattering from a 4%-thick aluminum shell for a 120-cycle sine burst with $x_O = 302$. The maximum amplitude agrees with the form function prediction.

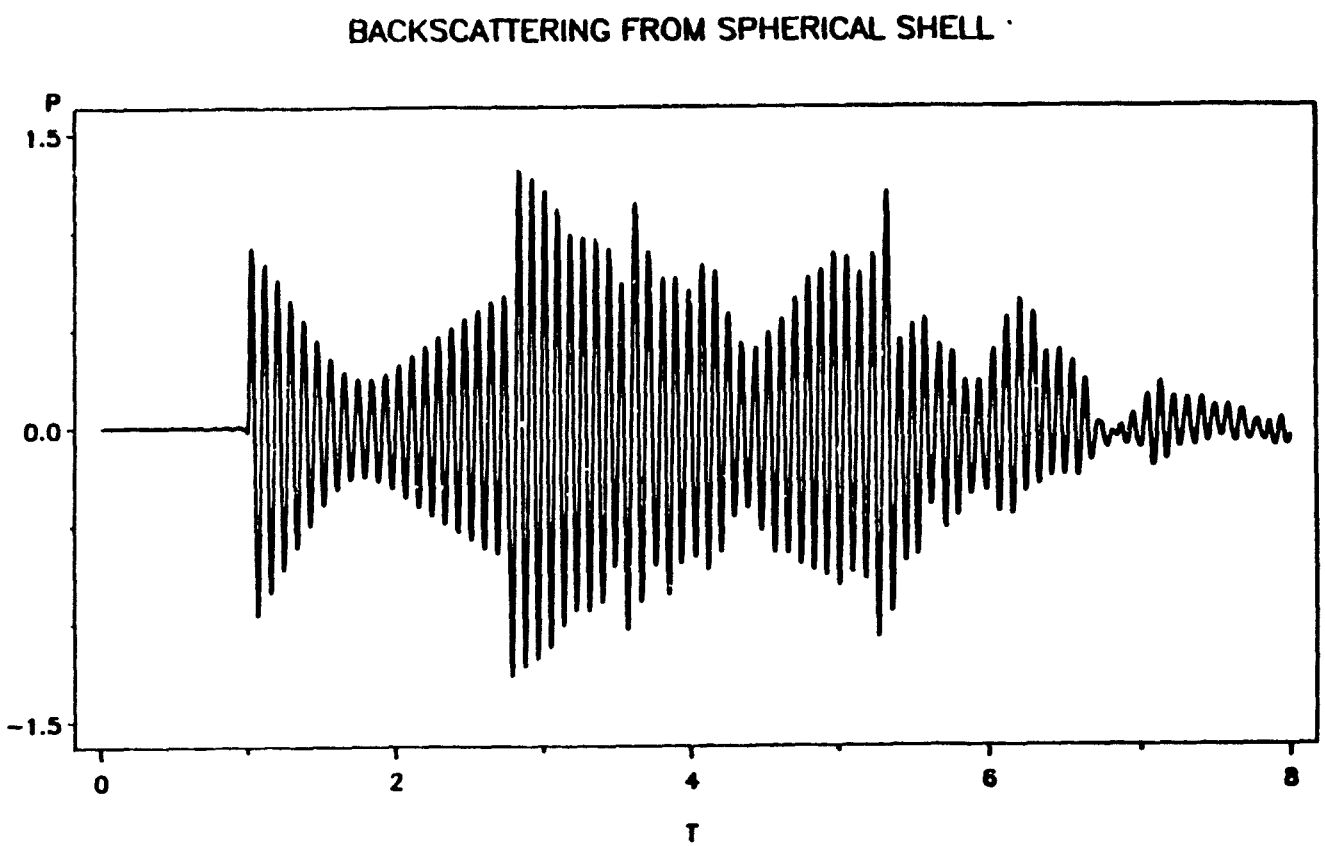

Fig. 18a. Computational backscattering from a 16.2%-thick SS440C shell for a 20-cycle sine burst with $x_o = 71.0$.

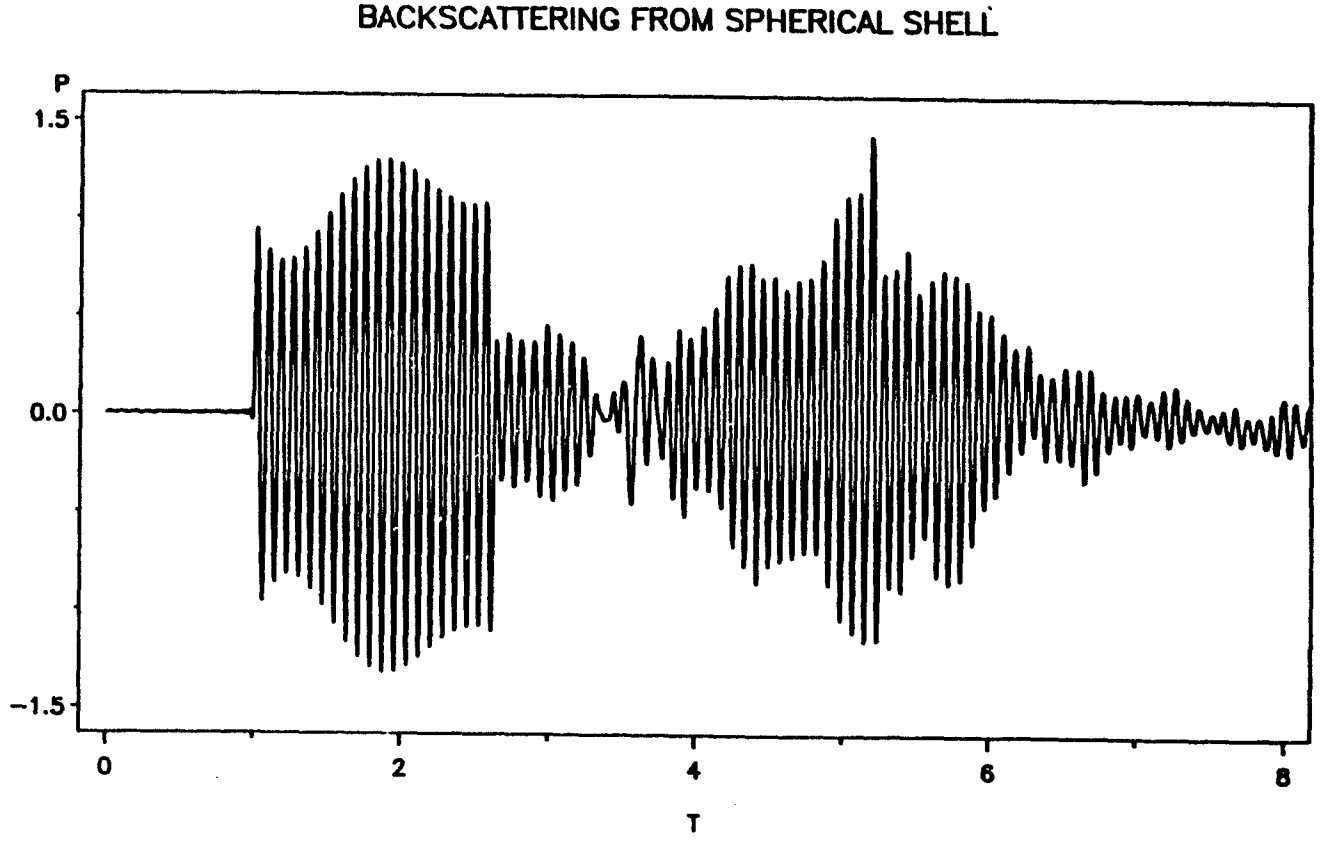

Fig.18b. Computational backscattering from a 16.2%-thick SS440C shell for a 20-cycle sine burst with $x_O = 76.8$.

which is far more complicated than the case of a SS440c/fluid shell. Difference between elastic and fluid shell results is rapidly evident in the time domain. It is seen by $\tau \approx 1.5$, which means there is a prompt mechanism for scattering in the elastic shell not included in the fluid case. We also see that the prompt radiation may be out of phase with the specular reflection therefore the effect can be either constructive or destructive, which is the case of aluminum shell and SS440C shell respectively.

Chapter 6

Discussion and Conclusion

The canonical problem of the backscattering of a short tone burst from elastic spherical shells has been computationally modeled and transient scattered waves has been calculated. The algorithms used are simple trapezoidal method to calculate the Fourier integral and FFT routines. Both methods have turned out to be equally successful, except that the physical meanings are more clear in the former case while the latter can do the transformations much faster. Most results presented in the report are from the calculation of FFT routines. No fundamental complications is in this approach. Any imperfection in the calculation appears to be due to the necessity of assuming a finite bandwidth. This was taken to be much larger than the carrier frequency for all cases shown.

Previous measurements by Williams and Marston for the tungsten carbide sphere and by S. Kargl and P.L.Marston for the 16.2%-thick elastic SS440c shell have been confirmed. Along with Fourier Transform calculations, a ray model of Sun and Marston[19] for the backscattering from thin shells has been carefully investigated. The results demonstrate that the thin elastic shells like 5%-thick SS440c and 2.5%-thick SS304 shells support a_0' wave which can be "creeping" and "trapped" waves. The phase and group velocities for a_0' are both close to the sound speed in the surrounding water. This particular surface wave contributes to the form function in the form of a big hump or mid-frequency enhancement for thin shells. The central frequency of the hump varies inversely with the thickness of the shell but the backscattered echoes due to the effect have an almost constant arrival time (in units of a/c) relative to the specular reflection. In the system point of view,

the scatterer is like a band-pass filter. The frequency components in the range of the hump are relatively enhanced. Because of its large magnitude, this enhancement and other properties of the associated surface wave may be of great practical use. Appendix C shows that the enhancement also contributes in a distinct way to the sphere's impulse response.

The thickness resonance conditions are also examined by computing the backscattering under those conditions. For the fluid stainless steel and aluminum shell cases, the agreement between the calculated backscattering and the prediction by PWS form function under the longitudinal thickness resonance is good. Since the fluid shell case has been well modeled by a ray method, this also indicates a good agreement with the ray prediction. A prompt radiation that is currently being modeled appears to be important in elastic shell cases and the amplitude of the computed backscattering for the aluminum shell does reach the limit predicted by the PWS form function. The case of a thick elastic SS440C shell (16.2%-thick) is more complicated in that the prompt radiation appears to interfere destructively with the specular reflection.

Appendix

A. List of programs

A1. Program computing the form function of elastic spheres

```
ccccccccccccccccccccccccccccccccccccccccccccccccccccccccccccc
C                                                             C
C THIS PROGRAM CALCULATES FORM FUNCTIONS USING CHIVERS        C
C PROGRAMS.                                                   C
C                                                             C
ccccccccccccccccccccccccccccccccccccccccccccccccccccccccccccc
C
      IMPLICIT DOUBLE PRECISION (P)
      DIMENSION PB(800),PCB(800),PSB(800)
c     REAL KAM
      COMPLEX CFAC
      DATA RHO,VC,VS,VW/13.80,6860.0,4185.0,1476.0/
c     data rho,vc,vs,vw/7.70, 5960.0,3240.0,1410.0/
      RH=1.0/(RHO*2.0)
      RAT1=    VW/VC
      RAT2=    VW/VS
      XMAX= 400.0
      X0=0.0
      K=0
 10   k=k+1
      x=x0+k*0.05
      T=1.25*X
      X1=RAT1*X
      X2=RAT2*X
      X2S=X2**2
      XSN=SIN(X)
      XCS=COS(X)
      CALL BESS(X,PB,T)
      TERM=     (XSN/X)/PB(1)
      BN1=     PB(2)*TERM
      CALL BESS(X1,PCB,T)
      CBN1=     PCB(2)/PCB(1)
      CALL BESS(X2,PSB,T)
      SNN0=-XCS/X
      XSIGN=1.0
      SBET=0.0
      SALP=0.0
      N=0
      SUM=0.0
      CALL STVAL(X,X1,X2,ALPN,BETN,CBN1,BN1,SNN1,RH,XSN,X2S,XCS)
 20   CONTINUE
      CBN2=     PCB(N+3)/PCB(N+2)
      Q=FLOAT(N+1)
```

```
      ANUM=(Q*CBN1)-(X1*CBN2)
      ADEN=((Q-1.0)*CBN1)-(X1*CBN2)
      DNUM=(((X2S/2.0)-Q*(Q-1.0))*CBN1)-(2.0*X1*CBN2)
      SBN1=1.0
      SBN2=     PSB(N+3)/PSB(N+2)
      BNUM=(2.0*Q*(Q+1.0))*SBN1
      EDEN=(((2.0*(Q**2))-(X2S+2.0))*SBN1)+(2.0*SBN2*X2)
      ENUM=2.0*Q*(Q+1.0)*(((1.0-Q)*SBN1)+(X2*SBN2))
      FN1=X2S*RH*((ANUM/ADEN)-(BNUM/EDEN))/((DNUM/ADEN)
     &-(ENUM/EDEN))
   30 CONTINUE
      BN2=     PB(N+3)*TERM
      GN1=((FN1-Q)*BN1)+(X*BN2)
      BN1=BN2
      SNN2=(((2.0*Q)+1.0)*SNN1/X)-SNN0
      HN1=((FN1-Q)*SNN1)+(X*SNN2)
      SNN0=SNN1
      SNN1=SNN2
      DEN=(GN1**2)+(HN1**2)
      ALPN1=-(GN1**2)/DEN
      BETN1=-(GN1*HN1)/DEN
      ADD=Q*(ALPN+ALPN1+(2.0*ALPN*ALPN1)+(2.0*BETN*BETN1))
      FAC=XSIGN*(2.0*Q-1.0)
      SALP=SALP+FAC*ALPN
      SBET=SBET+FAC*BETN
      ALPN=ALPN1
      BETN=BETN1
      SUM=SUM+ADD
      IF ((ABS(ADD/SUM)).LT.1.0E-8) GO TO 90
      J=0
      N=N+1
      XSIGN=-XSIGN
      GO TO 20
   90 J=J+1
      IF (J.EQ.5) GO TO 100
      N=N+1
      XSIGN=-XSIGN
      GO TO 20
  100 YP=(-4.0/(X**2))*SUM
      FAC=-XSIGN*(2.0*Q+1.0)
      SALP=SALP+FAC*ALPN1
      SBET=SBET+FAC*BETN1
      CFAC=CMPLX(SBET,-SALP)*(2.0/X)
      FINF=CABS(CFAC)
C     KAM(K)=X
C     FABS(K)=FINF
C     WRITE(7,40) KAM(K),FABS(K)
      WRITE(7,40)       X,CFAC
   40 FORMAT(   3f12.6)
      IF(X.Gt.XMAX) GO TO 50
      GO TO 10
   50 CONTINUE
```

```
      STOP
      END
C
C
      SUBROUTINE STVAL(X,X1,X2,ALPN,BETN,CBN1,BN1,SNN1,RH,XSN,X2S
     &,XCS)
      TERM=CBN1*X1
      FN=-X2S*RH*TERM/((X2S/2.0)-2.0*TERM)
      SNN1=-((XCS/(X**2))+(XSN/X))
      GN=(FN*(XSN/X))+(BN1*X)
      HN=(-(FN*XCS)/X)+(X*SNN1)
      DEN=(GN**2)+(HN**2)
      ALPN=-(GN**2)/DEN
      BETN=-(GN*HN)/DEN
      RETURN
      END
C
C
      SUBROUTINE BESS(X,PA,T)
      IMPLICIT DOUBLE PRECISION (P)
      DIMENSION PA(800)
      L=IFIX(T)+15
      PA(L+2)=0.0
      PA(L+1)=1.0E-30
      DO 10 I=1,L
      M=(L+1)-I
      R=FLOAT(M)
      PA(M)=(((2.0*R)+1.0)*PA(M+1)/X)-PA(M+2)
 10   CONTINUE
      RETURN
      END
```

A2. Program computing the form function of elastic spherical shells

```
 REAL*8 X,XT,XL,QT,QL,BA,RHO,RHOE,XMIN,XMAX,DX,JX(900),
+  JXT(900),JXL(900),JQT(900),JQL(900),YX(900),YXT(900),
+  YXL(900),YQT(900),YQL(900),D(5,5),DI(5,5),
+  C,DETDR,DETDI,
+  CT,CL,XTS,QTS,DNR,DNI,COEF,FORM,SUMR,SUMI
 INTEGER NMAX,I,J,MAX,K,INDX(5)
 C=1.4790D0
 CT=3.1410D0
 CL=5.6750D0
 RHO=1.0D0
 RHOE=7.570D0
 BA=0.9750D0

 XMIN=478.0D0
 XMAX=480.0D0
 X=XMIN
 DX=0.050D0

 MAX=INT((XMAX-XMIN)/DX)
 DO 1000 I=1, MAX

  X=X+DX
  XT=X*C/CT
  XL=X*C/CL
  QT=XT*BA
  QL=XL*BA
  QTS=QT*QT
  XTS=XT*XT

  IF ( (0.20 .LT. X) .AND. (X .LT. 8.0)) THEN
    NMAX=2+NINT(X+4.0*DEXP(DLOG(X)/3.0))
  ELSE
    NMAX=3+NINT(X+4.05*DEXP(DLOG(X)/3.0))
  ENDIF

  CALL BESSEL(NMAX+2,X,JX)
  CALL BESSEL(NMAX+2,XT,JXT)
  CALL BESSEL(NMAX+2,XL,JXL)
  CALL BESSEL(NMAX+2,QT,JQT)
  CALL BESSEL(NMAX+2,QL,JQL)

  CALL NEUMANN(NMAX+2,X,YX)
  CALL NEUMANN(NMAX+2,XL,YXL)
  CALL NEUMANN(NMAX+2,XT,YXT)
  CALL NEUMANN(NMAX+2,QL,YQL)
  CALL NEUMANN(NMAX+2,QT,YQT)

  SUMR=0.0
  SUMI=0.0
```

```
      DO 500 J=1, NMAX
        FJ=DBLE(J-1)
        D(1,1)=(RHO/RHOE)*XTS*JX(J)
        D(1,2)=(2.0*FJ*(FJ-1.0)-XTS)*JXL(J)
        D(1,2)=D(1,2)+4.0*XL*JXL(J+1)
        D(1,3)=(2.0*FJ*(FJ-1.0)-XTS)*YXL(J)
        D(1,3)=D(1,3)+4.0*XL*YXL(J+1)
        D(1,4)=(FJ-1.0)*JXT(J)-XT*JXT(J+1)
        D(1,4)=2.0*FJ*(FJ+1)*D(1,4)
        D(1,5)=(FJ-1.0)*YXT(J)-XT*YXT(J+1)
        D(1,5)=2.0*FJ*(FJ+1)*D(1,5)
        D(2,1)=-FJ*JX(J)+X*JX(J+1)
        D(2,2)=FJ*JXL(J)-XL*JXL(J+1)
        D(2,3)=FJ*YXL(J)-XL*YXL(J+1)
        D(2,4)=FJ*(FJ+1.0)*JXT(J)
        D(2,5)=FJ*(FJ+1.0)*YXT(J)
        D(3,1)=0.0D0
        D(3,2)=2.0*((1.0-FJ)*JXL(J)+XL*JXL(J+1))
        D(3,3)=2.0*((1.0-FJ)*YXL(J)+XL*YXL(J+1))
        D(3,4)=(XTS-2.0*(FJ**2)+2.0)*JXT(J)-2.0*XT*JXT(J+1)
        D(3,5)=(XTS-2.0*(FJ**2)+2.0)*YXT(J)-2.0*XT*YXT(J+1)
        D(4,1)=0.0D0
        D(4,2)=(2.0*FJ*(FJ-1.0)-QTS)*JQL(J)
        D(4,2)=D(4,2)+4.0*QL*JQL(J+1)
        D(4,3)=(2.0*FJ*(FJ-1.0)-QTS)*YQL(J)
        D(4,3)=D(4,3)+4.0*QL*YQL(J+1)
        D(4,4)=2.0*FJ*(FJ+1.0)*((FJ-1.0)*JQT(J)-QT*JQT(J+1))
        D(4,5)=2.0*FJ*(FJ+1.0)*((FJ-1.0)*YQT(J)-QT*YQT(J+1))
        D(5,1)=0.0D0
        D(5,2)=2.0*((1.0-FJ)*JQL(J)+QL*JQL(J+1))
        D(5,3)=2.0*((1.0-FJ)*YQL(J)+QL*YQL(J+1))
        D(5,4)=(QTS-2.0*(FJ**2)+2.0)*JQT(J)-2.0*QT*JQT(J+1)
        D(5,5)=(QTS-2.0*(FJ**2)+2.0)*YQT(J)-2.0*QT*YQT(J+1)

        DI(1,1)=(RHO/RHOE)*XTS*YX(J)
        DI(2,1)=-FJ*YX(J)+X*YX(J+1)
        DI(3,1)=0.0D0
        DI(4,1)=0.0D0
        DI(5,1)=0.0D0
        DO 200 K=2, 5
             DI(1,K)=D(1,K)
             DI(2,K)=D(2,K)
             DI(3,K)=D(3,K)
             DI(4,K)=D(4,K)
             DI(5,K)=D(5,K)
200     CONTINUE

             CALL LUDCMP(D,5,5,INDX,DETDR)
             CALL LUDCMP(DI,5,5,INDX,DETDI)

        DO 300 K=1, 5
             DETDR=DETDR*D(K,K)
             DETDI=DETDI*DI(K,K)
```

```
300      CONTINUE
         DNR=DETDR
         DNI=DETDI
         COEF=((-1.0)**(J+1))*(2.0*FJ+1.0)
         SUMR=SUMR+COEF*(DNI/(DNR+DNI*(DNI/DNR)))
         SUMI=SUMI+COEF*(DNR/(DNR+DNI*(DNI/DNR)))
500      CONTINUF
         FORM=(2.0/X)*DSQRT(SUMR**2+SUMI**2)
             SUMR= SUMR*2.0/X
             SUMI= SUMI*2.0/X
         WRITE(7,2000) X,SUMR,SUMI
1000     CONTINUE
2000     FORMAT(3F12.6)
   END

       SUBROUTINE NEUMANN(N,X,YN)

       REAL*8 X,YN(900)
       INTEGER I,N
       IF ( (X .LT. 0.0) .OR. (N .LT. 2) ) THEN
       WRITE(6,*) 'FAILURE IN NEUMANN FCN ROUTINE'
       GOTO 30
       ENDIF
       YN(1)=-DCOS(X)/X
       YN(2)=-DCOS(X)/(X**2)-DSIN(X)/X
       DO 10 I=1,N-1
       YN(I+2)=((2.0*DBLE(I-1)+3.0)/X)*YN(I+1)-YN(I)
10     CONTINUE
30     RETURN
       END

       SUBROUTINE BESSEL(N,X,JN)

       REAL*8 X,JN(900),RATIO,J0,JMX,JMX1
       INTEGER I,MAX,N,NT
       JMX=1.0
       JMX1=1.0D-100
       MAX=N+20
       IF ( (X .LT. 0.0) .OR. (N .GT. 900) ) THEN
       WRITE(6,*) 'FAILURE IN BESSEL FCN ROUTINE'
       GOTO 90
       ENDIF
       J0=DSIN(X)/X
       IF (N .GT. INT(X)) THEN
       DO 10 I=1,MAX-1
           NT=MAX-I
           JN(NT)=((2.0*DBLE(NT)+1.0)/X)*JMX-JMX1
           JMX1=JMX
           JMX=JN(NT)
10     CONTINUE
       RATIO=J0/JN(1)
       DO 20 I=1,N+1
           JN(I)=RATIO*JN(I)
```

```
20      CONTINUE
        ELSE
        JN(1)=J0
        JN(2)=DSIN(X)/(X**2)-DCOS(X)/X
        DO 35 I=1, N-2
            JN(I+2)=((2.0*DBLE(I)+1.0)/X)*JN(I+1)-JN(I)
35      CONTINUE
        ENDIF
90      RETURN
        END

        SUBROUTINE LUDCMP(A,N,NP,INDX,D)

        IMPLICIT REAL*8 (A-H, O-Z)
        PARAMETER(NMAX=100, TINY=1.0D-100)
        DIMENSION A(NP,NP),INDX(N),VV(NMAX)
        D=1.0
        DO 12 I=1, N
              AAMAX=0.0
        DO 11 J=1, N
         IF (DABS(A(I,J)) .GT. AAMAX) AAMAX=DABS(A(I,J))
11       CONTINUE
         IF (AAMAX .EQ. 0.0) PAUSE 'SINGULAR MATRIX'
         VV(I)=1.0/AAMAX
12       CONTINUE
         DO 19 J=1, N
         IF (J .GT. 1) THEN
            DO 14 I=1, J-1
             SUM=A(I,J)
             IF (I .GT. 1) THEN
                DO 13 K=1, I-1
                 SUM=SUM-A(I,K)*A(K,J)
13              CONTINUE
                      A(I,J)=SUM
             ENDIF
14          CONTINUE
         ENDIF
         AAMAX=0.0
         DO 16 I=J, N
             SUM=A(I,J)
             IF (J .GT. 1) THEN
             DO 15 K=1, J-1
                 SUM=SUM-A(I,K)*A(K,J)
15           CONTINUE
             A(I,J)=SUM
          ENDIF
          DUM=VV(I)*DABS(SUM)
          IF (DUM .GE. AAMAX) THEN
             IMAX=I
             AAMAX=DUM
          ENDIF
16       CONTINUE
         IF (J .NE. IMAX) THEN
```

```
          DO 17 K=1, N
              DUM=A(IMAX,K)
              A(IMAX,K)=A(J,K)
              A(J,K)=DUM
17        CONTINUE
          D=-D
          VV(IMAX)=VV(J)
        ENDIF
        INDX(J)=IMAX
        IF (J .NE. N) THEN
          IF (A(J,J) .EQ. 0.0) A(J,J)=TINY
          DUM=1.0/A(J,J)
          DO 18 I=J+1, N
           A(I,J)=A(I,J)*DUM
18        CONTINUE
        ENDIF
19    CONTINUE
      IF (A(N,N) .EQ. 0.0) A(N,N)=TINY
      RETURN
      END
```

A3. Program computing the form function of fluid spherical shells

```
      REAL*8 X,XL,QL,BA,RHO,RHOE,XMIN,XMAX,DX,JX(600),
     +  JXL(600),JQL(600),YX(600),YXL(600),YQL(600),D(3,3),DI(3,3),
     +  C,DETDR,DETDI,CL,DNR,DNI,COEF,FORM,SUMR,SUMI

      INTEGER NMAX,I,J,MAX,K,INDX(3)
      C=1.4790D0
      RHO=1.0D0
      RHOE=7.840D0
      CL=5.854D0
      BA=0.838D0
      XMIN=0.0D0
      XMAX=400.0D0
      X=XMIN
      DX=0.050D0

      PI=3.1415926
      MAX=INT((XMAX-XMIN)/DX)
      DO 1000 I=1,MAX

       X=I*DX
       XL=X*C/CL
       QL=XL*BA

       IF ( (0.20 .LT. X) .AND. (X .LT. 8.0)) THEN
         NMAX=2+NINT(X+4.0*DEXP(DLOG(X)/3.0))
       ELSE
         NMAX=3+NINT(X+4.05*DEXP(DLOG(X)/3.0))
       ENDIF

       CALL BESSEL(NMAX+2,X,JX)
       CALL BESSEL(NMAX+2,XL,JXL)
       CALL BESSEL(NMAX+2,QL,JQL)

       CALL NEUMANN(NMAX+2,X,YX)
       CALL NEUMANN(NMAX+2,XL,YXL)
       CALL NEUMANN(NMAX+2,QL,YQL)

       SUMR=0.0
       SUMI=0.0

       DO 500 J=1, NMAX
         FJ=DBLE(J-1)
         D(1,1)=(RHO/RHOE)*(C/CL)*JX(J)
         D(1,2)=JXL(J)
         D(1,3)=YXL(J)

         D(2,1)=FJ*JX(J)/X-JX(J+1)
         D(2,2)=FJ*JXL(J)/XL-JXL(J+1)
         D(2,3)=FJ*YXL(J)/XL-YXL(J+1)
```

```
          D(3,1)=0.0D0
          D(3,2)=JQL(J)
          D(3,3)=YQL(J)

          DI(1,1)=(RHO/RHOE)*(C/CL)*YX(J)
          DI(2,1)=FJ*YX(J)/X-YX(J+1)
          DI(3,1)=0.0D0
          DO 200 K=2, 3
               DI(1,K)=D(1,K)
               DI(2,K)=D(2,K)
               DI(3,K)=D(3,K)
200              continue

               CALL LUDCMP(D,3,3,INDX,DETDR)
               CALL LUDCMP(DI,3,3,INDX,DETDI)

          DO 300 K=1, 3
               DETDR=DETDR*D(K,K)
               DETDI=DETDI*DI(K,K)
300            CONTINUE
               DNR=DETDR
          DNI=DETDI
          COEF=((-1.0)**(J+1))*(2.0*FJ+1.0)
          SUMR=SUMR+COEF*(DNI/(DNR+DNI*(DNI/DNR)))
          SUMI=SUMI+COEF*(DNR/(DNR+DNI*(DNI/DNR)))
500           CONTINUE

              SUMR=(2.0/X)*SUMR
              SUMI=(2.0/X)*SUMI
              write (7,2000) x,sumr,sumi
1000      CONTINUE
2000      FORMAT(3F12.6)
          END

        SUBROUTINE NEUMANN(N,X,YN)

        REAL*8 X,YN(600)
        INTEGER I,N
        IF ( (X .LT. 0.0) .OR. (N .LT. 2) ) THEN
        WRITE(6,*) 'FAILURE IN NEUMANN FCN ROUTINE'
        GOTO 30
        ENDIF
        YN(1)=-DCOS(X)/X
        YN(2)=-DCOS(X)/(X**2)-DSIN(X)/X
        DO 10 I=1,N-1
        YN(I+2)=((2.0*DBLE(I-1)+3.0)/X)*YN(I+1)-YN(I)
10      CONTINUE
30      RETURN
        END
```

```
      SUBROUTINE BESSEL(N,X,JN)

      REAL*8 X,JN(600),RATIO,J0,JMX,JMX1
      INTEGER I,MAX,N,NT
      JMX=1.0
      JMX1=1.0D-100
      MAX=N+20
      IF ( (X .LT. 0.0) .OR. (N .GT. 500) ) THEN
      WRITE(6,*) 'FAILURE IN BESSEL FCN ROUTINE'
      GOTO 90
      ENDIF
      J0=DSIN(X)/X
      IF (N .GT. INT(X)) THEN
      DO 10 I=1,MAX-1
           NT=MAX-I
           JN(NT)=((2.0*DBLE(NT)+1.0)/X)*JMX-JMX1
           JMX1=JMX
           JMX=JN(NT)
10     CONTINUE
       RATIO=J0/JN(1)
       DO 20 I=1,N+1
           JN(I)=RATIO*JN(I)
20     CONTINUE
       ELSE
       JN(1)=J0
       JN(2)=DSIN(X)/(X**2)-DCOS(X)/X
       DO 35 I=1, N-2
       JN(I+2)=((2.0*DBLE(I)+1.0)/X)*JN(I+1)-JN(I)
35     CONTINUE
       ENDIF
90     RETURN
       END

       SUBROUTINE LUDCMP(A,N,NP,INDX,D)

      IMPLICIT REAL*8 (A-H, O-Z)
      PARAMETER(NMAX=100, TINY=1.0D-150)
      DIMENSION A(NP,NP),INDX(N),VV(NMAX)
      D=1.0
      DO 12 I=1, N
            AAMAX=0.0
        DO 11 J=1, N
         IF (DABS(A(I,J)) .GT. AAMAX) AAMAX=DABS(A(I,J))
11      CONTINUE
        IF (AAMAX .EQ. 0.0) PAUSE 'SINGULAR MATRIX'
        VV(I)=1.0/AAMAX
12    CONTINUE
        DO 19 J=1, N
        IF (J .GT. 1) THEN
           DO 14 I=1, J-1
            SUM=A(I,J)
            IF (I .GT. 1) THEN
               DO 13 K=1, I-1
                SUM=SUM-A(I,K)*A(K,J)
```

```
13              CONTINUE
                      A(I,J)=SUM
            ENDIF
14          CONTINUE
        ENDIF
        AAMAX=0.0
        DO 16 I=J, N
            SUM=A(I,J)
            IF (J .GT. 1) THEN
            DO 15 K=1, J-1
                SUM=SUM-A(I,K)*A(K,J)
15          CONTINUE
            A(I,J)=SUM
         ENDIF
         DUM=VV(I)*DABS(SUM)
         IF (DUM .GE. AAMAX) THEN
            IMAX=I
            AAMAX=DUM
         ENDIF
16      CONTINUE
        IF (J .NE. IMAX) THEN
         DO 17 K=1, N
             DUM=A(IMAX,K)
             A(IMAX,K)=A(J,K)
             A(J,K)=DUM
17       CONTINUE
         D=-D
         VV(IMAX)=VV(J)
        ENDIF
        INDX(J)=IMAX
        IF (J .NE. N) THEN
           IF (A(J,J) .EQ. 0.0) A(J,J)=TINY
           DUM=1.0/A(J,J)
           DO 18 I=J+1, N
            A(I,J)=A(I,J)*DUM
18         CONTINUE
        ENDIF
19      CONTINUE
        IF (A(N,N) .EQ. 0.0) A(N,N)=TINY
        RETURN
        END
```

A4. Program computing transient scattering: integration

```
      REAL M,A,B,X0,X,X1,X2, TWOPI,G,REG,IMG, ARG,REF,IMF,REAL,
     $     IMAG, P(5000),B0
      INTEGER I,N,J,N1
      WRITE(5,10)
   10 FORMAT('READ IN N & N1')
      READ (5,20) N,N1
   20 FORMAT(2I4)
      X0=49.1
      B0=4.
      TWOPI=2*3.1415926
      M=TWOPI*B0/X0
      X1=0.05
      T1=20*M/N1
      DO 200 J=1,N1
      P(J)=00.0
  200 CONTINUE
      DO 100 I=1,N
      T =  -6.*M
C     X=I*X1
      READ (9,500      ) X,REF,IMF
      REF=-REF
      IMF=+IMF
  500 FORMAT(3F12.6)
      X2=X-X0
      X2=ABS(X2)
      A=X+X0
      B=X-X0
      IF (X2.LT.1.0E-8) GO TO 30
      REG=(1-COS(M*A))/A-(1-COS(M*B))/B
      IMG=SIN(M*A)/A-SIN(M*B)/B
C     IF(REG.EQ.0.0) GO TO 25
C     ARG   =ATAN2(IMG, REG)
C     GO TO 28
C  25 ARG  =3.1415926/2
C  28 ARG   = ARG/3.1415926
      GO TO 40
   30 REG=(1-COS(M*A))/A
      IMG=SIN(M*A)/A-M
   40 IMG=-IMG
C     G=(REG**2+IMG**2)**0.5
C     ARG   = ATAN2(IMG, REG)/3.1415926
C     WRITE (7,50) X,G
C
      REAL=REG*REF -IMG*IMF
      IMAG=IMG*REF +REG*IMF
      DO 300 J=1,N1
      P(J)=(REAL*COS(X*T)+IMAG*SIN(X*T))*X1+P(J)
      T=T+T1
  300 CONTINUE
  100 CONTINUE
```

```
      T= -6.0*M-T1
      DO 400 J=1,N1
      T=T+T1
      P(J)=P(J)/TWOPI
      WRITE(8,50)  T, P(J)
400   CONTINUE
 50   FORMAT(2F12.6)
      STOP
      END
```

Program A4. This program computes the transient backscattering from any scatterer for a B0-cycle sine burst with a carrier frequency x_0. A simple trapezoidal method is used in doing the integration in Eq.(3.10). The disk defined as device 9 contains the data for the form function of any scatterer. The N and N1 are parameters which specify, respectively, the number of data for the form function and the number of points you want for each cycle of the incident burst.

A5. Program computing transient scattering: FFT routines

```
      INTEGER I, N, M, N1
      REAL CONST, TWOPI, X0,B, UL,T,T1,MODSEQ ,MODCOEF,KA,
     $ REF,IMF,T2,Y
      COMPLEX C, COEF(34280),H, SEQ(34280)
      EXTERNAL CONST, FFTCF, FFTCB
      COMMON /WORKSP/  RWKSP
      REAL RWKSP(206000)
      CALL IWKIN(206000)
      X0=49.1
      B=4.
      M=INT(B*25.)
      N=INT(X0*M/B/0.05)
      IF (N/2.GT.0) N=N+1
      TWOPI= 2.0*CONST('PI')
      UL=TWOPI*B/X0
      T =0.
      T2=0.
      T1=UL/M
      Y = 3*FLOAT(M)/UL
      N1= IFIX(Y)+1
      DO 30 I=1,N1
         SEQ(I)=0.
         MODSEQ   =REAL(SEQ(I))
         WRITE (6,300) T,MODSEQ
         T=T+T1
   30 CONTINUE
      DO 10 I=N1+1 ,N1+1+  M
         SEQ(I)= SIN(X0*T2)
         MODSEQ   =REAL(SEQ(I))
         WRITE (6,300) T,MODSEQ
         T2=T2+T1
         T =T +T1
   10 CONTINUE
      DO 20 I=N1+2+M , N
         SEQ(I)=0.
         MODSEQ   =REAL(SEQ(I))
         IF (T.GT.5) GO TO 20
         WRITE (6,300) T,MODSEQ
         T=T+T1
   20 CONTINUE
      CALL FFTCF (N, SEQ, COEF)
      DO 1000 I=1,     N
      KA=FLOAT(I-1)*X0*M/B/FLOAT(N)
      MODCOEF  =CABS(COEF(I))/FLOAT(M)
      BETA=ATAN2(AIMAG(COEF(I)), REAL(COEF(I)))/CONST('PI')*180
      WRITE (7,300) KA,MODCOEF
      WRITE (2,300) KA,BETA
 1000 CONTINUE
      DO 4000 I=2,8001
```

```
      READ (9, 5000) X,REF,IMF
5000  FORMAT (3F12.6)
      COEF(I)=COEF(I)*CMPLX(-REF, -IMF)
4000  CONTINUE
      DO 3000 I= 8001 ,N
      COEF(I)=(0.,0.)
3000  CONTINUE
      CALL FFTCB (N,COEF,SEQ)
      T=-UL/FLOAT(M)
      DO 2000 I=1,N
      SEQ(I)=SEQ(I)*2./FLOAT(N)
      MODSEQ  = REAL(SEQ(I))
      T= T    +T1
      IF (T.GE.10.) GO TO 2500
      WRITE(8,300) T,       MODSEQ
 300  FORMAT(2F12.6)
2000  CONTINUE
2500  STOP
      END
```

Program A5. This program computes the transient backscattering from any scatterer for a B-cycle sine burst with a carrier frequency x_0. Two FFT routines, namely, FFTCF and FFTCB, in the CMS main frame Fortran routines bank are utilized. The parameters N and M specify, respectively, the total number of points for the input sequence and the number of points per cycle for the input burst. The disk defined as device 9 contains the data for the form function of any scatterer. The sign of these data may have to be changed depending on the time convention the form function program is using.

A6. Illustration about writing and using the programs

The program computing the form function of an elastic sphere was written by Chivers and Anson[22]. Both the program computing the form function of elastic spherical shells and that of fluid shells were written by S. Kargl. They are presented here just for user's convenience. These programs are found written in $e^{-i\omega t}$ time convention whose results can be used in present computation without any change. To compute the form function for high ka values, which is often the case for transient calculations, one needs to expand the dimension of the arrays defined in the programs. But this is not limitless. These programs can not calculate the form function for arbitrarily high ka values. This could be a problem sometimes. As in the case of resonance scattering by aluminum shell, the carrier frequency is as high as $x_0 = 340$, but the form function can only be calculated up to $x = 480$ for the material constants we are using. The cut-off high frequency of 480 gives us a real incident burst as shown in Fig. A1 which is far from perfect. When interpreting the transient scattering in this case, one has to take into the consideration the no longer small difference between the ideal and real incident bursts.

The programs computing the transient scattering are also written in $e^{-i\omega t}$ time convention but the FFT routines called from IMSL bank are in $e^{+i\omega t}$ time convention. Since our input is a real sequence, the difference in time convention gives a different sign for the imaginary part of the result. That is why the sentence img = -img is used in the program calling the routines.

In order for the set of samples of a signal to correctly represent that signal, the sampling theorem has to be satisfied. Since an upper limit of integration or summation xmax has been assumed, the sampling frequency can not be less than 2xmax. Suppose we want

L points per cycle for the incident burst, then the sampling theorem states the following condition

$$Lx_o \geq 2x_{max} . \qquad (A6.1)$$

Throughout the report, xmax = 400 and $\Delta x = 0.05$ have been chosen except for the aluminum and aluminum/fluid shell cases where xmax = 480 and $\Delta x = 0.1$. When $x_o < 40$, we can either let L be greater or reduce the value of xmax a little bit. We decided to adopt the former solution, namely, changing L while keeping xmax = 400. Examples are Fig.6d where L = 40 and Fig 5c(a),11a,11b,B1(a) and B1(b) where L = 25.

As stated in Chapter 4, large value of N could be a calculation problem. A 10-cylinder account on the CMS main frame can only support the calculation of N=34000. When computing the backscattering from aluminum or aluminum/fluid shell, the carrier frequencies we are interested in are $x_o = 302$ and 340. Since we have $N = Lx_o/\Delta x$, L has to be decreased and Δx has to be increased in order to keep N under this limit. Therefore $\Delta x = 0.1$ and L = 10 have been chosen, which also assures the sampling theorem condition for xmax = 480.

It should be pointed out that the upper limit of the summation in Eq.(4.15) should be the same as xmax. In other words $\Delta x N/2$ = xmax, or $Lx_o = 2x_{max}$. Fortunately, the components above xmax for all the bursts considered in this report is small enough that as far as the physics in the scattering process is concerned, the inequality (A6.1) can be regarded as the proper condition which has been assured throughout the work.

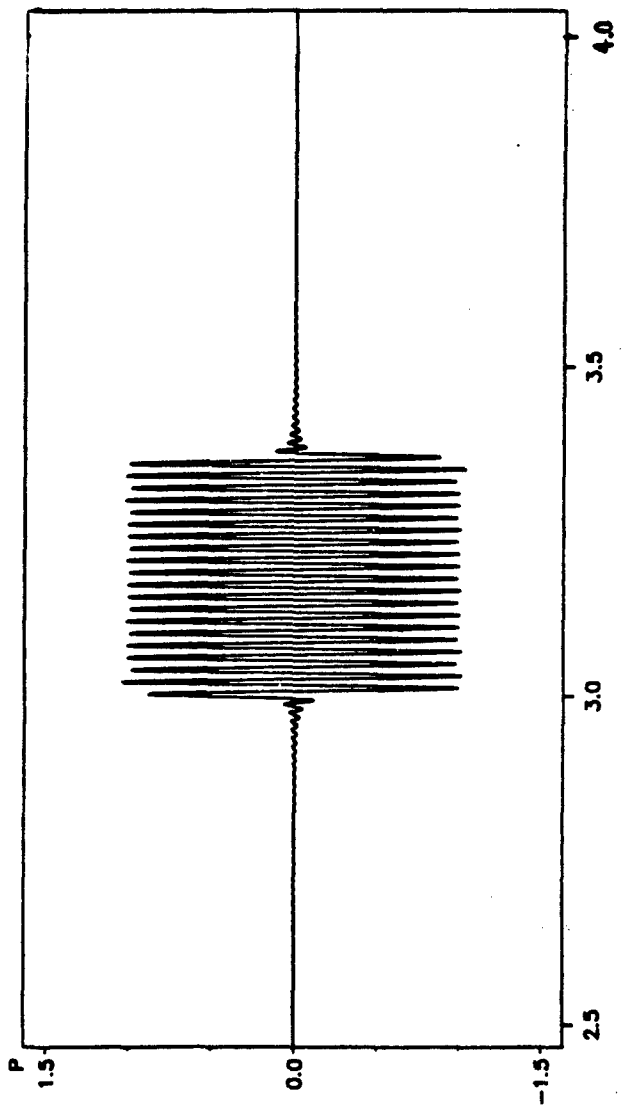

Fig.A1. Real incident burst with $x_0 = 340$ for the backscattering computation from aluminum and aluminum/fluid shell. The cut-off frequency is xmax = 480. The imperfection is mainly at the two edges.

B. Additional Data and Graphs

B1. Mid-frequency enhancement of the backscattering for 4-cycle burst

B2. Resonance backscattering from aluminum/fluid shell: 1-cycle

B3. Resonance backscattering from aluminum/fluid shell: 4-cycle

B4. Resonance backscattering from SS440c/fluid shell: 1-cycle

B5. Resonance backscattering from SS440c/fluid shell: 4-cycle

B6. Resonance backscattering from real aluminum shell: 1-cycle

B7. Resonance backscattering from real aluminum shell: 4-cycle

B8. Resonance backscattering from real SS440c shell: 1-cycle

B9. Resonance backscattering from real SS440c shell: 4-cycle

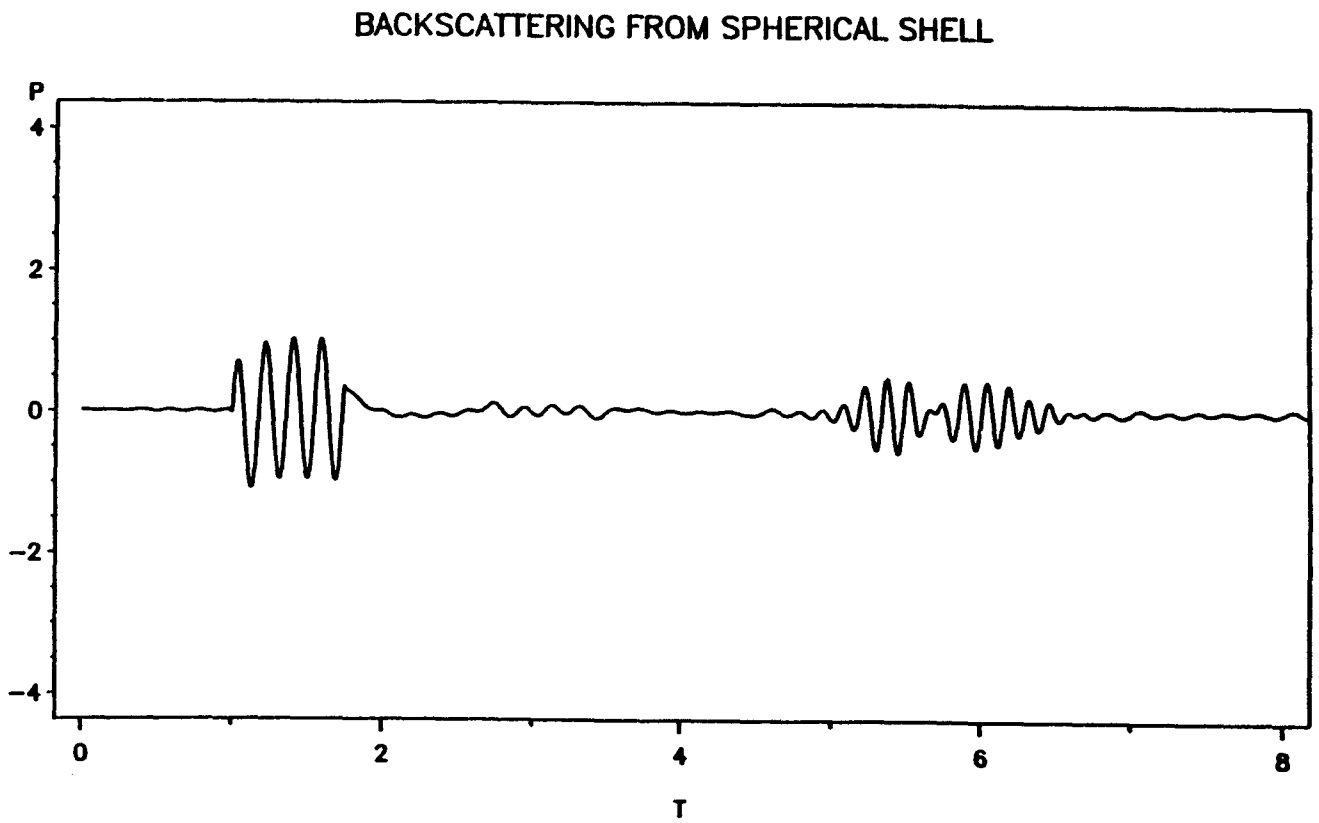

Fig. B1(a). Computational backscattering from a 2.5%-thick SS304 shell for a 4-cycle sine burst with $x_o = 34.0$.

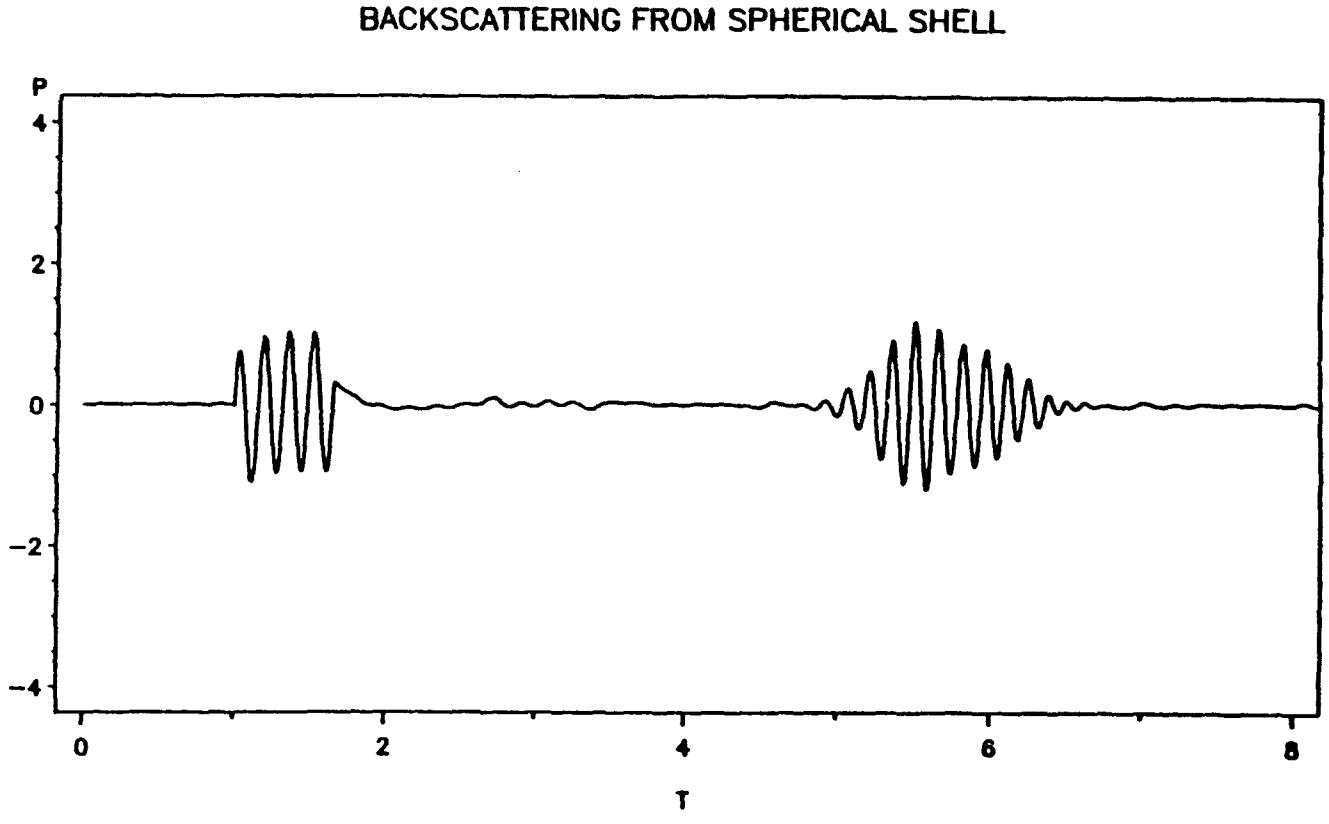

Fig. B1(b). Computational backscattering from a 2.5%-thick SS304 shell for a 4-cycle sine burst with $x_O = 38.0$.

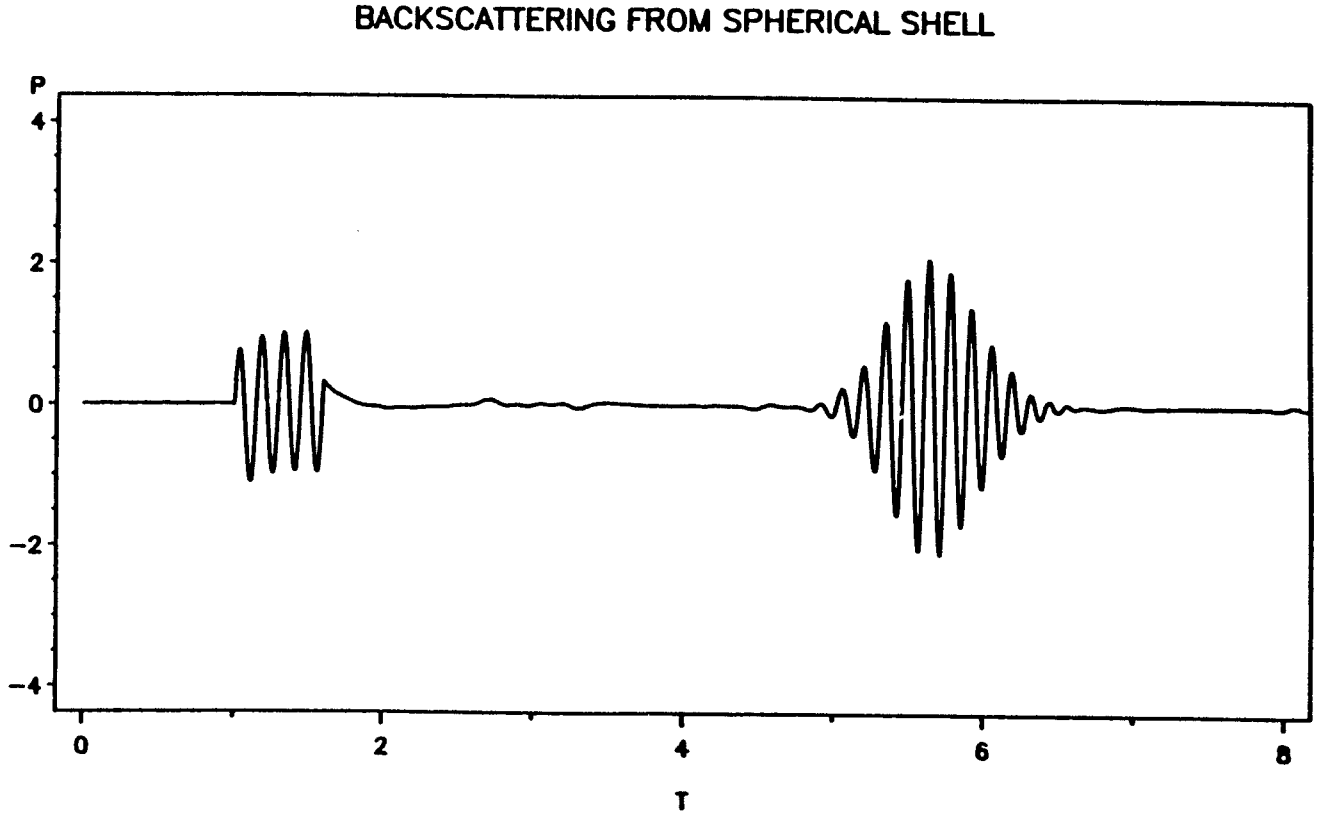

Fig. B1(c). Computational backscattering from a 2.5%-thick SS304 shell for a 4-cycle sine burst with $x_O = 42.0$.

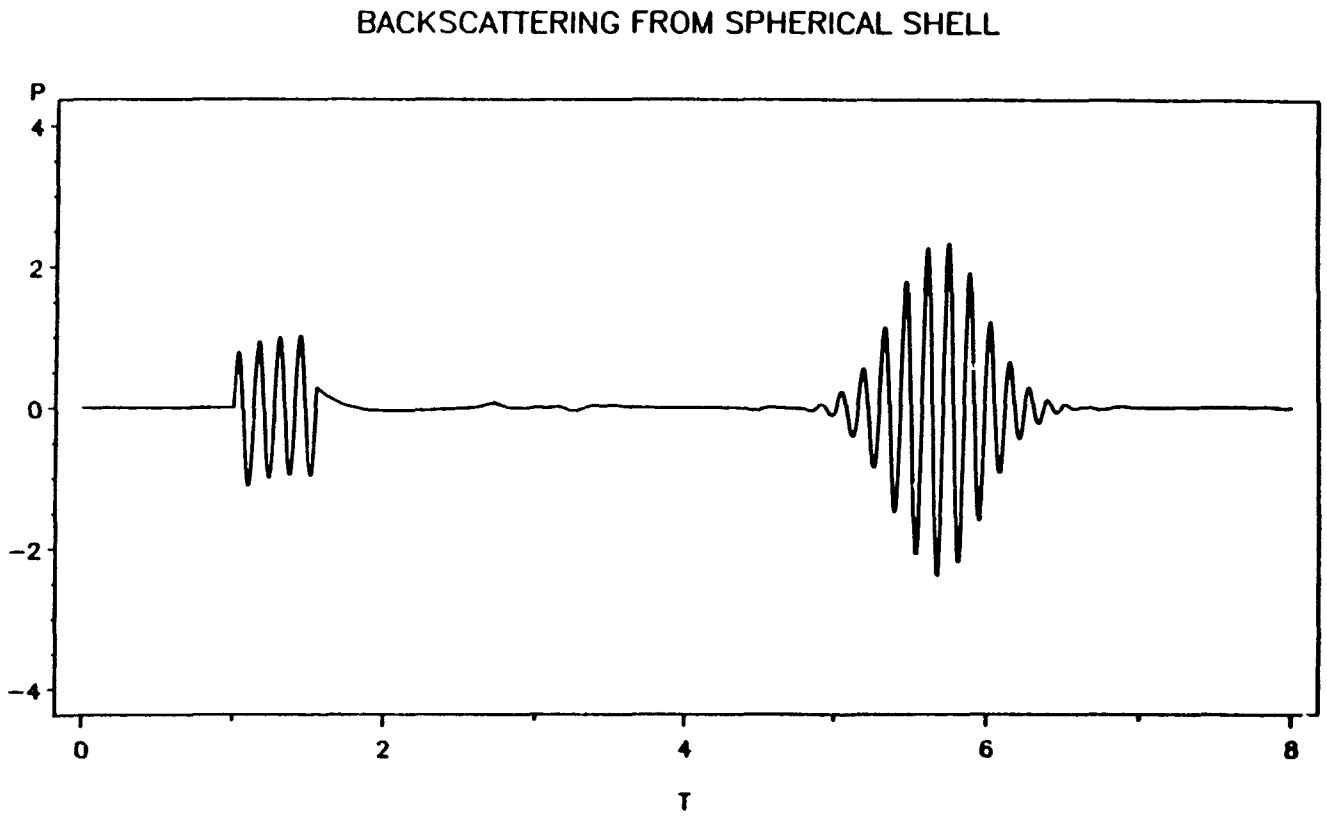

Fig. B1(d). Computational backscattering from a 2.5%-thick SS304 shell for a 4-cycle sine burst with $x_0 = 46.0$.

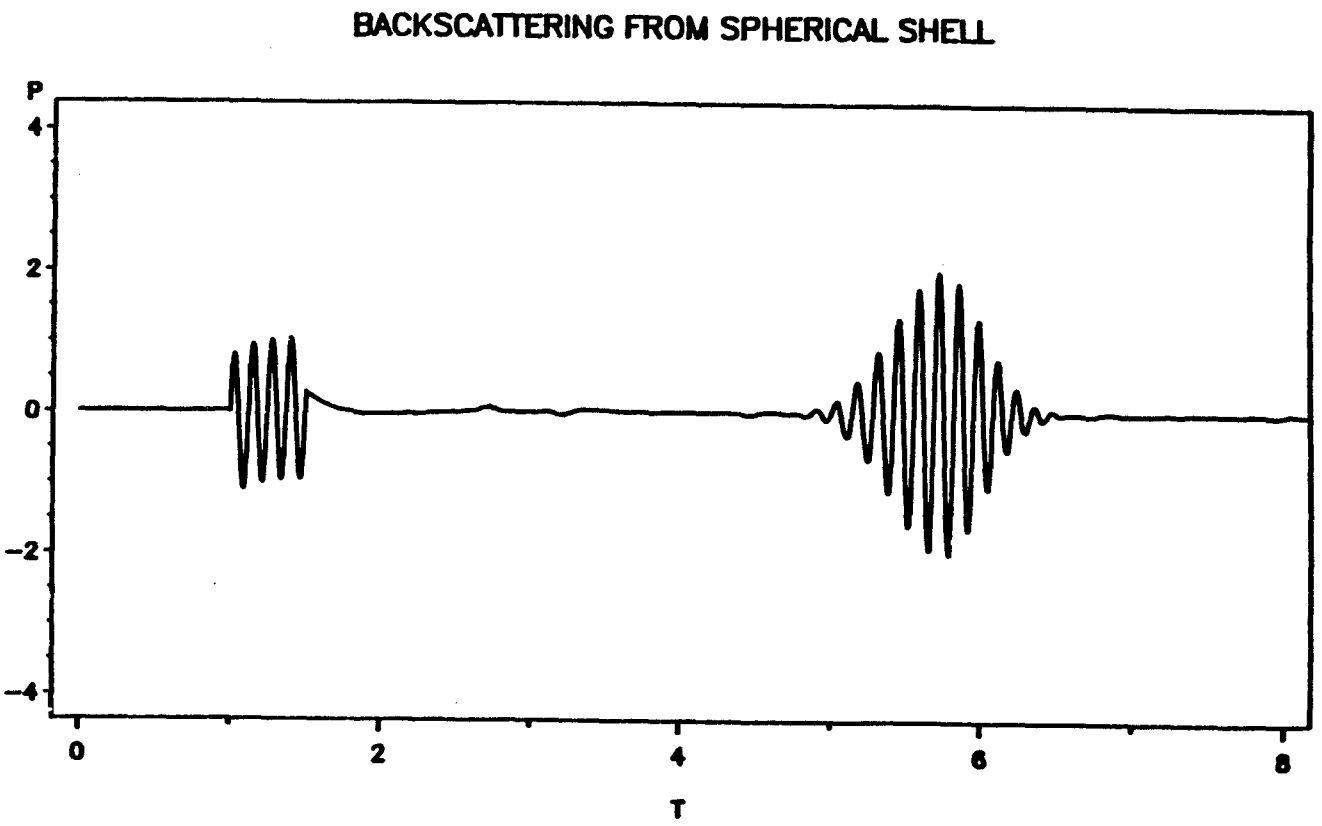

Fig. B1(e). Computational backscattering from a 2.5%-thick SS304 shell for a 4-cycle sine burst with $x_O = 50.0$.

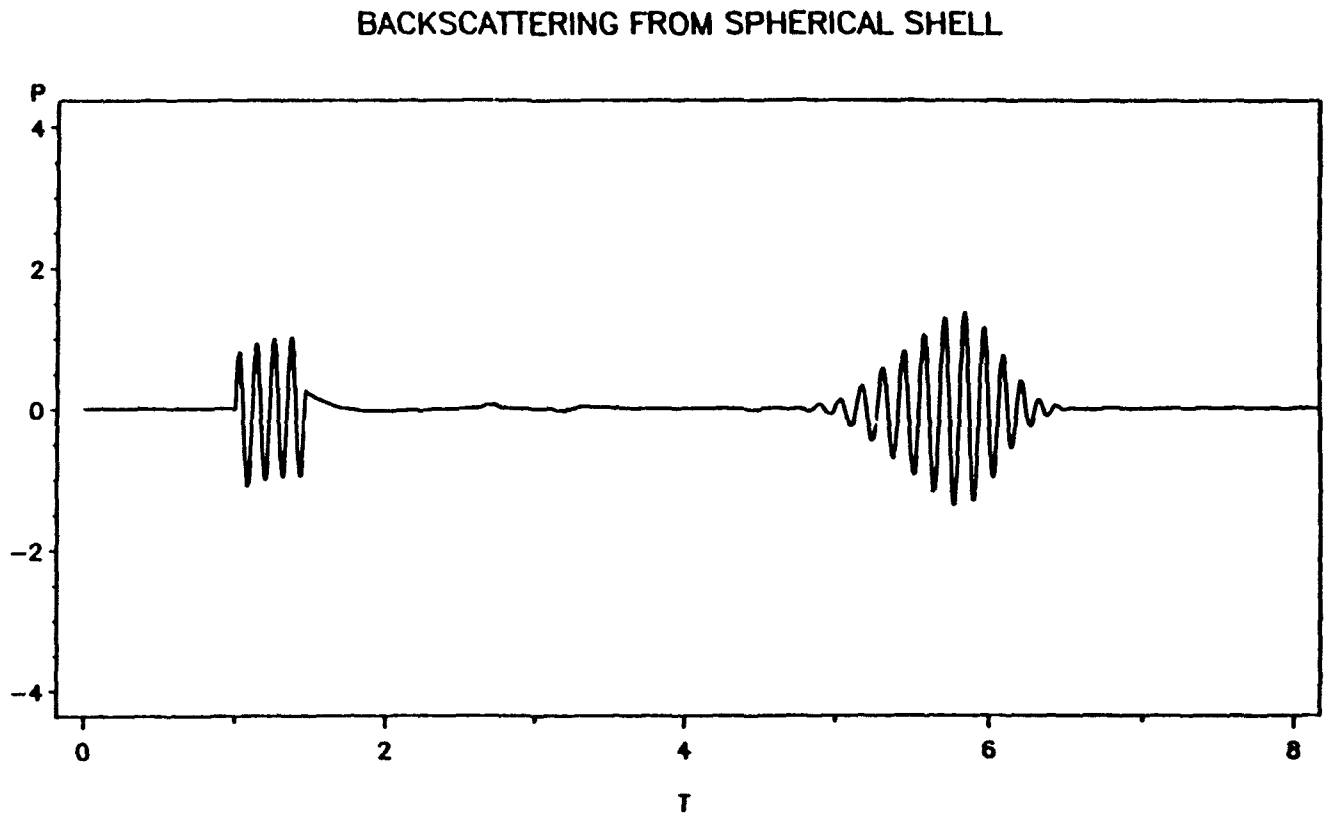

Fig. B1(f). Computational backscattering from a 2.5%-thick SS304 shell for a 4-cycle sine burst with $x_o = 54.0$.

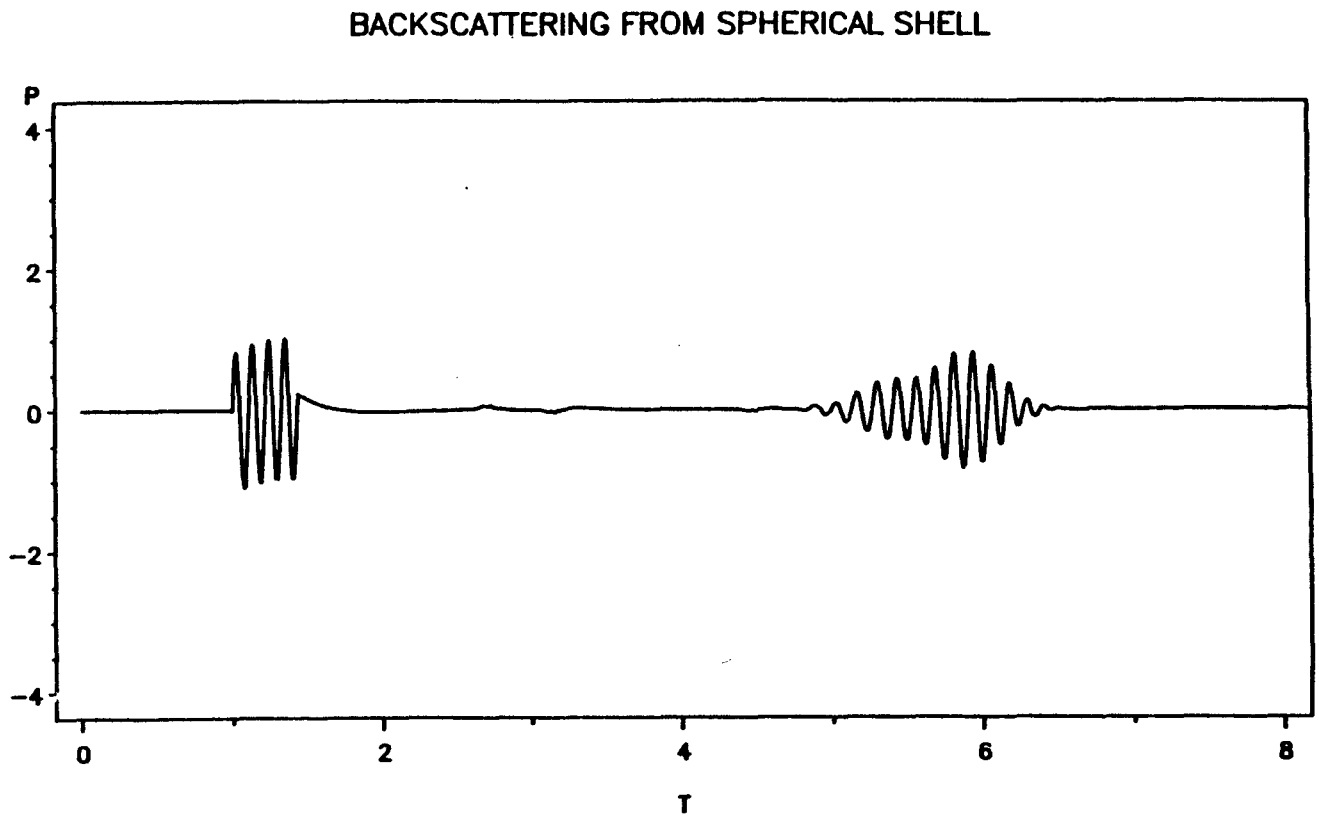

Fig. B1(g). Computational backscattering from a 2.5%-thick SS304 shell for a 4-cycle sine burst with $x_o = 58.0$.

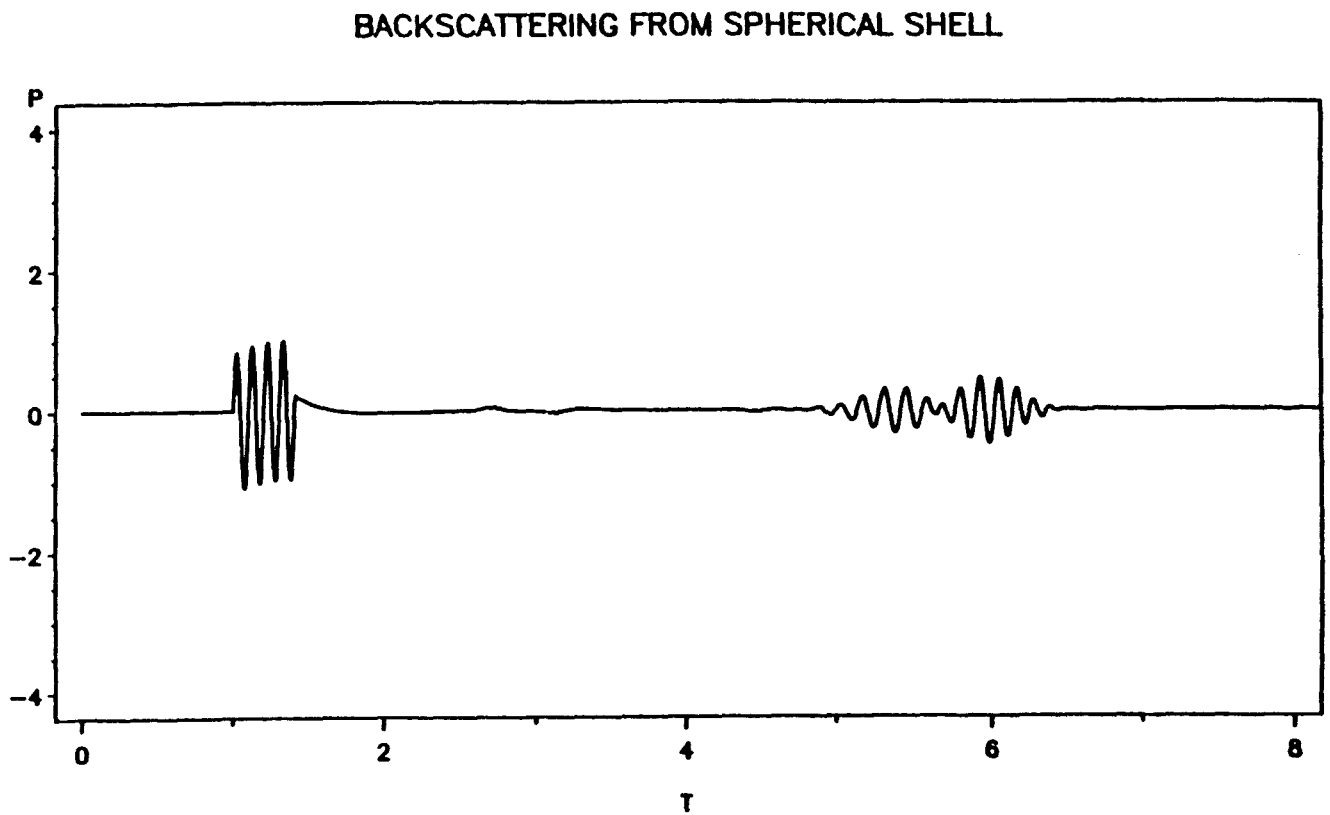

Fig. B1(h). Computational backscattering from a 2.5%-thick SS304 shell for a 4-cycle sine burst with $x_O = 62.0$.

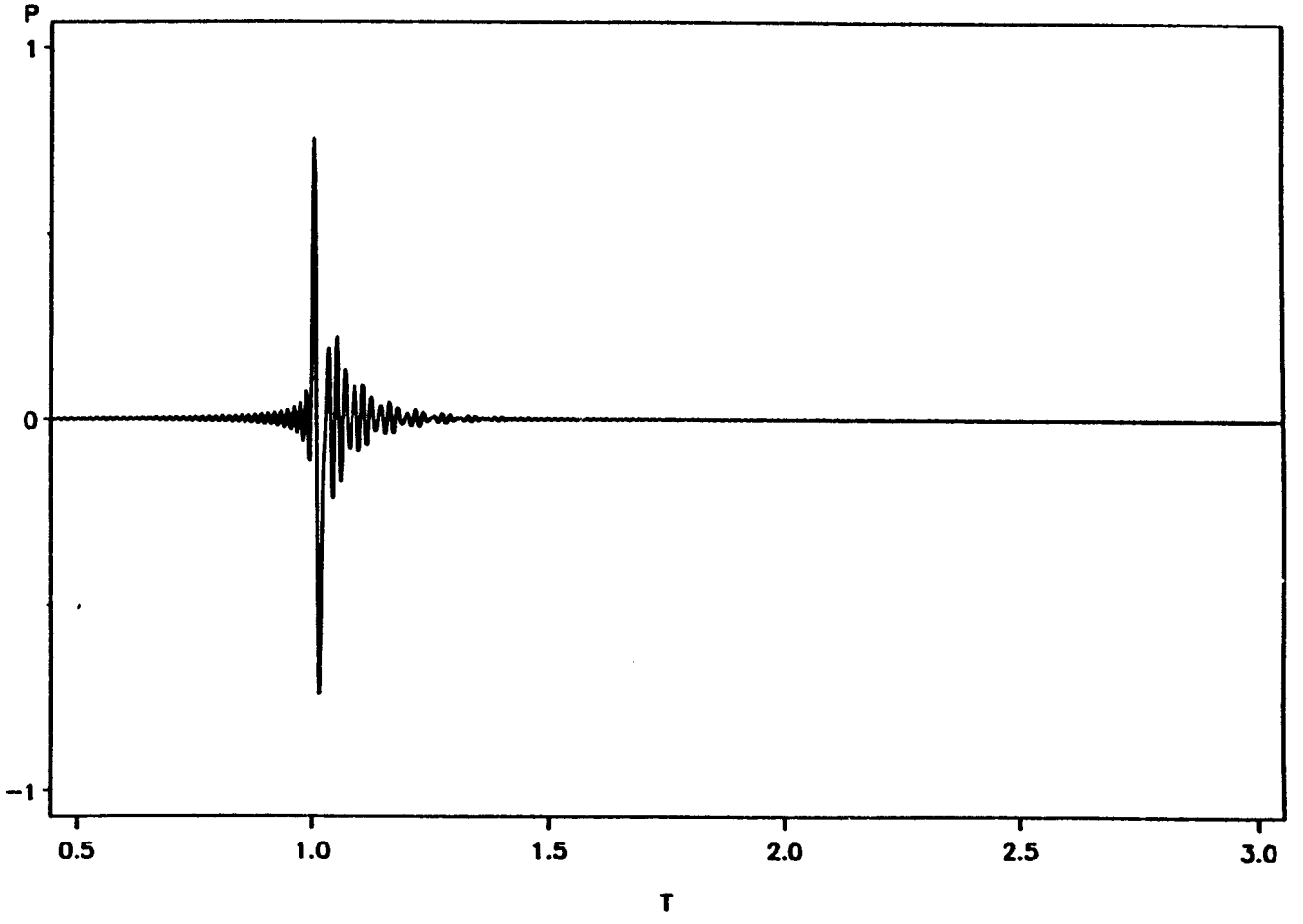

Fig.B2(a). Computational backscattering from a 4%-thick aluminum/fluid shell for a 1-cycle sine burst with $x_0 = 302$.

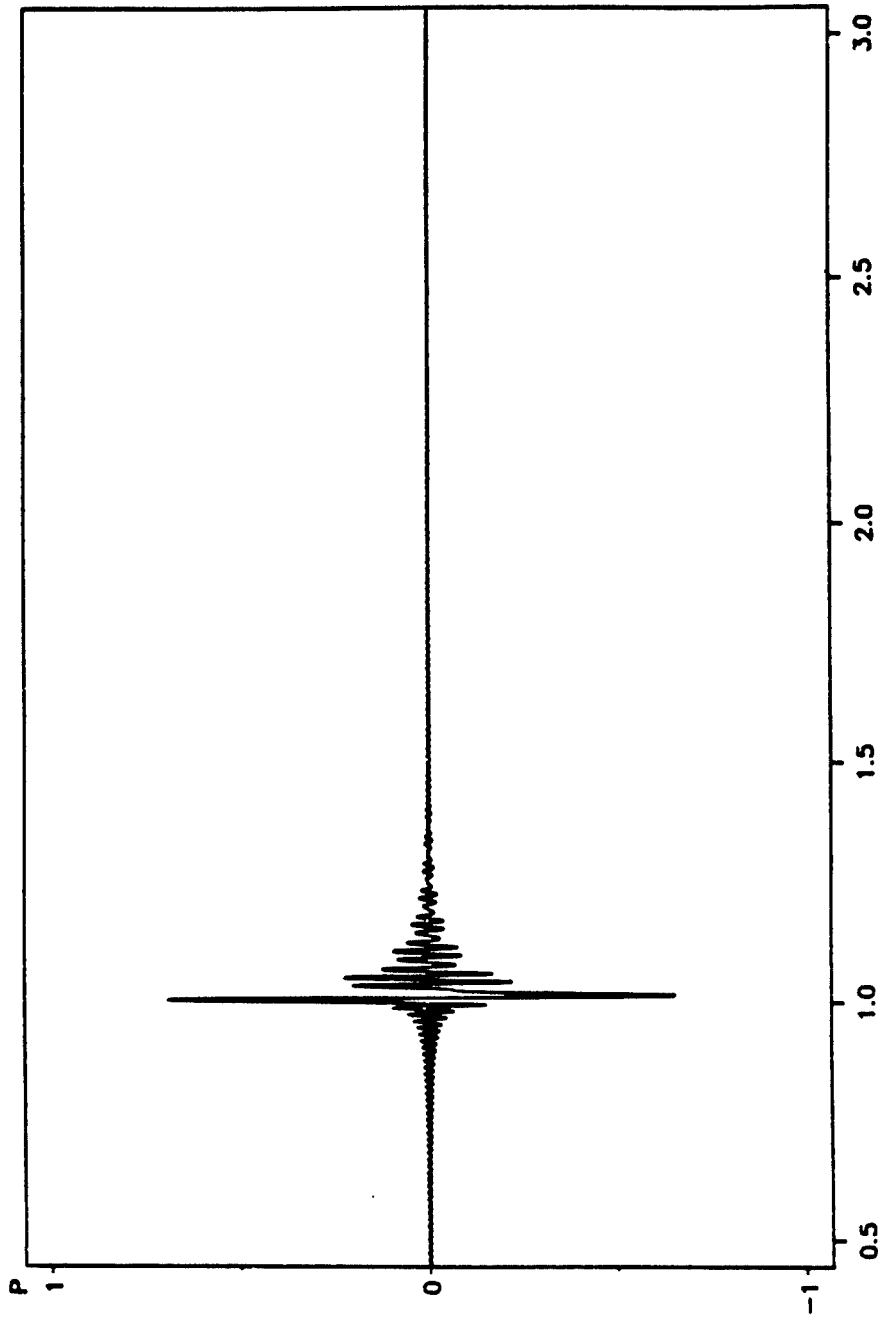

Fig.B2(b). Computational backscattering from a 4%-thick aluminum/fluid shell for a 1-cycle sine burst with $x_O = 340$.

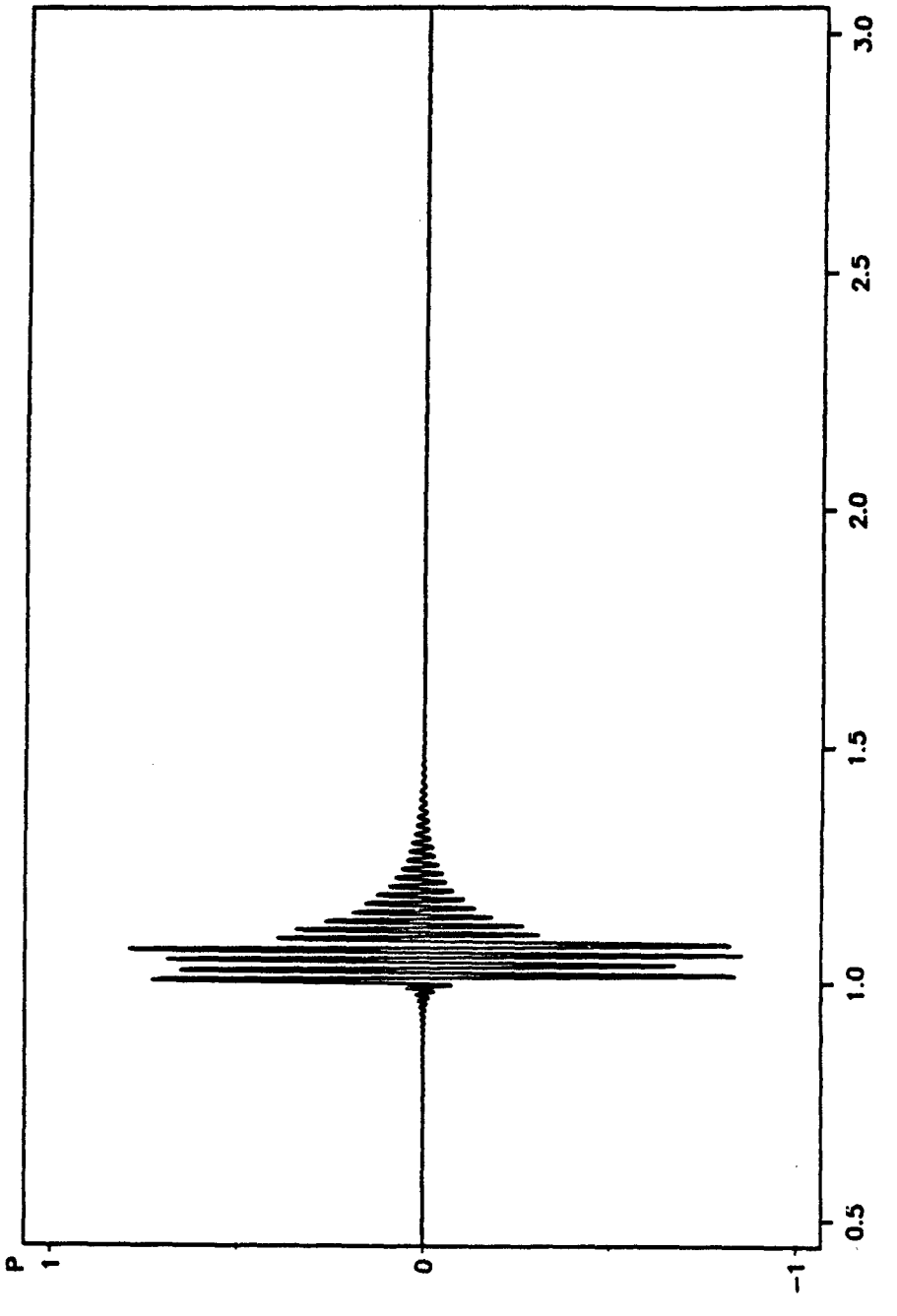

Fig.B3(a). Computational backscattering from a 4%-thick aluminum/fluid shell for a 4-cycle sine burst with $x_0 = 302$.

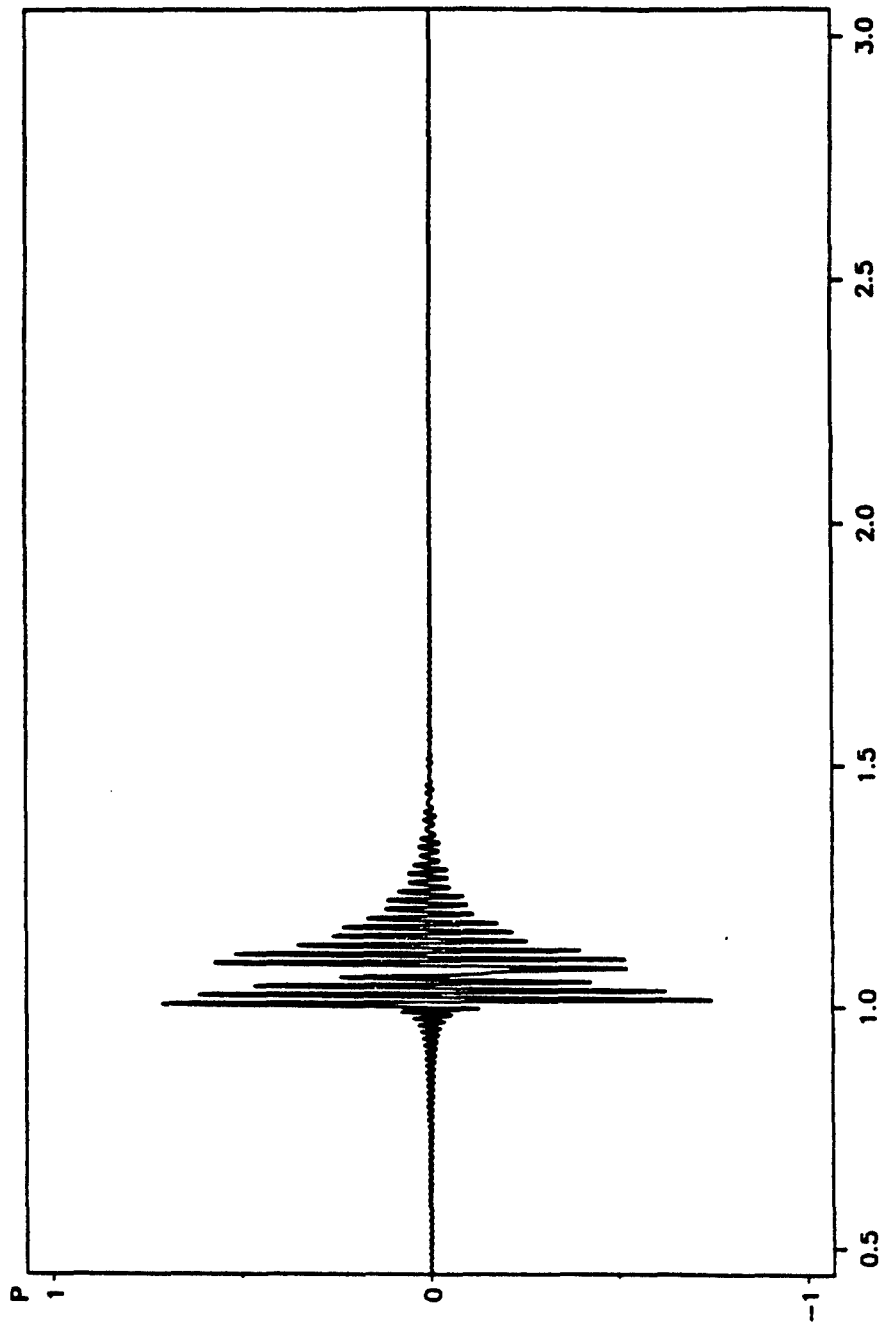

Fig.B3(b). Computational backscattering from a 4%-thick aluminum/fluid shell for a 4-cycle sine burst with $x_0 = 340$.

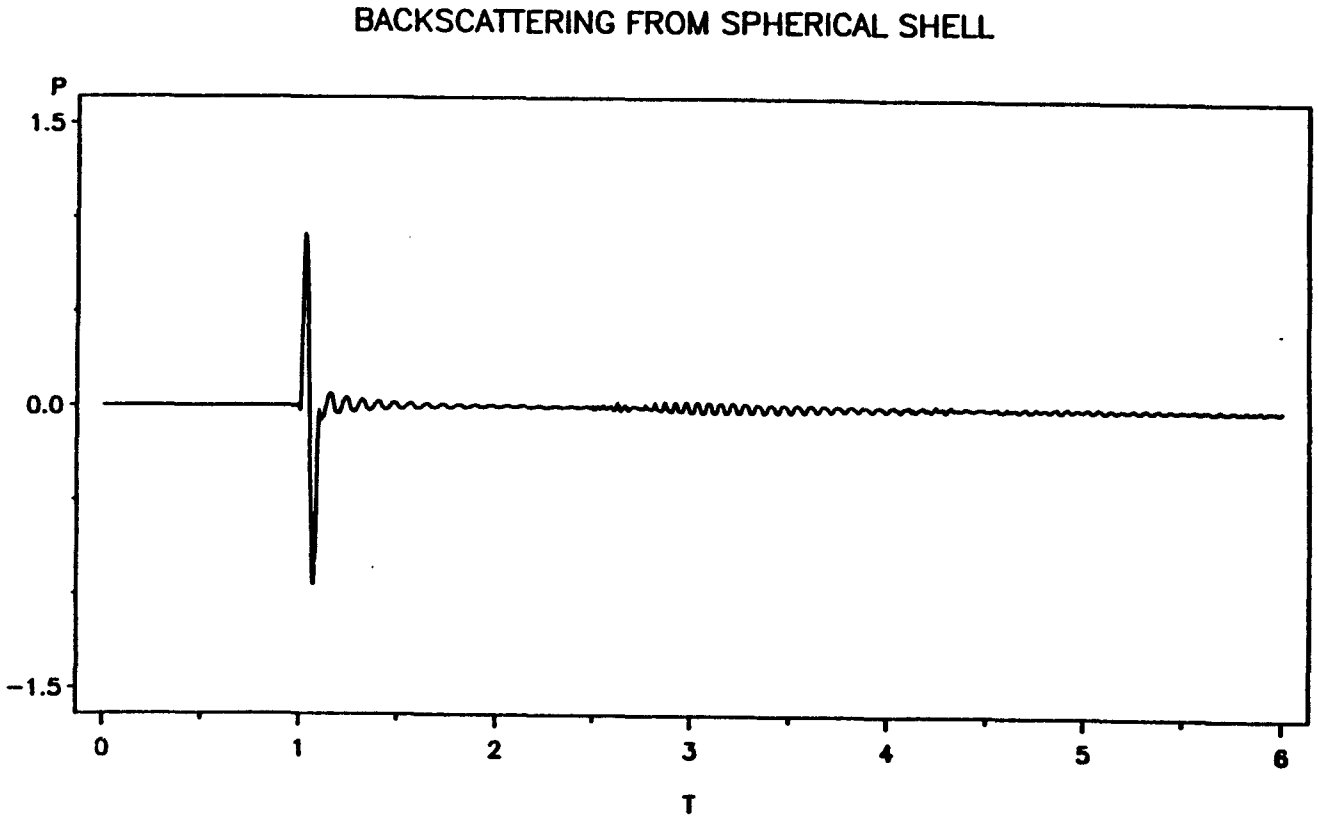

Fig.B4(a). Computational backscattering from a 16.2%-thick *SS440C*/fluid shell for a 1-cycle sine burst with $x_0 = 71.0$.

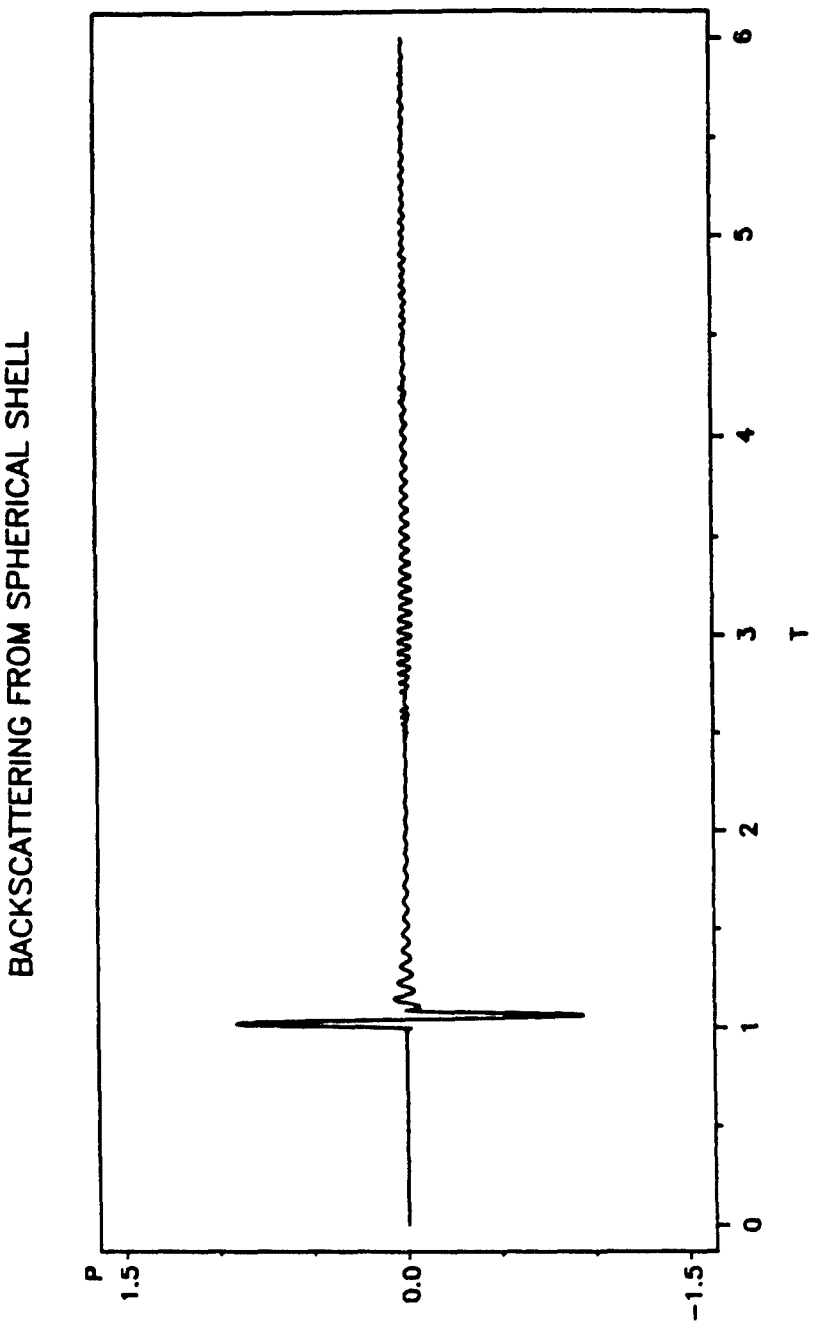

Fig.B4(b). Computational backscattering from a 16.2%-thick SS440C/fluid shell for a 1-cycle sine burst with $x_0 = 76.8$.

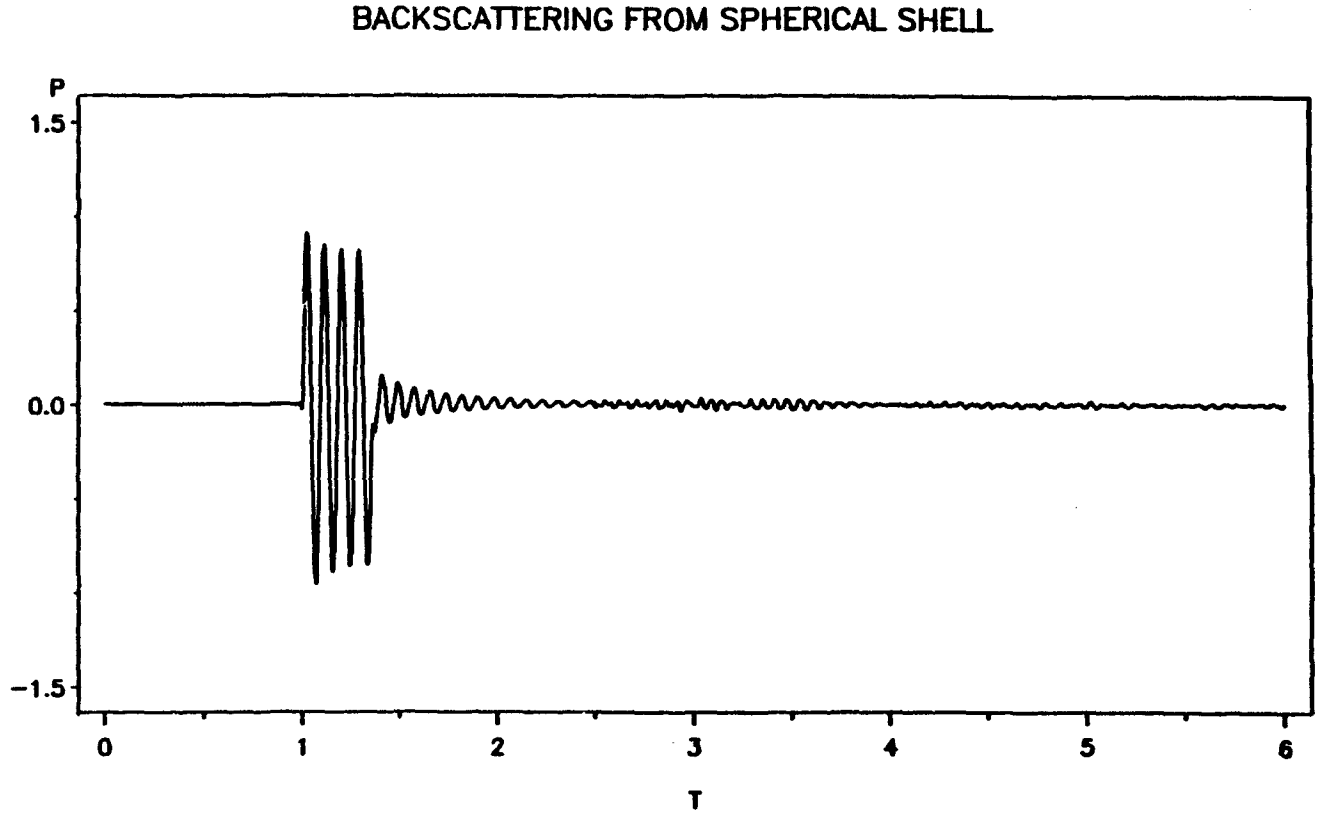

Fig.B5(a). Computational backscattering from a 16.2%-thick SS440C/fluid shell for a 4-cycle sine burst with $x_o = 71.0$.

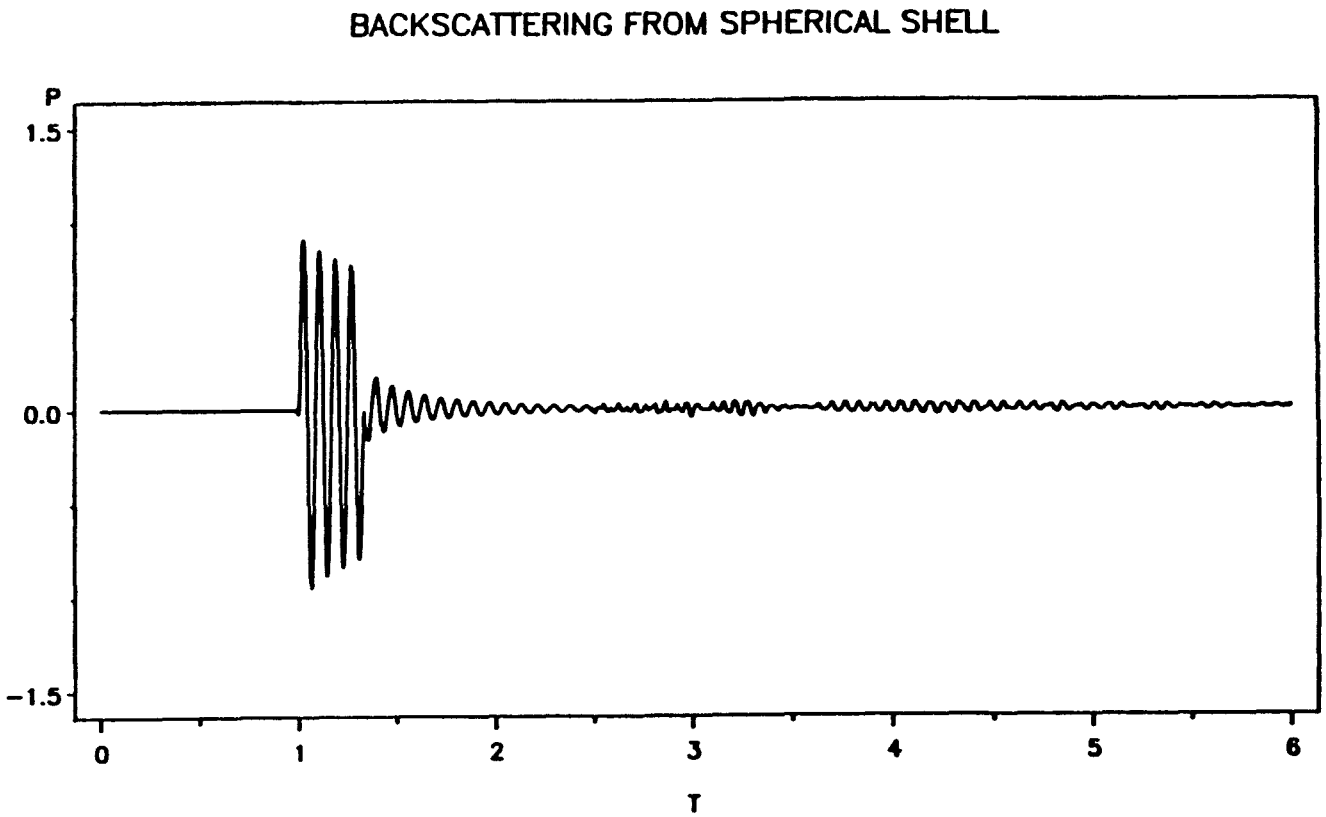

Fig.B5(b). Computational backscattering from a 16.2%-thick SS440C/fluid shell for a 4-cycle sine burst with $x_0 = 76.8$.

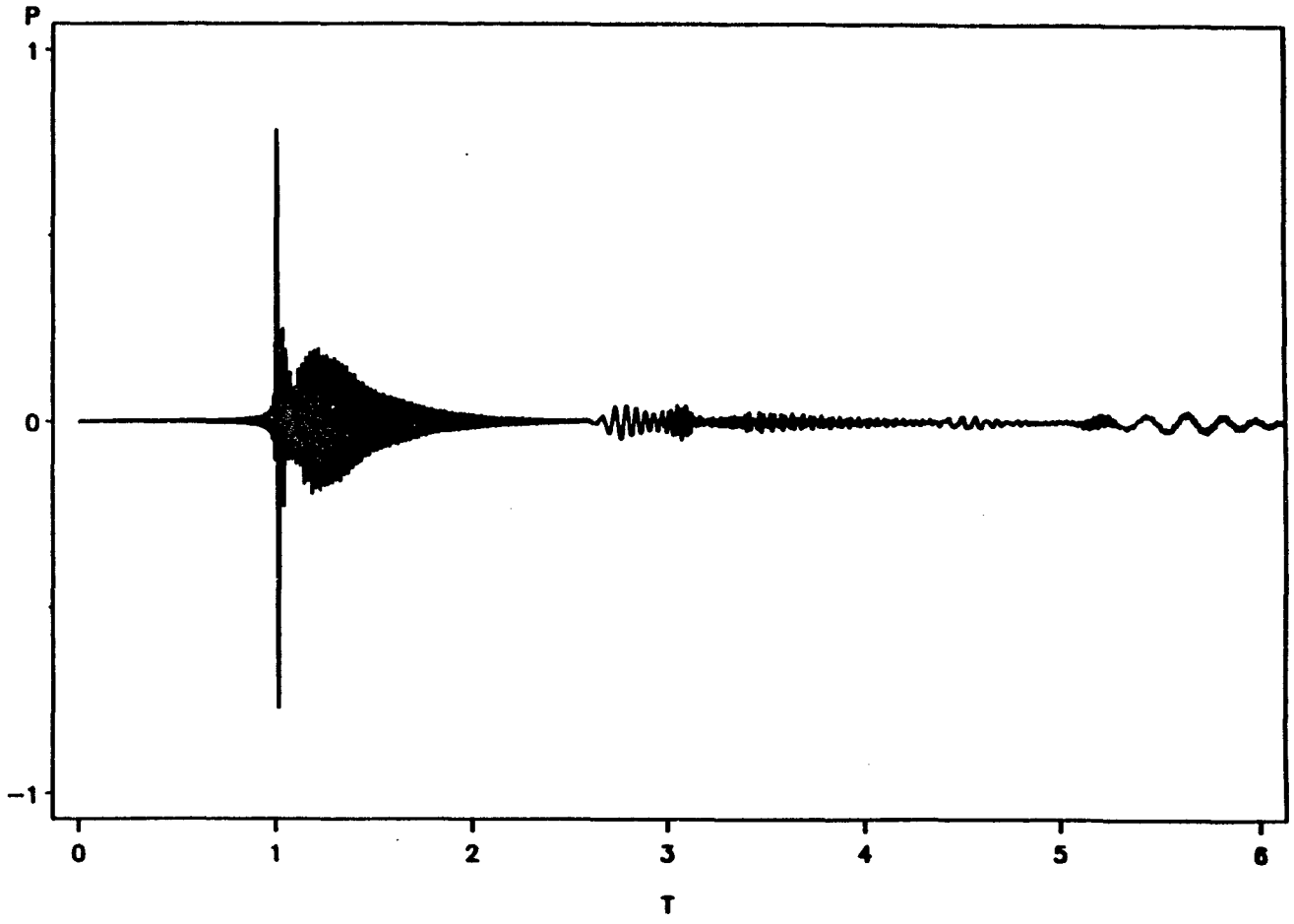

Fig.B6(a). Computational backscattering from a 4%-thick real aluminum shell for a 1-cycle sine burst with $x_0 = 302$.

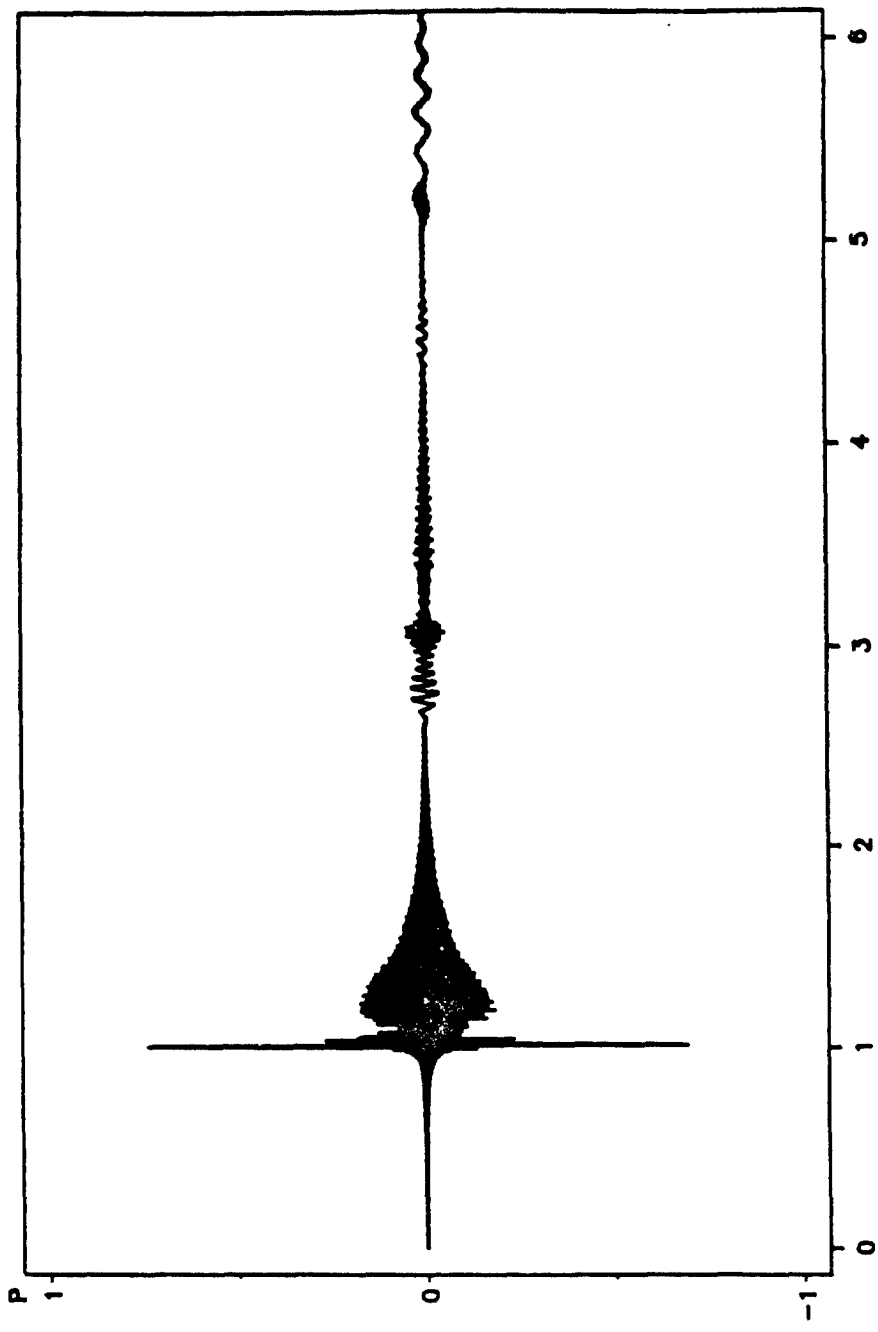

Fig.B6(b). Computational backscattering from a 4%-thick real aluminum shell for a 1-cycle sine burst with $x_0 = 340$.

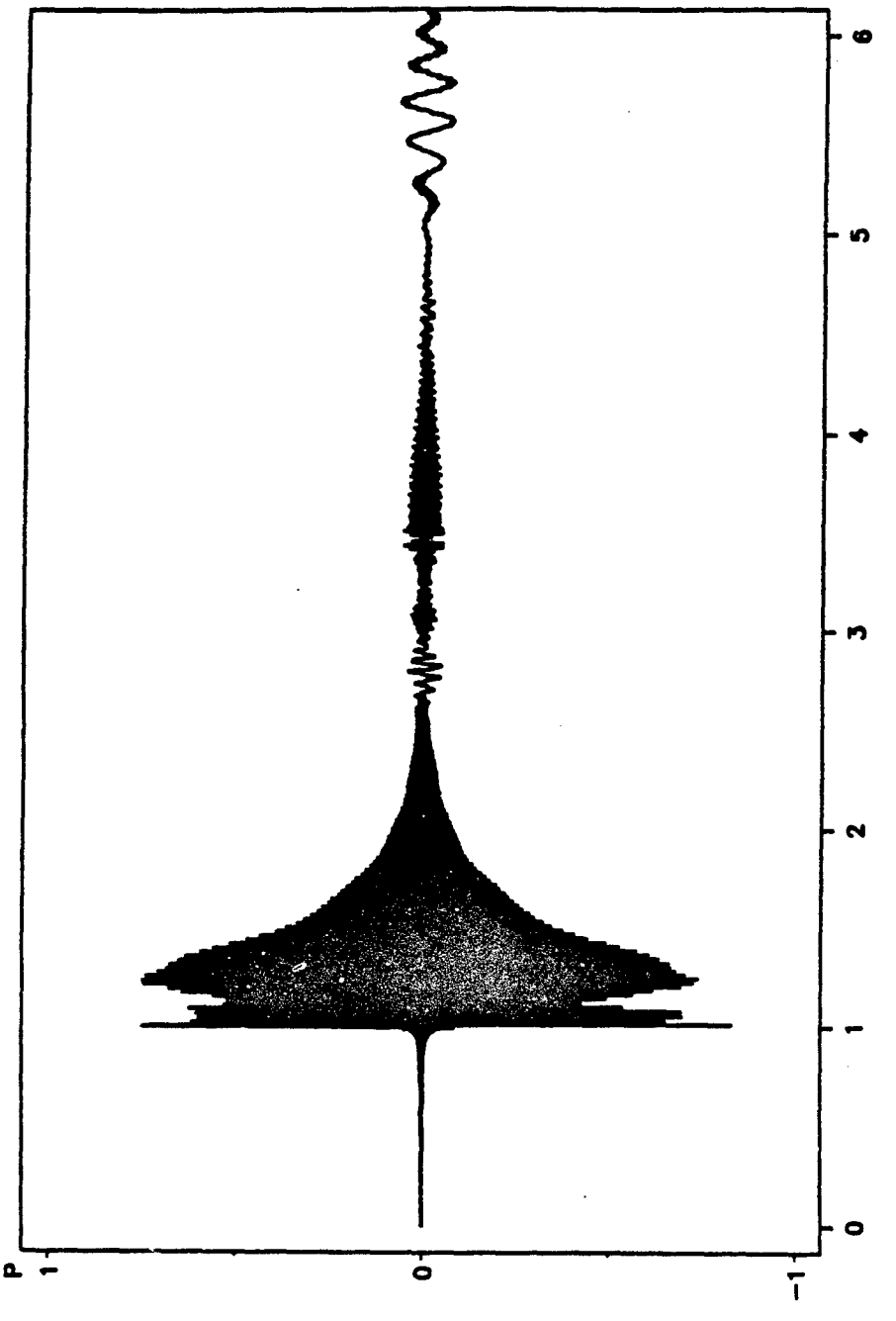

Fig.B7(a). Computational backscattering from a 4%-thick real aluminum shell for a 4-cycle sinc burst with $x_0 = 302$.

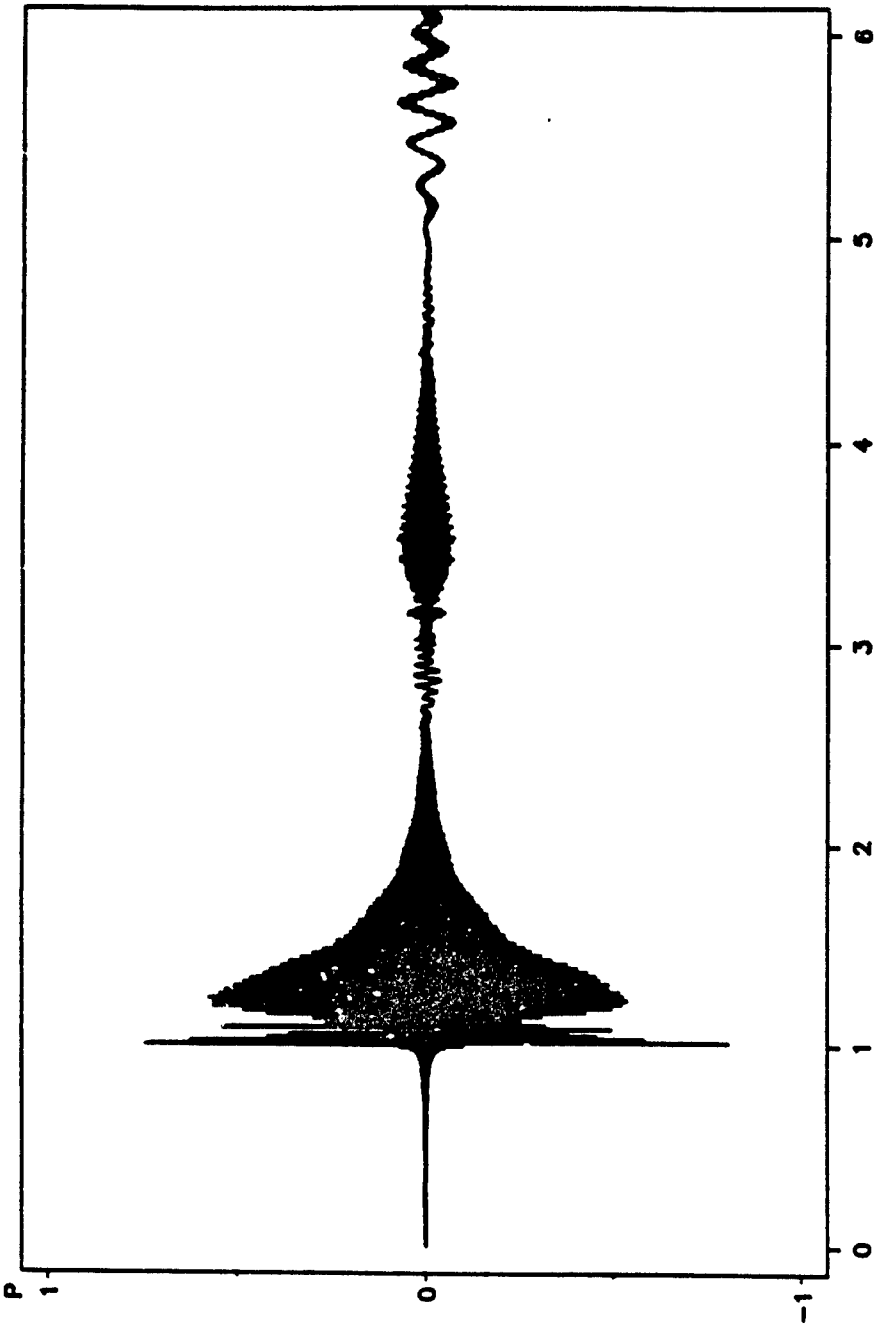

Fig.B7(b). Computational backscattering from a 4%-thick real aluminum shell for a 4-cycle sine burst with $x_O = 340$.

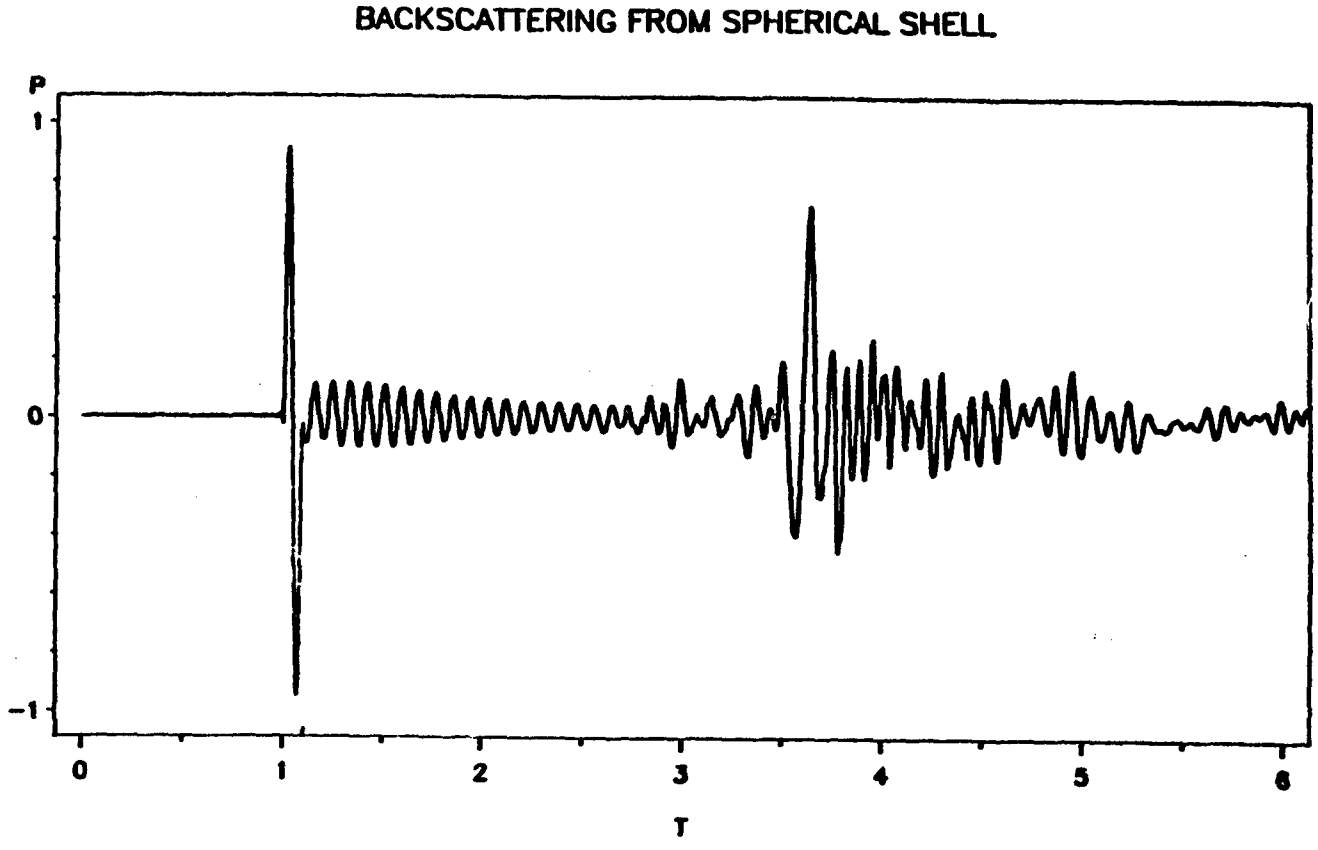

Fig.B8(a). Computational backscattering from a 16.2%-thick real SS440C shell for a 1-cycle sine burst with $x_0 = 71.0$.

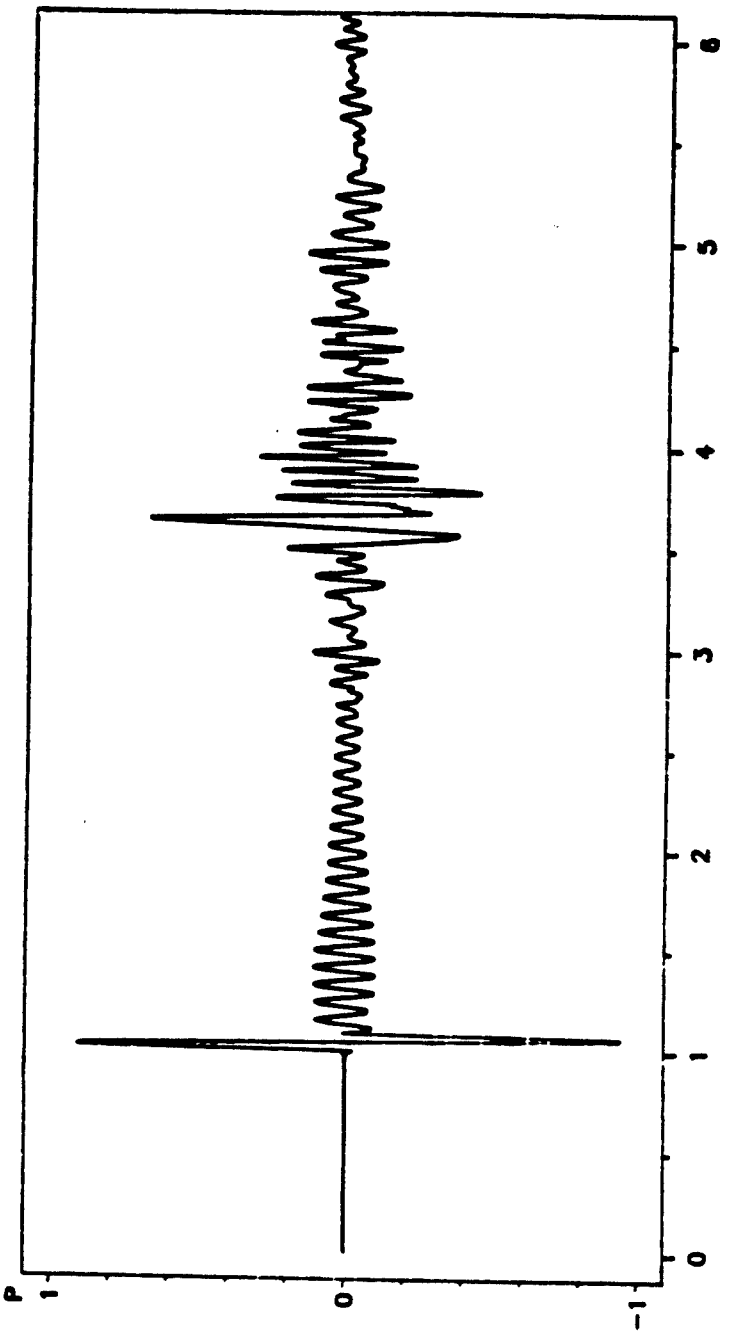

Fig.B8(b). Computational backscattering from a 16.2%-thick real SS440C shell for a 1-cycle sine burst with $x_0 = 76.8$.

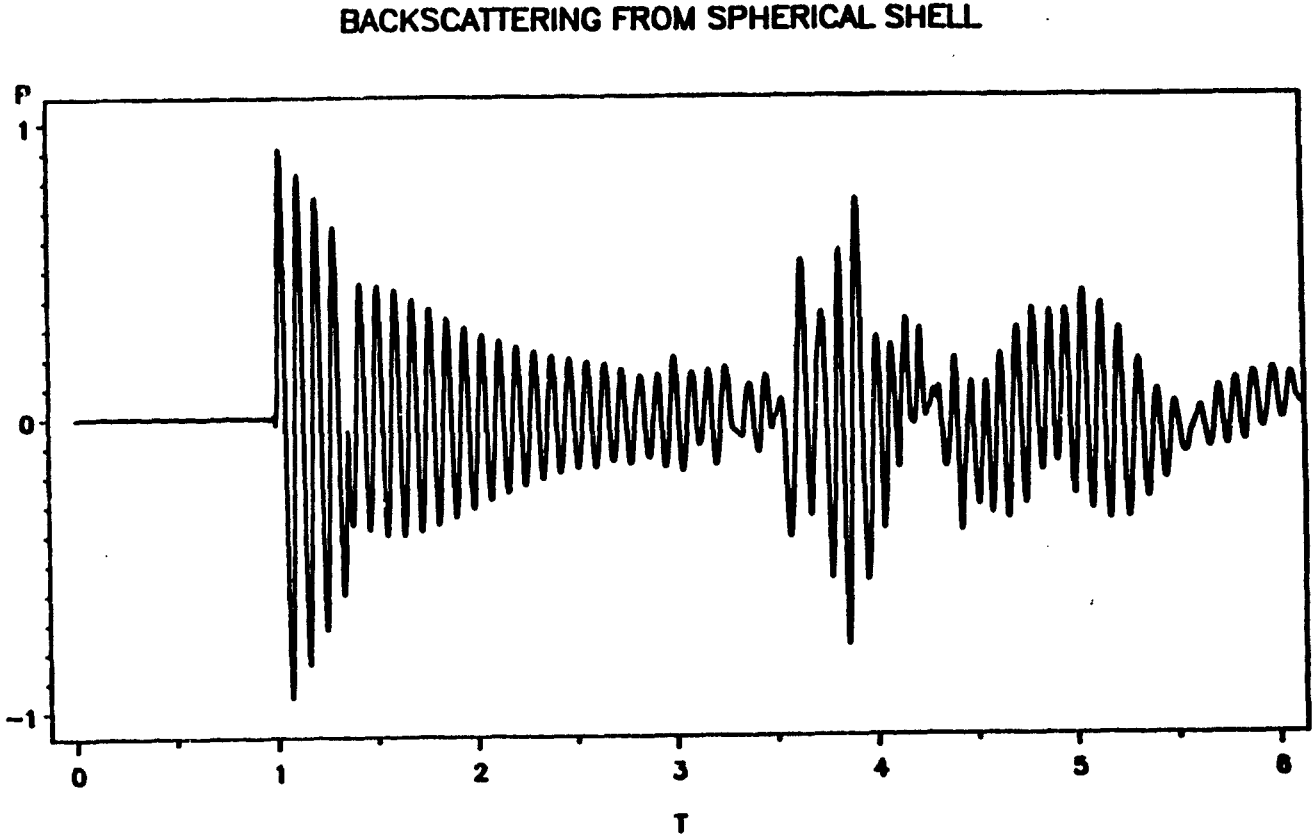

Fig.B9(a). Computational backscattering from a 16.2%-thick real SS440C shell for a 4-cycle sine burst with $x_0 = 71.0$.

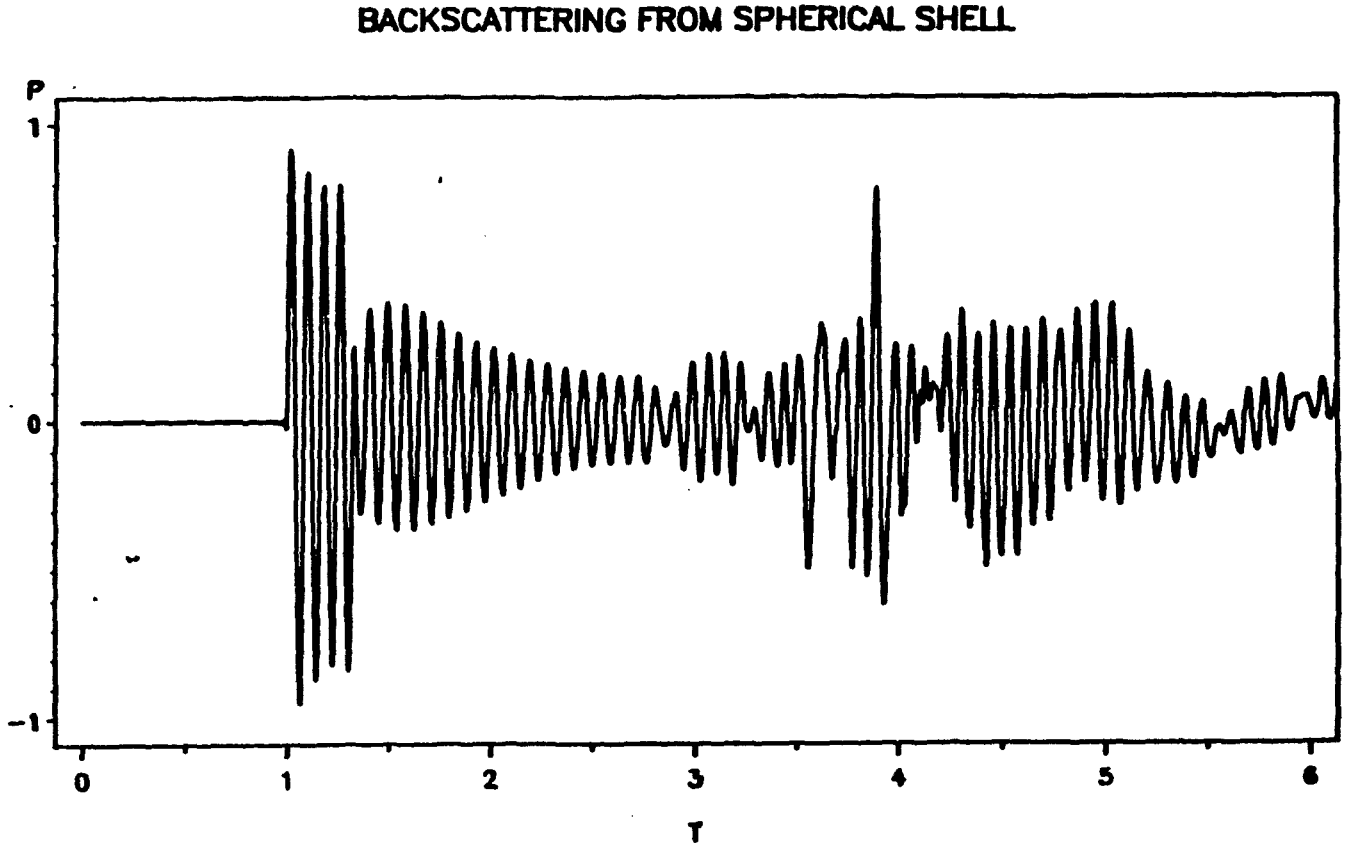

Fig.B9(b). Computational backscattering from a 16.2%-thick real SS440C shell for a 4-cycle sine burst with $\dot{x}_0 = 76.8$.

C. Impulse Response and Form Function

Eq.(3.7) states that $p'(\tau)$ and $F(x)$ are a Fourier Transform pair when $G(x) \equiv 1$, or in other words, when incident wave is a Dirac delta function $\delta(\tau)$. Therefore we would expect to obtain the impulse response of the scatterer by taking the inverse Fourier Transform of the form function. Considering the time reference point, we let the incident wave starting at $\tau = 3$ be a half cycle sine wave with $x_0 = 200$ and $L = 4$. It is equivalent to a delta function with nonzero value 1 only at $\tau = 3$. Its spectrum was checked to be unity for all x value. When taking the inverse Fourier Transform, the cut-off frequency is chosen to be 400. Computed backscattering, or the impulse response of a 2.5%-thick SS304 shell is shown in Fig.C1. We clearly see a low frequency response starting at $\tau \approx 5$ which is the manifestation of existence of a mid-frequency enhancement. The measured interval between the center of the response, assumed to be right at the peak indicated by an arrow, and the specular reflection is 4.44. The excellent agreement with the ray model calculation value (4.467) strongly suggests the validity of the coincident ray model.

Fig. 5c(a), 5c(b) and 5c(c) suggest a very low frequency enhancement. The impulse response of a 16.2%-thick SS440C shell, shown as Fig.C2, was computed by choosing a half-cycle sine burst with $x_0 = 200$ and $L = 4$. A low frequency response is evident, which shows that there does exist a low frequency enhancement for such a thick shell.

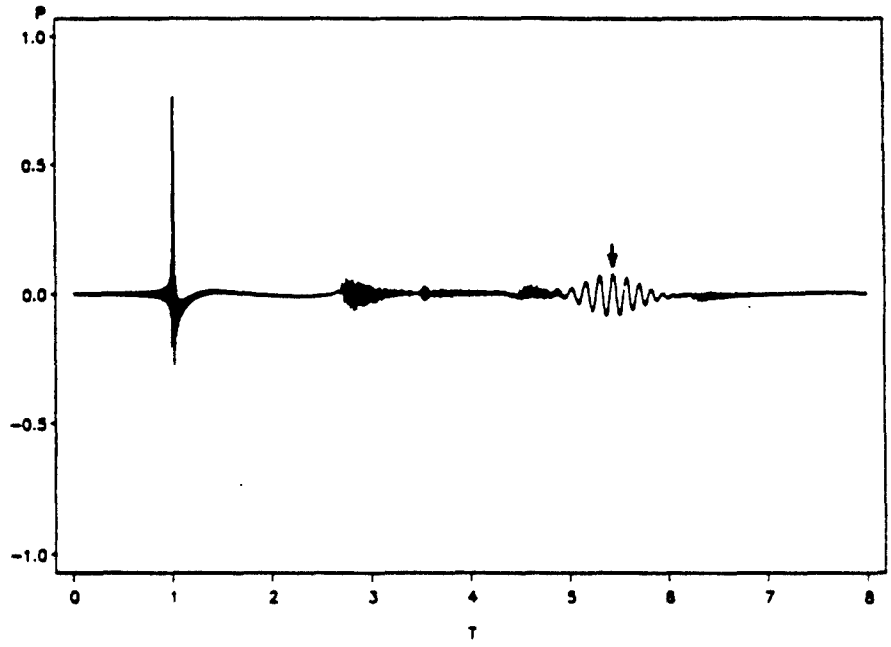

Fig.C1. The impulse response of a 2.5%-thick SS304 shell.

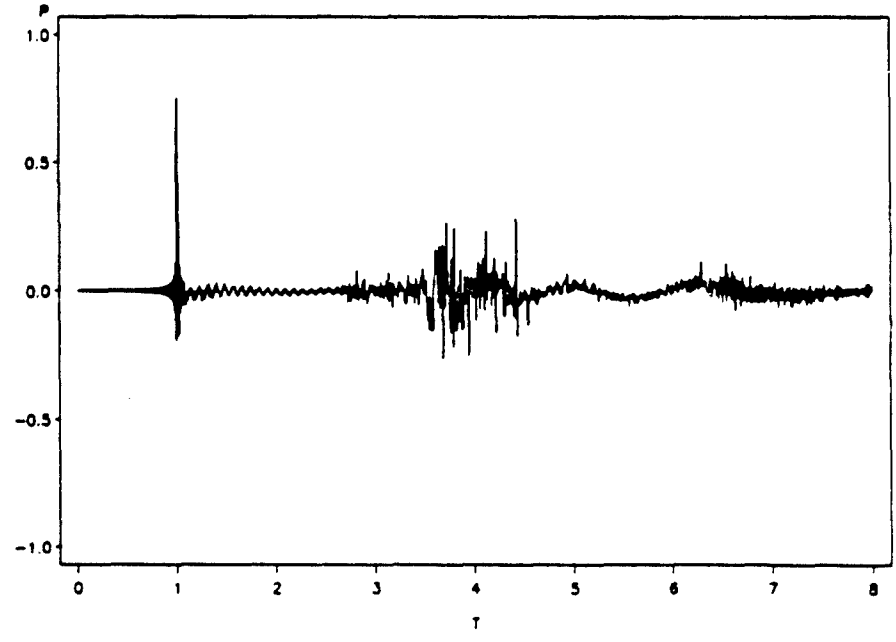

Fig.C2. The impulse response of a 16.2%-thick SS440C shell.

D. Additional Evidence of Mid-Frequency Enhancement: Arrival Time Check With Ray Model Calculation

The coincident ray model for the mid-frequency enhancement has predicted that relative to the specular reflection the arrival time of the echo due to the mid-frequency enhancement can be described by $\tau_d = 2 + \pi c/c_{gl}$. The calculated time interval between the center of the specular reflection and the center of the coincident echo by ray model is 4.467 for 2.5%-thick SS304 shell and $x_o = 46.0$. Fig.11d shows that at $x_o = 46.0$, the echo due to the mid-frequency enhancement is quite symmetric therefore it is easy to locate the center of the echo. Actually it can be determined as $\tau = 6.768$ by looking at the Table 4.4 and the center of the specular reflection can be calculated as $\tau = 1 + 10 \times 2\pi/x_o = 2.366$. The time interval between them is therefore 4.402 which is pretty much the same as the ray model prediction. This simple check gives additional evidence of the validity of the coincident ray model.

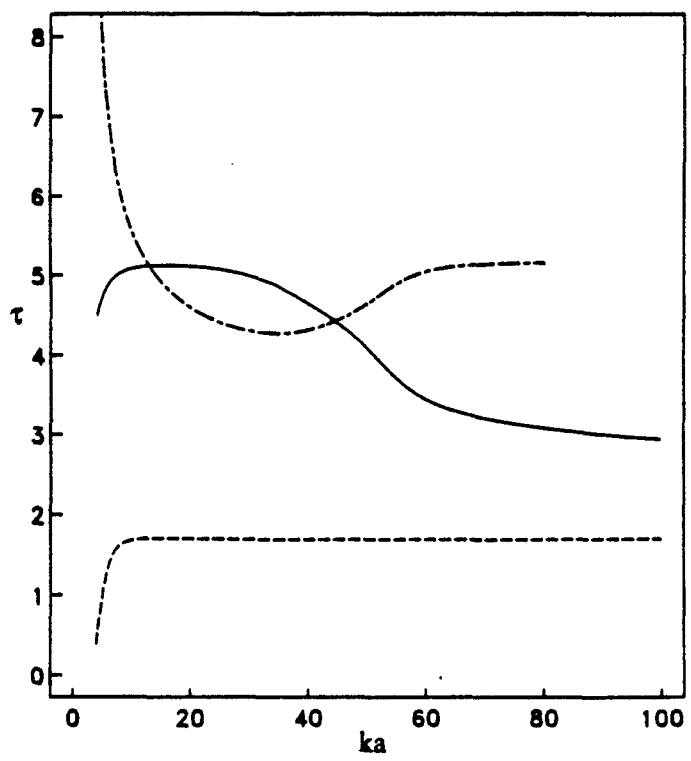

Fig.D1. The arrival time of various surface waves for 2.5%-thick SS304 shell. The solid curve is for $l = a_o$, the short-dashed curve is for $l = s_o$, and the short-long-dashed curve is for $l = a_o'$.

E. More on Prompt Radiation Effect

We have seen in section 5.5 that the prompt radiation can be out of phase with the specular reflection, which makes it difficult to infer the amplitude of the prompt radiation wave for the case of the backscattering from a SS440C shell (Fig.18a). In section 5.4 we have assumed a fluid shell to remove the effects due to the elastic surface waves and transverse waves. Here we want to single out the prompt radiation from the specular reflection background, which can be achieved by subtracting the backscattering by a fluid shell from that by an elastic shell. The results for aluminum and SS440C shell cases have been shown as Fig.E. The prompt radiation can be clearly seen for both aluminum (x_0 = 302) and SS440C (x_0 = 71.0) cases. Comparison of Figs. E1 and E2 for the aluminum case shows clear evidence of a substantial prompt contribution for x_0 = 302 and a much weaker prompt contribution for x_0 = 340. It is interesting to notice that Figs. E1 and E2 display a qualitative similarity with the burst response of a damped harmonic oscillator near and away from resonance respectively. For a review of the burst response of such systems see e.g. Pippard[23].

The arrival of other surface wave contributions makes the steady-state prompt radiation contribution hard to be determined for the SS440C case. Shown in Fig.E5 is the case of 80-cycle incident burst. If the backscattering reaches its steady state right before the burst turns off, which is a suggestion of the figure although it can not be fully trusted, then the measured amplitude value is 2.0. Neglecting the relatively weak contribution of other surface waves in this time interval, the value 2.0 becomes the estimate of the prompt radiation contribution. This value is remarkably close to the value of 1.95 at x_0 = 71.0 implicit in Fig.7 of Ref.20. That is the magnitude of the error in the steady-state ray synthesis, which neglects prompt radiation contribution. Thus 1.95 and 2.0 are consistent estimates of the prompt contribution for the SS440C case.

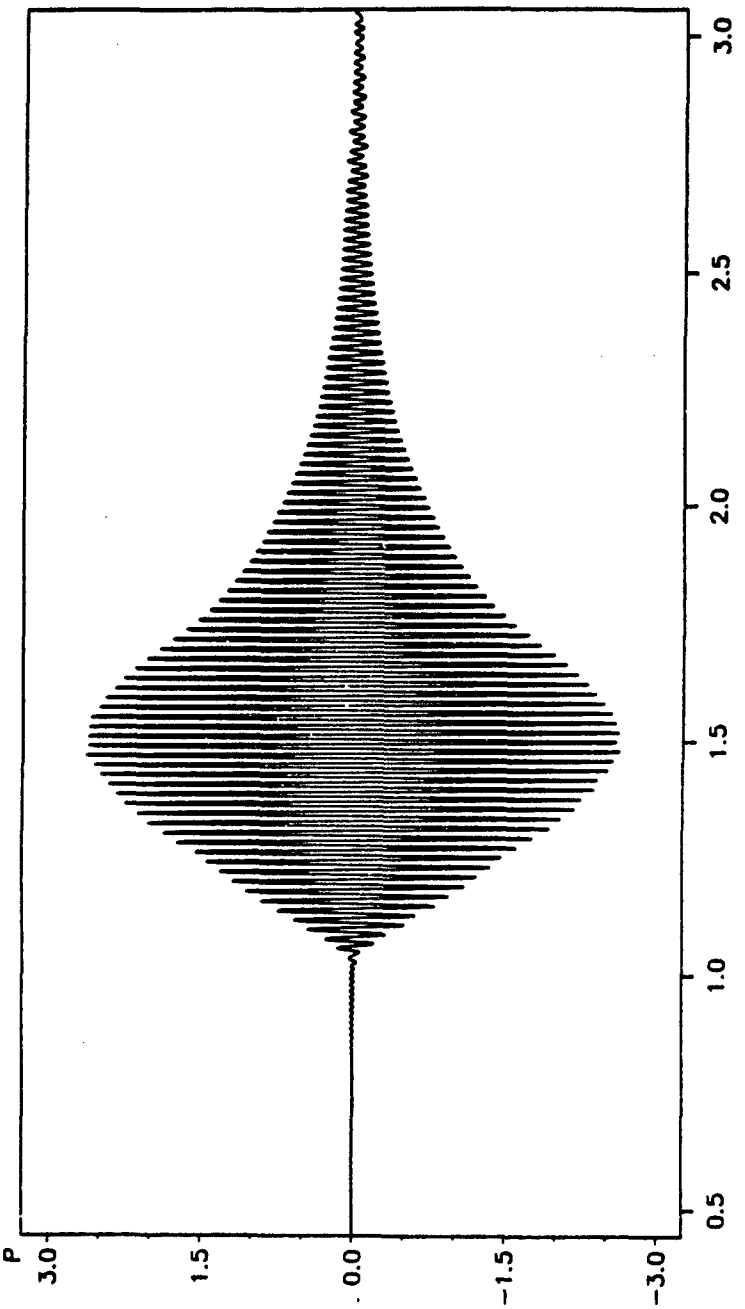

Fig.E1. The difference between the backscattering by a 4%-thick aluminum shell and that by a 4%-thick aluminum/fluid shell for a 20-cycle sine burst with x_0 = 302.

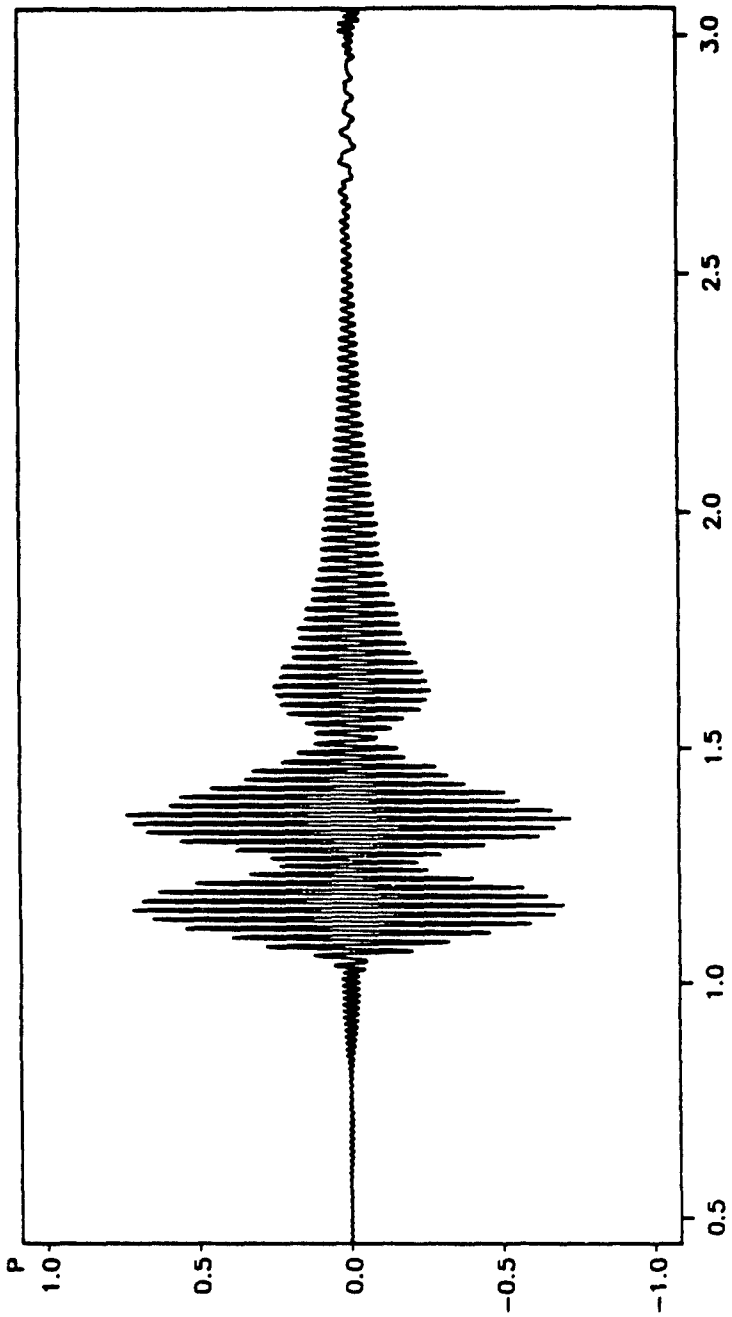

Fig.E2. The difference between the backscattering by a 4%-thick aluminum shell and that by a 4%-thick aluminum/fluid shell for a 20-cycle sine burst with x_0 = 340.

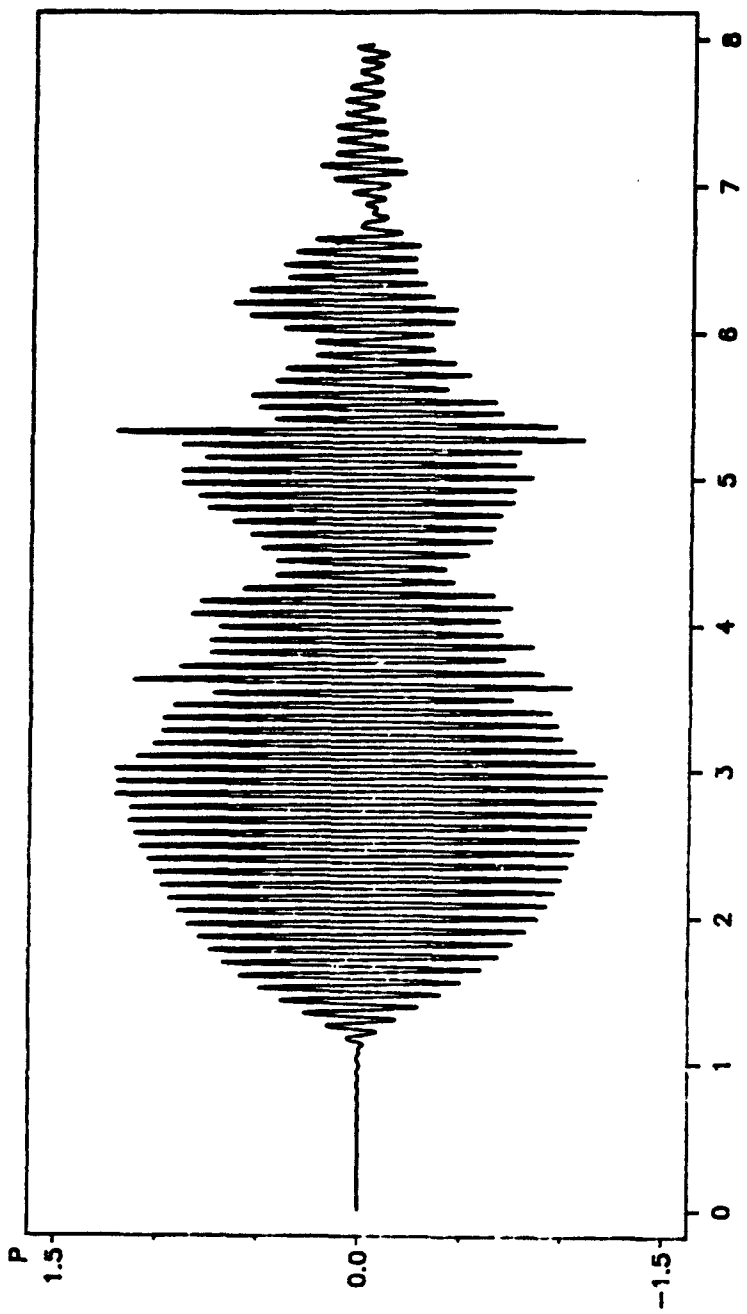

Fig.E3. The difference between the backscattering by a 16.2%-thick SS440C shell and that by a 16.2%-thick SS440C/fluid shell for a 20-cycle sine burst with x_O = 71.0.

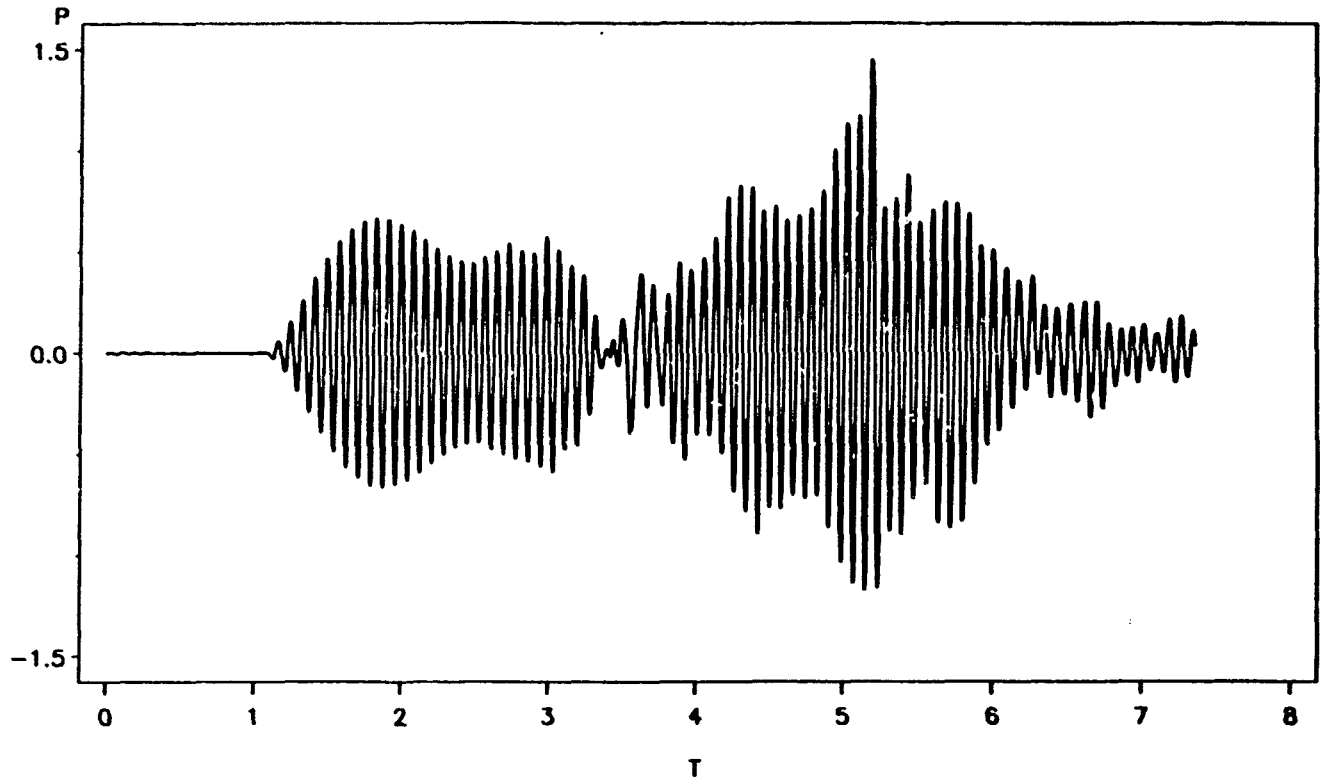

Fig.E4. The difference between the backscattering by a 16.2%-thick SS440C shell and that by a 16.2%-thick SS440C/fluid shell for a 20-cycle sine burst with x_0 = 76.8.

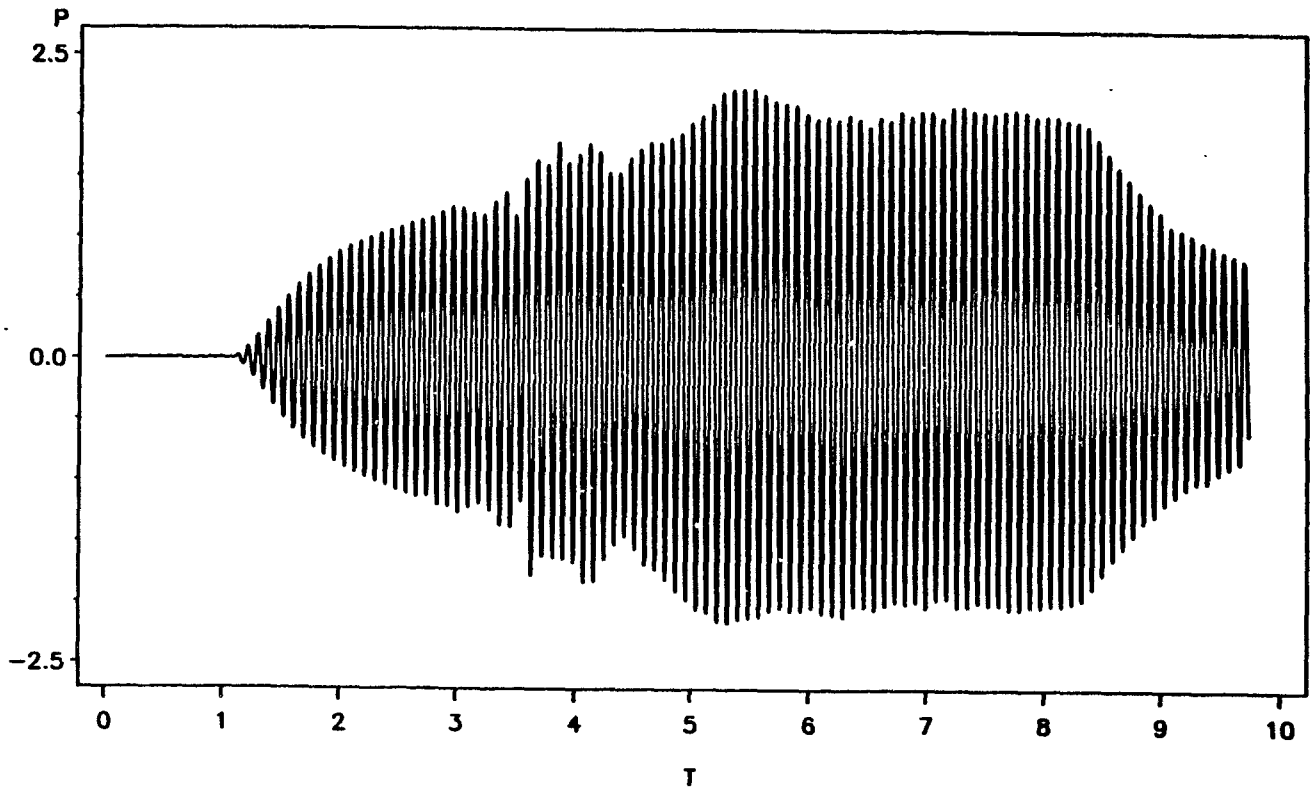

Fig.E5. The difference between the backscattering by a 16.2%-thick SS440C shell and that by a 16.2%-thick SS440C/fluid shell for a 80-cycle sine burst with x_0 = 71.0.

References

1. R.Hickling, "Analysis of echoes from a hollow metallic sphere in water," J. Acoust. Soc. Am. **36**, 1124 - 1137 (1964).

2. K.J.Diercks and R.Hickling, "Echoes from hollow aluminum spheres in water," J.Acoust. Soc. Am. **41**, 380 - 393 (1967).

3. A.J.Rudgers, "Acoustic pulses scattered by a rigid sphere immersed in a fluid," J.Acoust. Soc. Am. **45**, 900 - 910 (1969).

4. J.J.Stephens, P.S.Ray and R.J.Kurzeja, "Far-field transient backscattering by water drops," J. Atmospheric Sci. **28**, 785 - 793 (1971).

5. H.Inada, "Backscattered short pulse response of surface waves from dielectric spheres," Applied Optics **13**, 1928 - 1933 (1974).

6. P.S.Ray, J.J.Stephens and T.W.Kitterman, "Near-field impulse response examination of backscattering from dielectric spheres," Applied Optics **14**, 2492 - 2498 (1975).

7. I. A. Viktorov, Rayleigh and Lamb Waves: Physical Theory and Applications (Plenum, New York, 1967).

8. M.Talmant, H.Uberall, R.D.Miller and J.W.Dickey, "Lamb waves and fluid-borne waves on water-loaded, air-filled thin spherical shells," J. Acoust. Soc. Am. **86**, 278 - 289 (1989).

9. K.L.Williams and P.L.Marston, "Backscattering from an elastic sphere: Sommerfeld-Watson transformation and experimental confirmation," J. Acoust. Soc. Am. **78**, 1093 - 1102 (1985).

10. K.L.Williams and P.L.Marston, "Synthesis of backscattering from an elastic sphere using the Sommerfeld-Watson transformation and giving a Fabry-Perot analysis of resonances," J. Acoust. Soc. Am. **79**, 1702 - 1708 (1986).

11. S.G.Kargl and P.L.Marston, "Longitudinal resonances in the form function for backscattering from a spherical shell : Fluid shell case," J. Acoust. Soc. Am. **88**, 1114 - 1122 (1990).

12. S.G.Kargl and P.L.Marston, "Observation and modeling of the backscattering of short tone bursts from a spherical shell: Lamb wave echoes, glory and axial reverberations," J. Acoust. Soc. Am.**85**, 1014 - 1028 (1989).

13. S.G.Kargl and P.L.Marston, "Ray synthesis of Lamb wave contributions to the total scattering cross section for an elastic spherical shell," J. Acoust. Soc. Am. **88**, 1103 -1113 (1990).

14. B.Gold and C.M.Rader, Digital Processing of Signals, (McGraw-Hill 1969).

15. IMSL Stat/Library, Fortran subroutines for mathematical applications, version 1.0 April 1987.

16. G.S.Sammelmann, D.H.Trivett, and R.H.Hackman, "The acoustic scattering by a submerged, spherical shell.I: The bifurcation of the dispersion curve for the spherical antisymmetric Lamb wave," J. Acoust. Soc. Am.85, 114 - 124 (1989).

17. G.S.Sammelmann and R.H.Hackman, "The acoustic scattering by a submerged, spherical shell.II: The high-frequency region and the thickness quasiresonance," J. Acoust. Soc. Am. 89, 2096 - 2103 (1991).

18. P.L.Marston, "GTD for backscattering from elastic spheres and cylinders in water and the coupling of surface elastic waves with the acoustic field," J. Acoust. Soc. Am. 83, 25 - 37 (1988).

19. N.Sun and P.L.Marston, "Ray synthesis of backscattering by thin cylindrical shells (Abstract)," J. Acoust. Soc.Am. 89, 1949 (1991).

20. S.G.Kargl and P.L.Marston, "Ray synthesis of the form function for backscattering for an elastic spherical shell: leaky Lamb waves and longitudinal resonances," J. Acoust. Soc. Am. 89, 2545 - 2558 (1991).

21. J.M.Ho and L.B.Felsen, "Nonconventional traveling wave formulations and ray-acoustic reductions for source-excited fluid-loaded thin elastic spherical shells," J. Acoust. Soc. Am. 88, 2389 - 2414 (1990).

22. R.C.Chivers and L.W.Anson, "Calculations of the backscattering and radiation force functions of spherical targets for use in ultrasonic beam assessment," Ultrasonics 20, 25 - 34 (1982).

23. A.B.Pippard, The physics of vibration, Vol. 1, p.145, (Cambridge University Press 1978).

TECHNICAL REPORT DISTRIBUTION, UNCLASSIFIED CONTRACT

Defense Technical Information Center — 2 one-sided copies
Comeron Station
Alexandria, VA 22314

L. E. Hargrove — 1 two-sided copy
Physics Division, Code 1112
Office of Naval Research
800 N. Quincy Street
Arlington, VA 22217-5000

S. G. Kargl — 1 two-sided copy
Naval Coastal Systems Center
Physical Acoustics Branch
Code 2120
Panama City, FL 32407

L. G. Zhang — 1 two-sided copy
School of Electrical Engineering and Computer Science
Washington State University
Pullman, WA 99164-2752